Shadows as a tool to evaluate black hole parameters and a dimension of spacetime

- **А.Ф. Захаров (Alexander F. Zakharov)**
- **E-mail: zakharov@itep.ru**
-
- *Institute of Theoretical and Experimental Physics,*
- *B. Cheremushkinskaya, 25, 117218 Moscow;*

-
- **8th SCSLSA**
- **Special workshop "Black Holes and Spectral Lines"**
- in the frame of COST action MP0905 "Black Holes in an Violent Universe"

- Divcibare, Serbia,   **10 June, 2011**

SEARCH [   ] Go ▸ Advanced search

Home > News

NEWS

Black holes 'do not exist'

Philip Ball

These mysterious objects are dark-energy stars, physicist claims.

Black holes are staples of science fiction and many think astronomers have observed them indirectly. But according to a physicist at the Lawrence Livermore National Laboratory in California, these awesome breaches in space-time do not and indeed cannot exist.
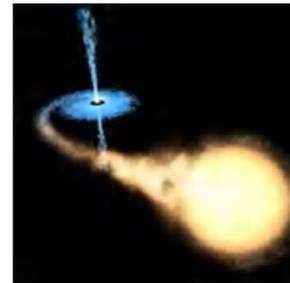
Black holes, such as the one pictured in this artist's impression, may in fact be pockets of 'dark energy'.

© ESA/NASA

Over the past few years, observations of the motions of galaxies have shown that some 70% the Universe seems to be composed of a strange 'dark energy' that is driving the Universe's accelerating expansion.

George Chapline thinks that the collapse of the massive stars, which was long believed to generate black holes, actually leads to the formation of stars that contain dark energy. "It's a near certainty that black holes don't exist," he claims.

Black holes are one of the most celebrated predictions of Einstein's general theory of relativity, which explains gravity as the warping of space-time caused by massive objects. The theory suggests that

a sufficiently massive star, when it dies, will collapse under its own gravity to a single point.

But Einstein didn't believe in black holes, Chapline argues. "Unfortunately", he adds, "he couldn't articulate why." At the root of the problem is the other revolutionary theory of twentieth-century physics, which Einstein also helped to formulate: quantum mechanics.

> **It's a near certainty that black holes don't exist.**
>
> George Chapline
> Lawrence Livermore National Laboratory

In general relativity, there is no such thing as a 'universal time' that makes clocks tick at the same rate everywhere. Instead, gravity makes clocks run at different rates in different places. But quantum mechanics, which describes physical phenomena at infinitesimally small scales, is meaningful only if time is universal; if not, its equations make no sense.

This problem is particularly pressing at the boundary, or event horizon, of a black hole. To a far-off observer, time seems to stand still here. A spacecraft falling into a black hole would seem, to someone watching it from afar, to be stuck forever at the event horizon, although the astronauts in the spacecraft would feel as if they were continuing to fall. "General relativity predicts that nothing happens at the event horizon," says Chapline.

Quantum transitions

However, as long ago as 1975 quantum physicists argued that strange things do happen at an event horizon: matter governed by quantum laws becomes hypersensitive to slight disturbances. "The result was quickly forgotten," says Chapline, "because it didn't agree with the prediction of general relativity. But actually, it was absolutely correct."

This strange behaviour, he says, is the signature of a 'quantum phase transition' of space-time. Chapline argues that a star doesn't simply collapse to form a black hole; instead, the space-time inside it becomes filled with dark energy and this has some intriguing gravitational effects.

Outside the 'surface' of a

dark-energy star, it behaves much like a black hole, producing a strong gravitational tug. But inside, the 'negative' gravity of dark energy may cause matter to bounce back out again.

HGM2005
Kyoto, Japan
18th – 21st April 2005
Register now for HUGO's 10th annual human genome meeting
Deadline for abstracts
January 21st 2005
HUGO

Click here for information on HGM2005

If the dark-energy star is big enough, Chapline predicts, any electrons bounced out will have been converted to positrons, which then annihilate other electrons in a burst of high-energy radiation. Chapline says that this could explain the radiation observed from the centre of our galaxy, previously interpreted as the signature of a huge black hole.

He also thinks that the Universe could be filled with 'primordial' dark-energy stars. These are formed not by stellar collapse but by fluctuations of space-time itself, like blobs of liquid condensing spontaneously out of a cooling gas. These, he suggests, could be stuff that has the same gravitational effect as normal matter, but cannot be seen: the elusive substance known as dark matter.

▲ Top

References

1. Chapline G. *Arxiv*, http://xxx.arxiv.org/abs/astro-ph/0503200 (2005).

▲ Top

Outline of my talk

- The iron K_α -line as a tool for BH characteristics
- Movies

Outline of my talk

- Mirages around BHs and retro-lensing
- Bright star trajectories around BH at GC as a tool
- Conclusions

VII. On the Means of discovering the Distance, Magnitude, &c. of the Fixed Stars, in consequence of the Diminution of the Velocity of their Light, in case such a Diminution should be found to take place in any of them, and such other Data should be procured from Observations, as would be farther necessary for that Purpose. By the Rev. John Michell, B. D. F. R. S. In a Letter to Henry Cavendish, Esq. F. R. S. and A. S.

Read November 27, 1783.

16. Hence, according to article 10, if the semi-diameter of a sphære of the same density with the sun were to exceed that of the sun in the proportion of 500 to 1, a body falling from an infinite height towards it, would have acquired at its surface a greater velocity than that of light, and consequently, supposing light to be attracted by the same force in proportion to its vis inertiæ, with other bodies, all light emitted from such a body would be made to return towards it, by its own proper gravity.

Black holes in galaxy centers

Black Hole Mass Scales with Galaxy Size

Ground — HST — Black Hole Mass

NGC 4649 — 2 billion suns

NGC 4291 — 200 million suns

NGC 2778 — 20 million suns

NGC 7457 — 3 million suns

Black hole event horizons

75000 light-years — 3000 light-years — Diameter of Earth's Orbit (186 million miles)

NASA and K. Gebhardt (Lick Observatory) • STScI-PRC00-22
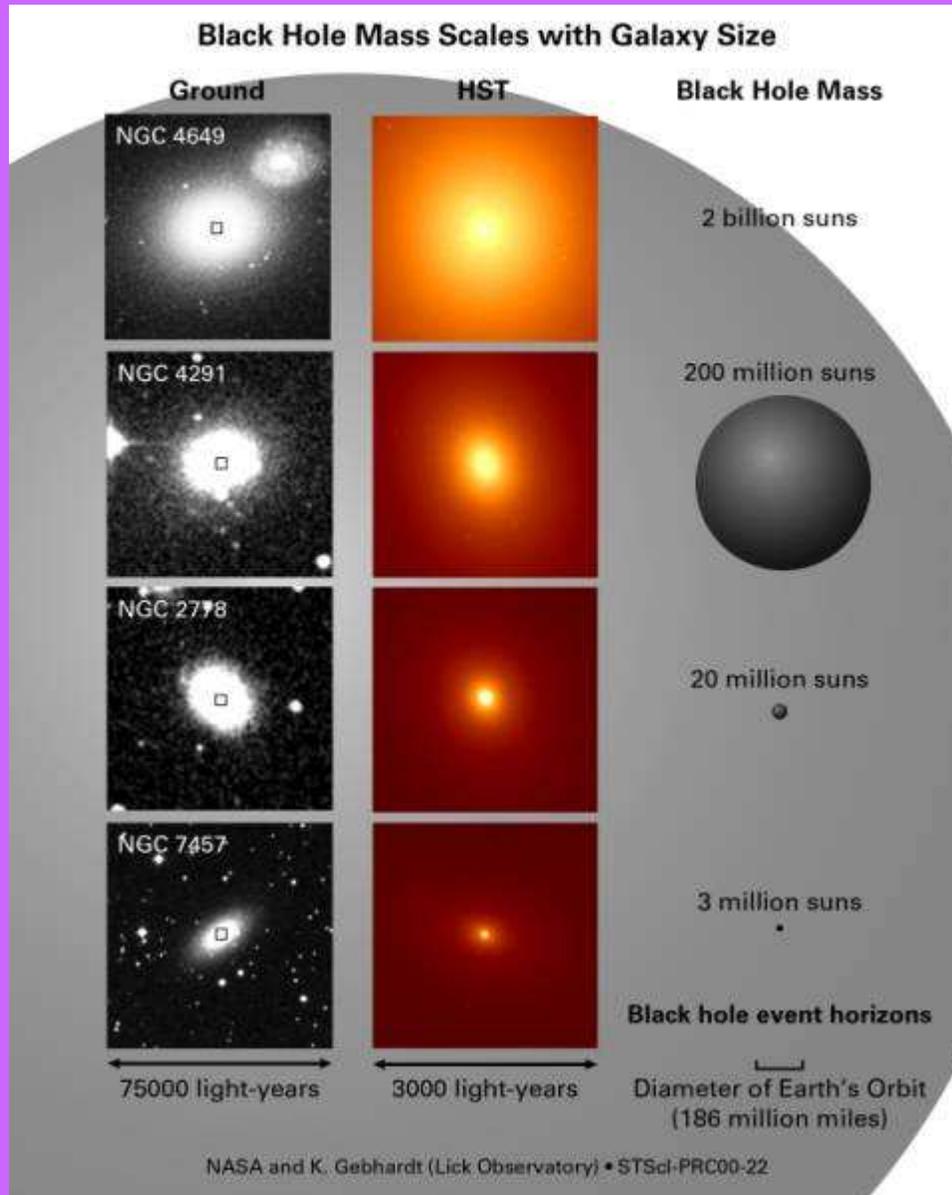
Many galaxies are assumed to have the black holes in their centers.

The black hole masses vary from million to dozens of billion Solar mass.

Because of the small size we cannot observe the black hole itself, but can register the emission of the accretion disk, rotating around the black hole.

Seyfert galaxies and Kα line

Seyfert Galaxy NGC 4151
PRC97-18 • ST ScI OPO • June 9, 1997
B. Woodgate (GSFC), J. Hutchings (DAO) and NASA
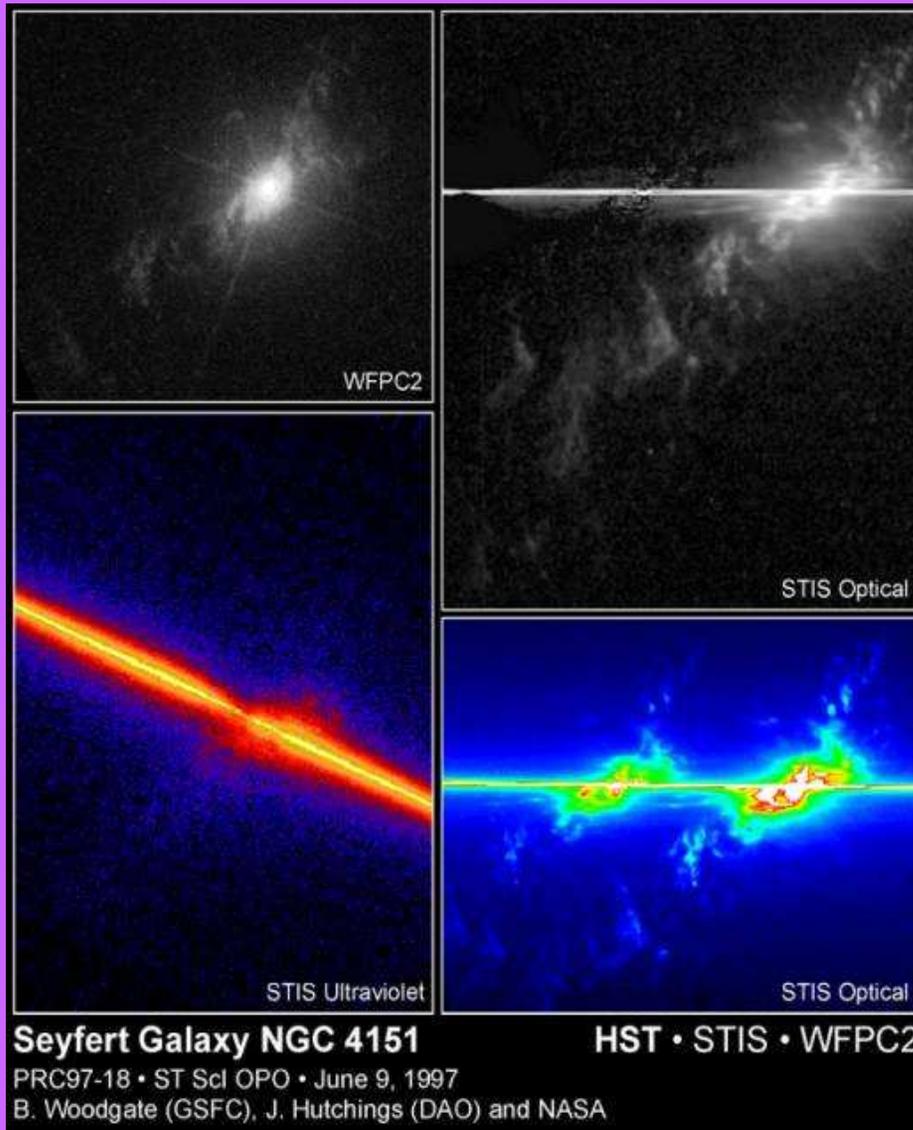
Seyfert galaxies give us a wonderful possibility of direct observations of black holes in their centers.

They often have a wide iron Kα line in their spectra, which seems to arise in the innermost part of the accretion disk close to the event horizon.

Hubble image of Seyfert galaxy NGC 4151 shown at the left.

Fe K α line origin
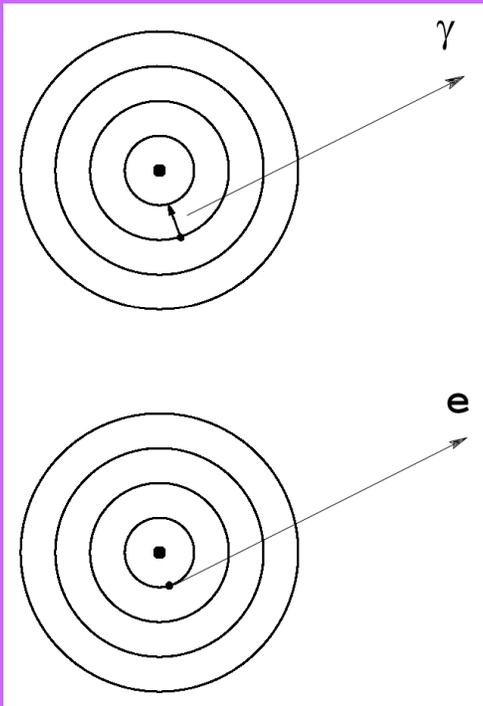
Kα   (6.4 keV)   analogous to Lα in hydrogen,
                          electron transition to the lowest level

                          excitation by electronic shock

hν > 7.1 keV   neutral iron
                          photoionization and recombination

            Fe XXV, XXVI – 6.9 keV   hydrogen-like Fe

Emission lines in Seyfert galaxies

O VIII	0.653 keV		Fe L	0.7– 0.8 keV
Ne IX	0.915 keV		Ne X	1.02 keV
Fe L	1.03 – 1.25 keV		Mg XI	1.34 keV
Mg XII	1.47 keV		Si XIII	1.85 keV
Si XIV	2.0 keV		S XIV	2.35 keV
S XV	2.45 keV		S XVI	2.62 keV
Ar XVII	3.10 keV		Ar XVIII	3.30 keV

Fe I – Fe XVI	6.4 keV
Fe XVII – Fe XXIII	6.5 keV
Fe XXV	6.68 keV
Fe XXVI	6.96 keV

K α

We find a 6.4 keV emission line in 72% of the sample (18 of 25 sources) at the 99% confidence level.

The 5 – 7 keV regime is dominated by emission from neutral iron (< Fe XVI).

Observations

Tanaka, Nandra, Fabian. Nature, 1995, **375**, 659.
Galaxy MCG-6-30-15, ASCA satellite, SIS detectors

Sy 1 type
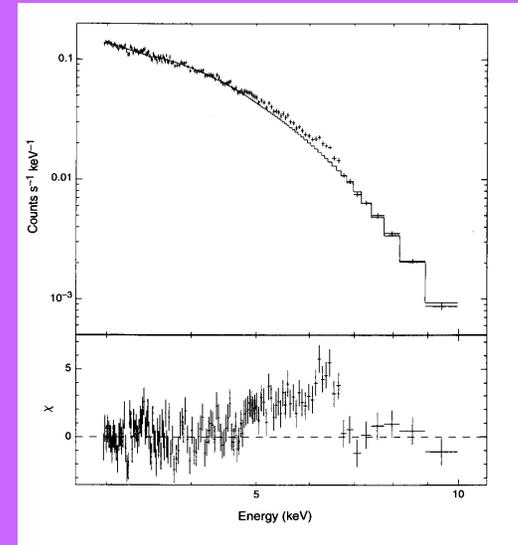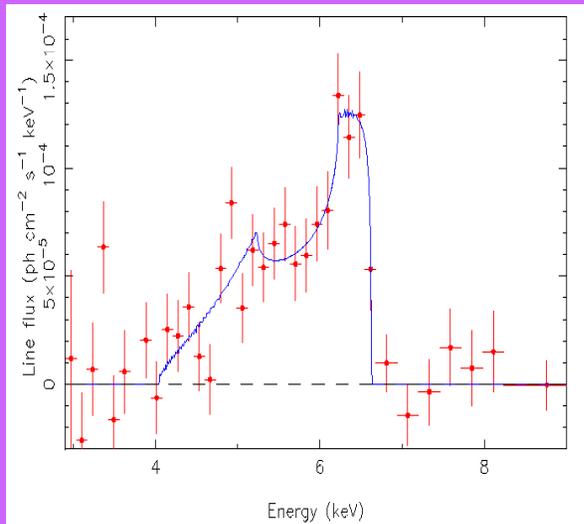
The line profile of iron Kα line in

X-ray emission from MCG-6-30-15.

Width corresponds to 80000 – 100000 km/s.

- **Variability**

Sulentic, Marziani, Calvani. ApJL, 1998, **497**, L65.

Properties of wide lines at 6.4 keV

- Line width corresponds to velocity
  - v ~ 80000 – 100000 km/s   MCG-6-30-15
  - v ~ 48000 km/s   MCG-5-23-16
  - v ~ 20000 – 30000 km/s   many other galaxies

- Asymmetric structure (profile)
  - two-peak shape
  - narrow bright **blue** wing
  - wide faint **red** wing

- Variability of both
  - line shape
  - intensity

Possible interpretation

- iron Kα emission line

  o 6.4 – 6.9 – 7.1 keV

- radiation of inner part of accretion disk around a supermassive
black hole in the center of the galaxy

  r emission ~ 1 – 4 r$_g$ $r_g = \dfrac{2km}{c^2}$
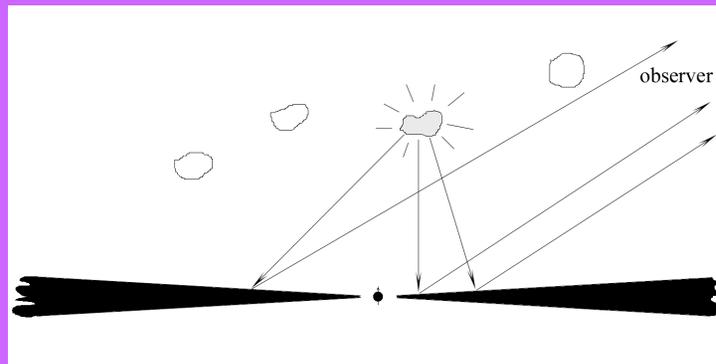
Equations of motion

Kerr metric

$$ds^2 = -\frac{\Delta}{\rho^2}\left(dt - a\sin^2\theta d\phi\right)^2 + \frac{\rho^2}{\Delta}dr^2 + \rho^2 d\theta^2 +$$

$$+\frac{\sin^2\theta}{\rho^2}\left[\left(r^2 + a^2\right)d\phi - adt\right]^2$$

or

$$ds^2 = -\left(1 - \frac{2Mr}{\rho^2}\right)dt^2 + \frac{\rho^2}{\Delta}dr^2 + \rho^2 d\theta^2 +$$

$$+\left(r^2 + a^2 + \frac{2Mra^2}{\rho^2}\sin^2\theta\right)\sin^2\theta\,d\phi^2 - \frac{4Mra}{\rho^2}\sin^2\theta\,d\phi dt,$$

Equations of motion

Equations of photon motion:

$$\frac{dt}{d\lambda} = -\frac{r_g r a}{\rho^2 \Delta} L + \frac{\omega_0}{\Delta}\left(r^2 + a^2 + \frac{r_r r a^2}{\rho^2}\sin^2\theta\right)$$

$$\frac{d\phi}{d\lambda} = \frac{L}{\Delta \sin^2\theta}\left(1 - \frac{r_g r}{\rho^2}\right) + \frac{r_g r a}{\rho^2 \Delta}\,\omega_0$$

$$\left(\frac{dr}{d\lambda}\right)^2 = \frac{1}{\rho^4}\left[\left(r^2 + a^2\right)\omega_0 - aL\right] - \frac{K\Delta}{\rho^4}$$

$$\left(\frac{d\theta}{d\lambda}\right)^2 = \frac{K}{\rho^4} - \frac{1}{\rho^4}\left[a\,\omega_0\sin\theta - \frac{L}{\sin\theta}\right]^2$$

where

$$\Delta = r^2 - r_g r + a^2, \qquad \rho^2 = r^2 + a^2\cos^2\theta,$$

$$r_g = 2km, \qquad a = M/m$$

Equations of motion

For numerical solution the system should be replaced with

$$\frac{dt'}{d\sigma} = -\hat{a}\left(\hat{a}\sin^2\theta - \xi\right) + \frac{\hat{r}^2 + \hat{a}^2}{\hat{\Delta}}\left(\hat{r}^2 + \hat{a}^2 - \xi\hat{a}\right),$$

$$\frac{d\hat{r}}{d\sigma} = r_1,$$

$$\frac{dr_1}{d\sigma} = 2\hat{r}^3 + \left(\hat{a}^2 - \xi^2 - \eta\right)\hat{r} + (\hat{a} - \xi) + \eta,$$

$$\frac{d\theta}{d\sigma} = \theta_1,$$

$$\frac{d\theta_1}{d\sigma} = \cos\theta\left(\frac{\xi^2}{\sin^3\theta} - \hat{a}^2\sin\theta\right),$$

$$\frac{d\phi}{d\sigma} = -\left(\hat{a} - \frac{\xi}{\sin^2\theta}\right) + \frac{\hat{a}}{\hat{\Delta}}\left(\hat{r}^2 + \hat{a}^2 - \xi\hat{a}\right).$$

The system has two integrals:

$$\epsilon_1 \equiv r_1^2 - \hat{r}^4 - \left(\hat{a}^2 - \xi^2 - \eta\right)\hat{r}^2 - 2\left[(\hat{a} - \xi)^2 + \eta\right]\hat{r} + \hat{a}^2\eta = 0,$$

$$\epsilon_2 \equiv \theta_1^2 - \eta - \cos^2\theta\left(\hat{a}^2 - \frac{\xi^2}{\sin^2\theta}\right) = 0,$$

Simulation result
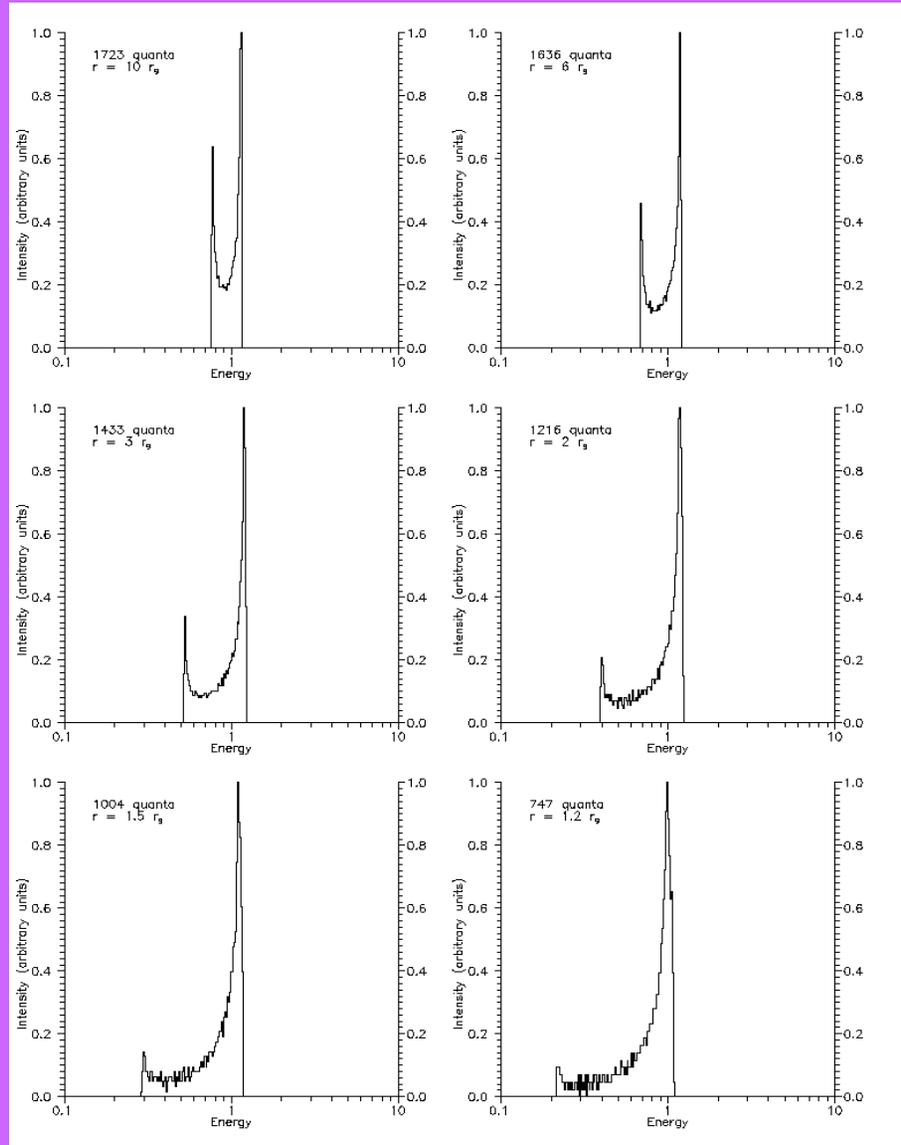
Spectrum of a hot spot for a=0.9, θ=60 deg. and different values of radial coordinate.

Marginally stable orbit lays at r = 1.16 r$_g$.

Gallery of profiles
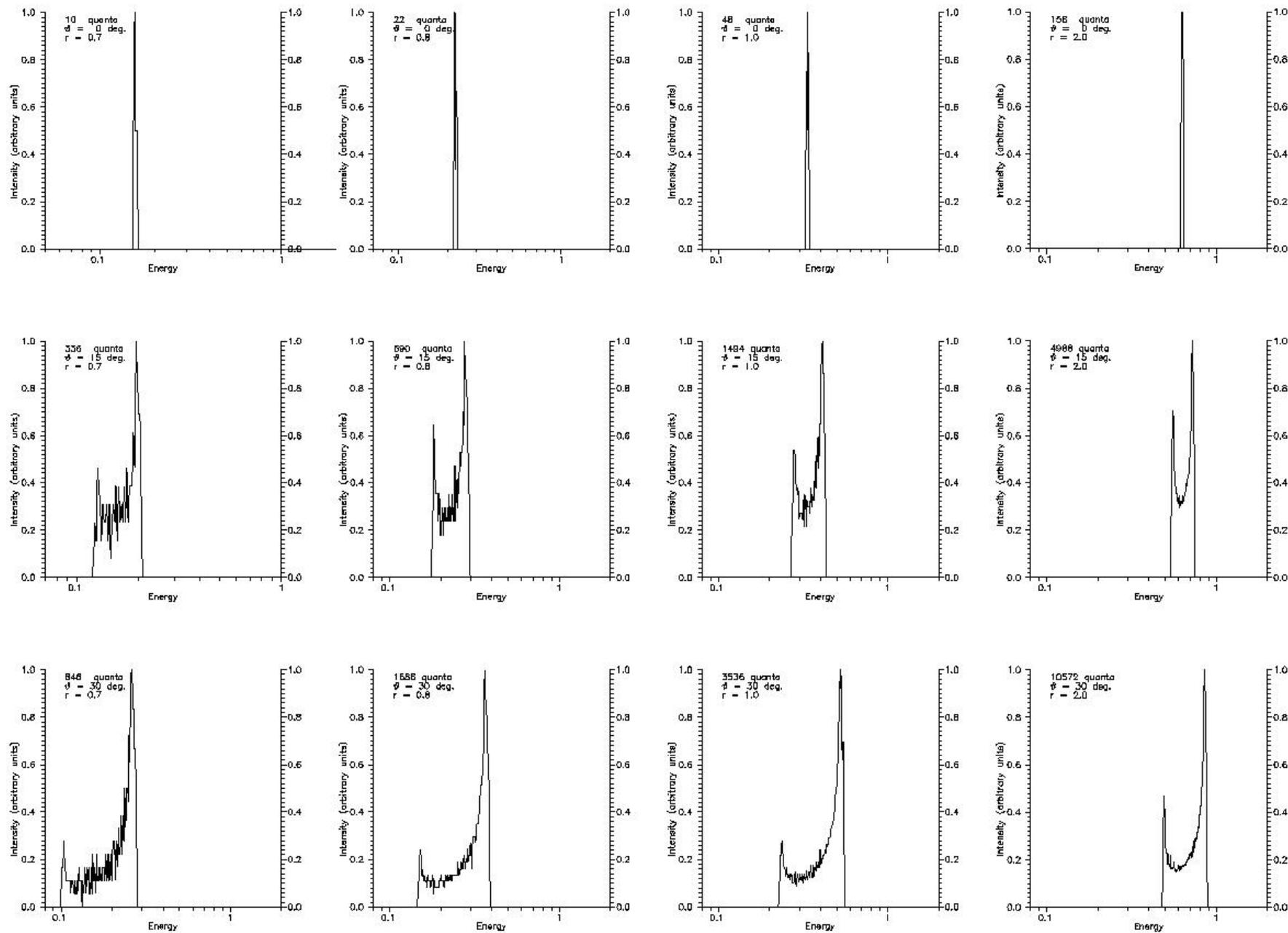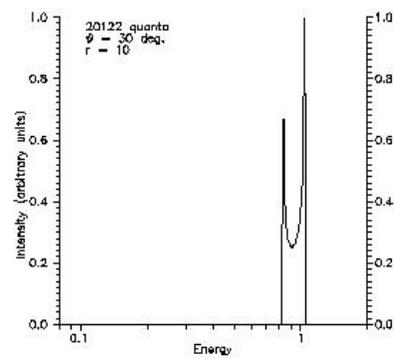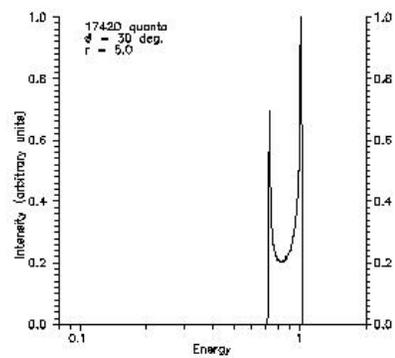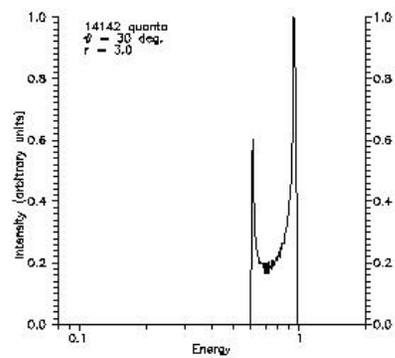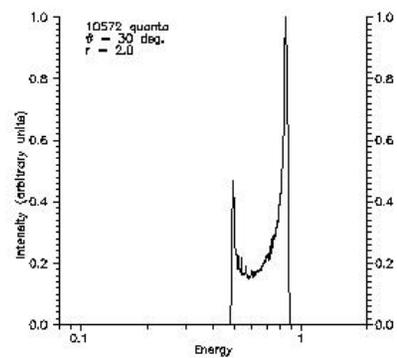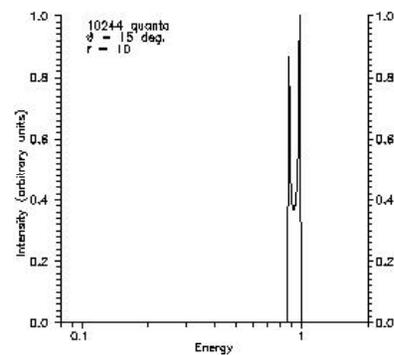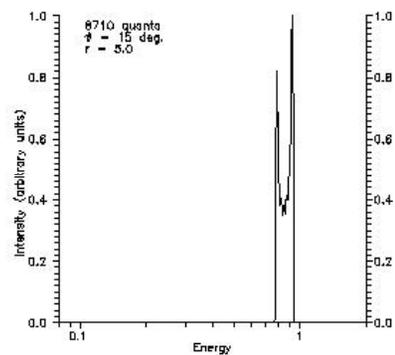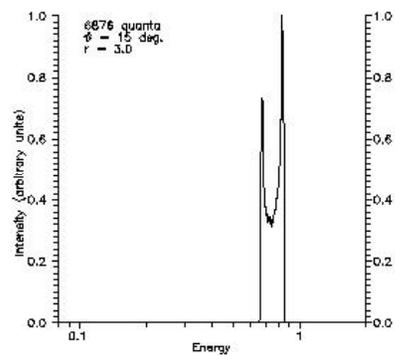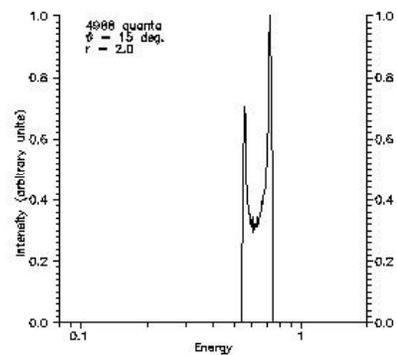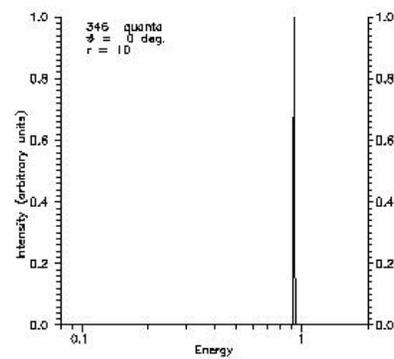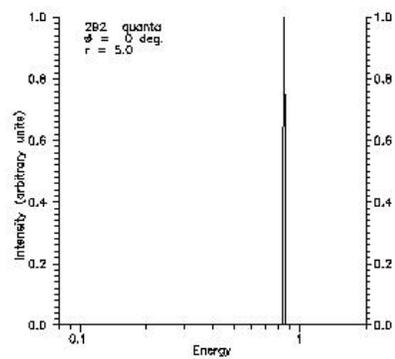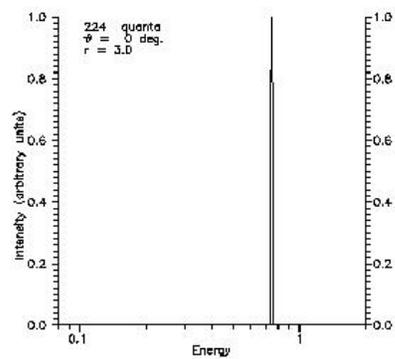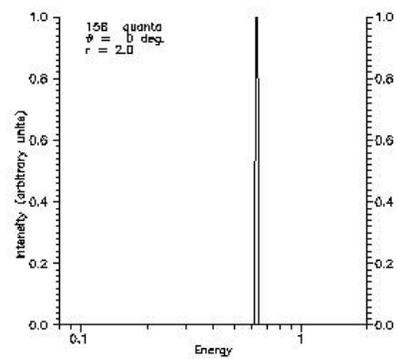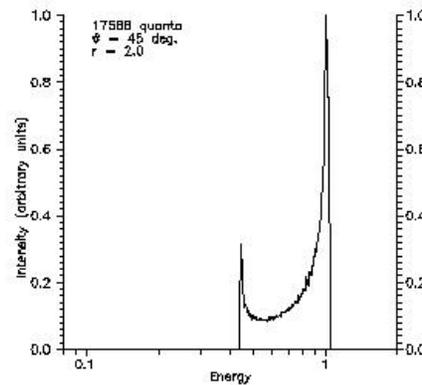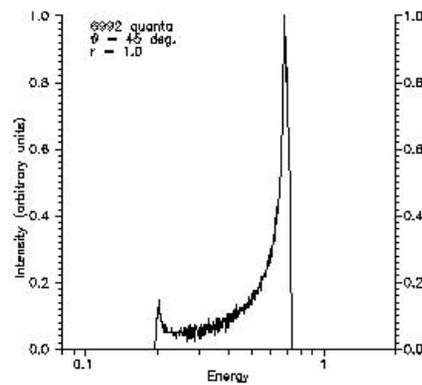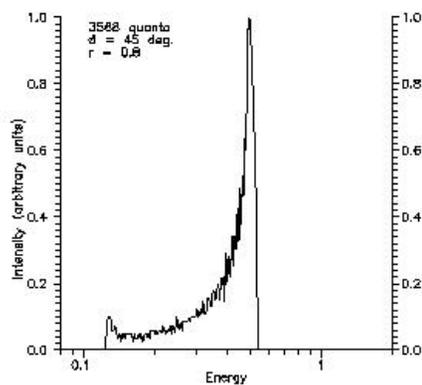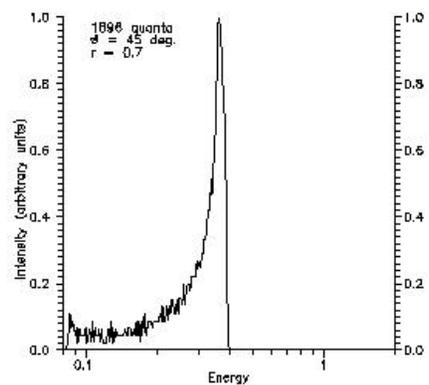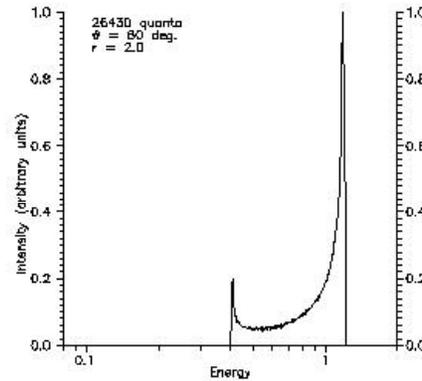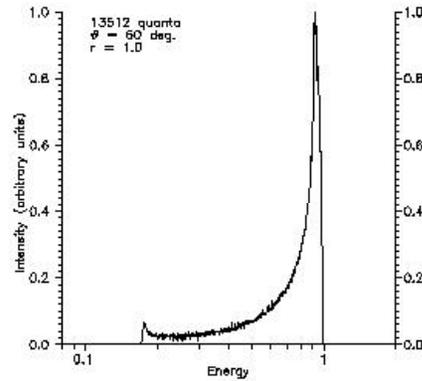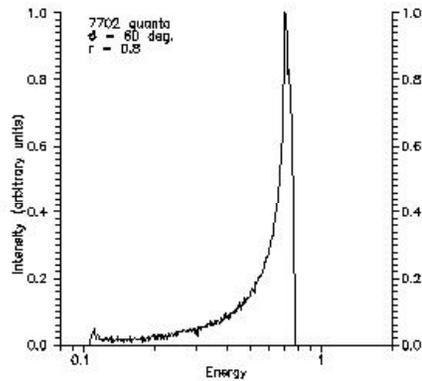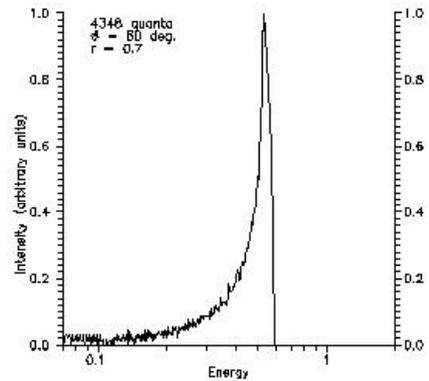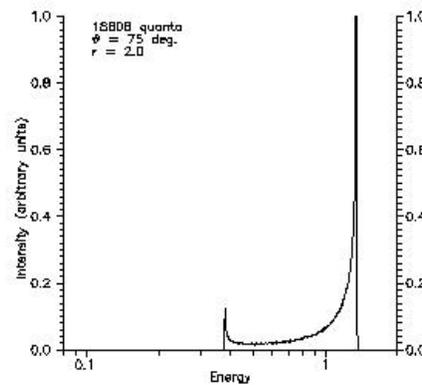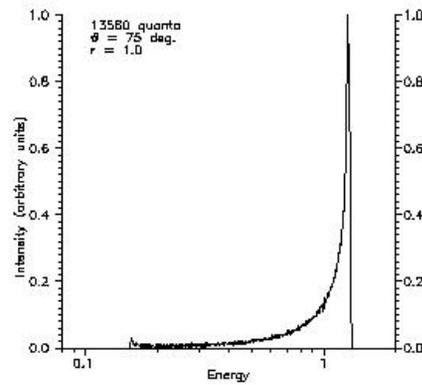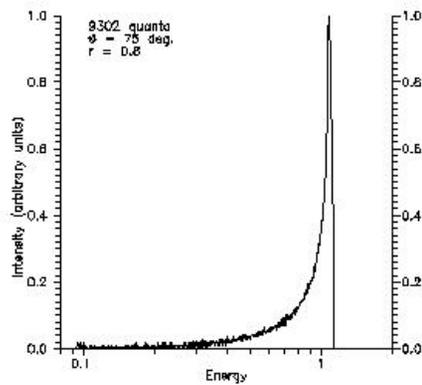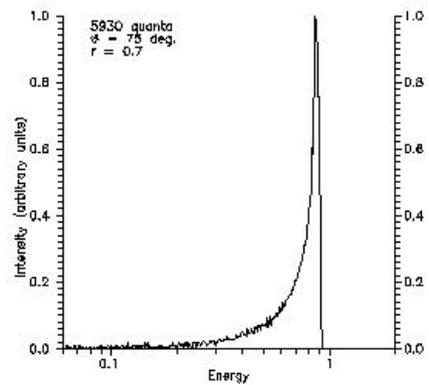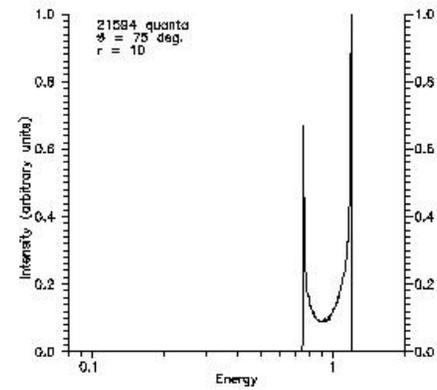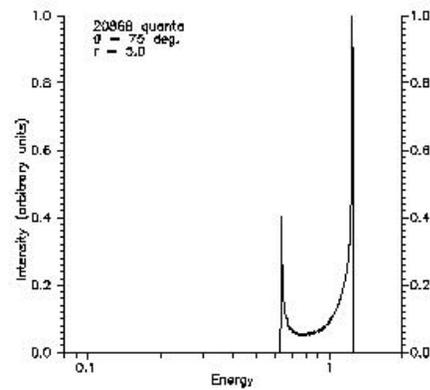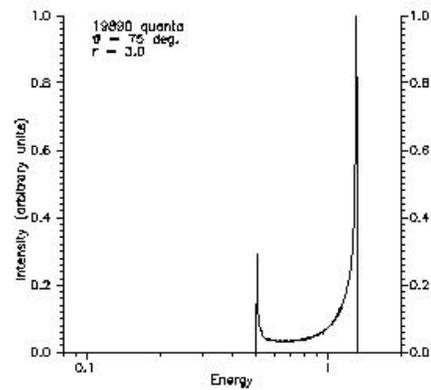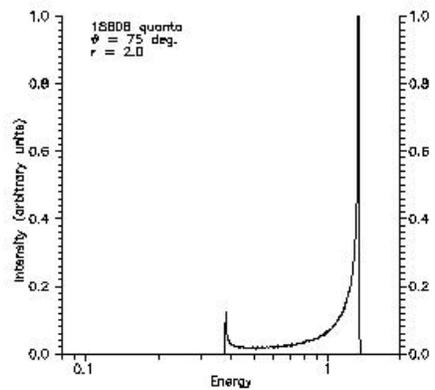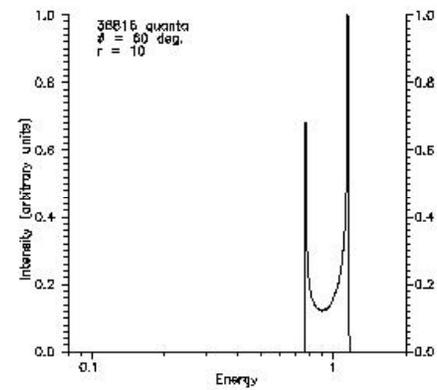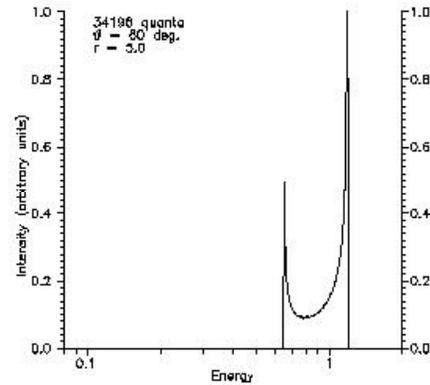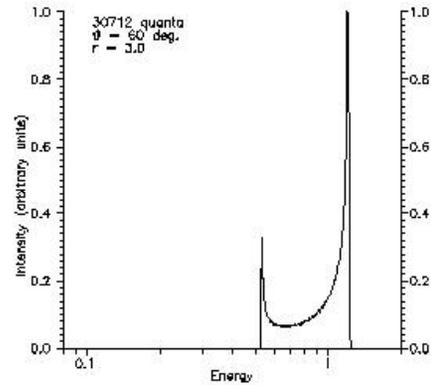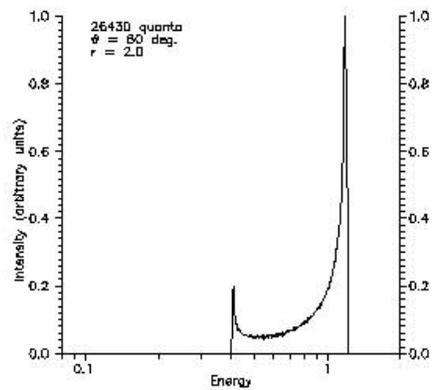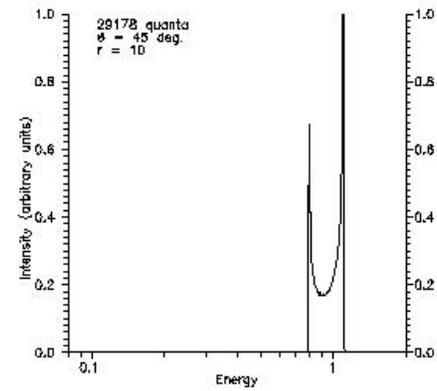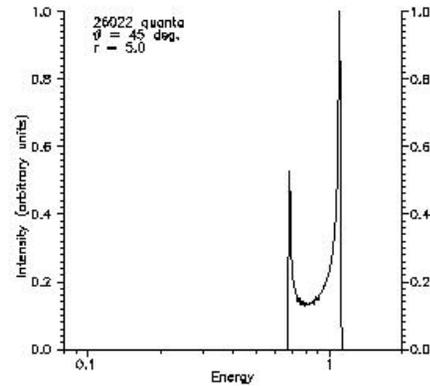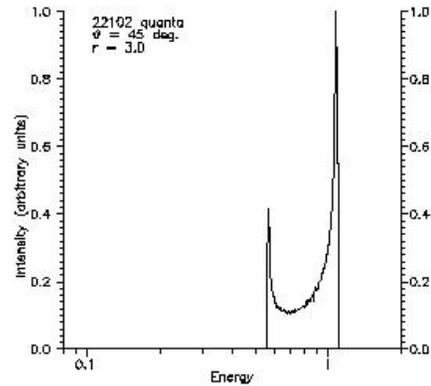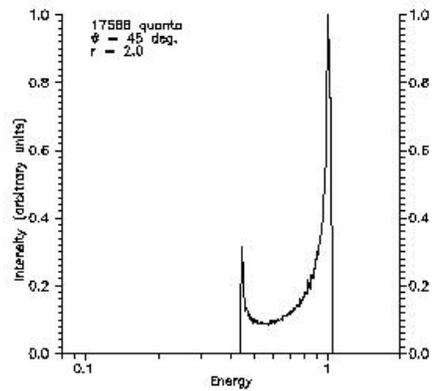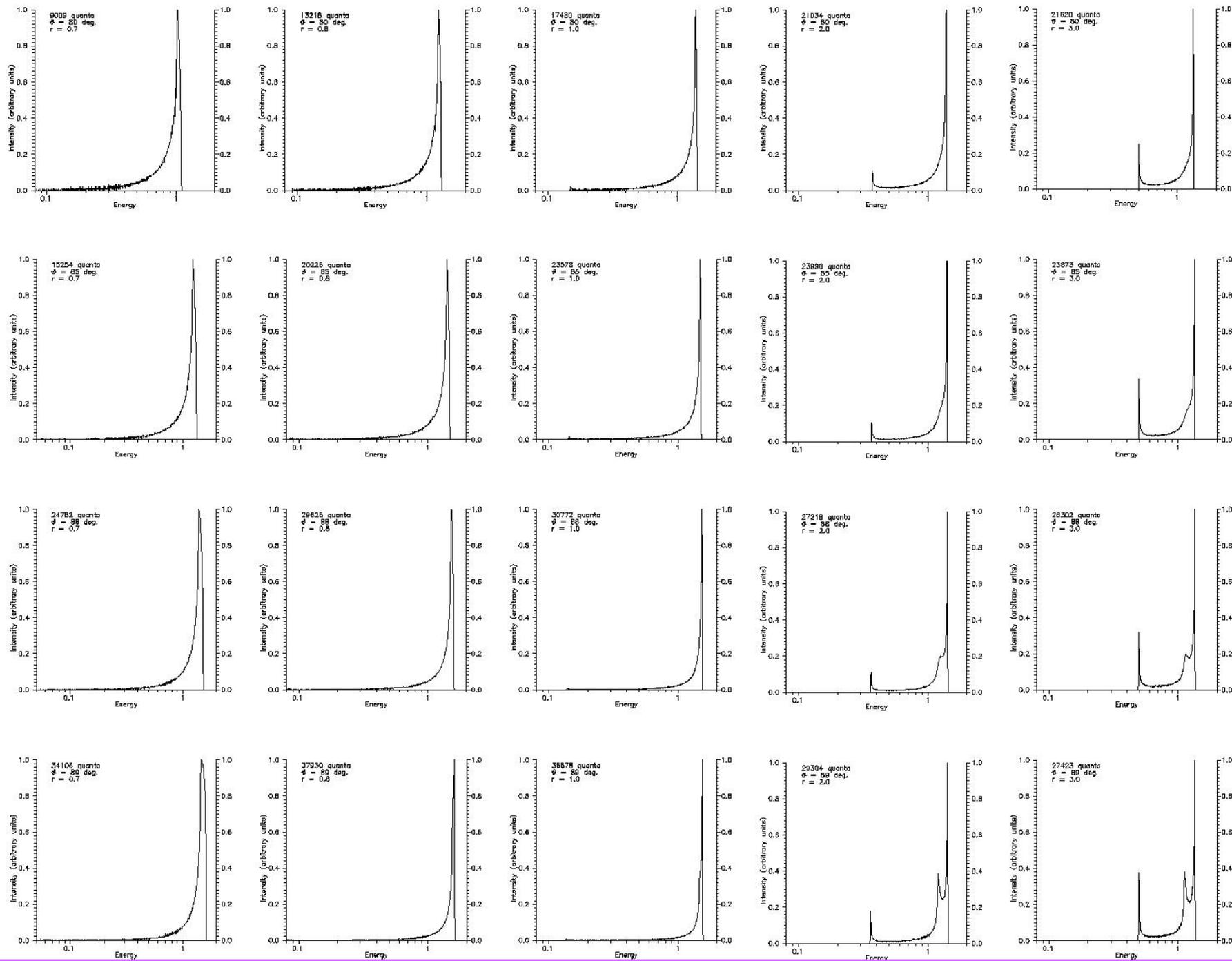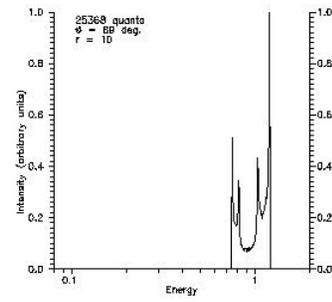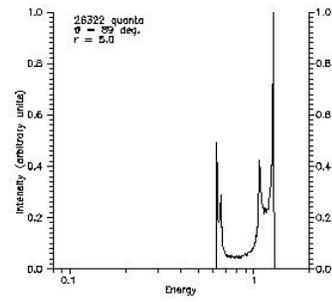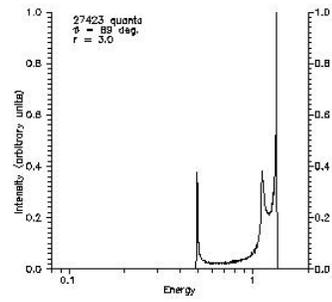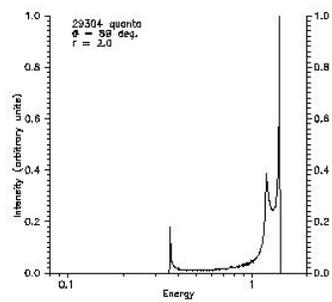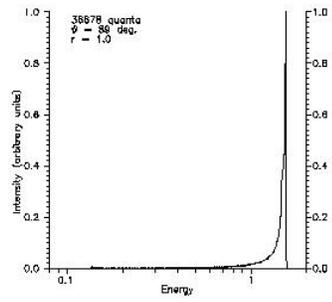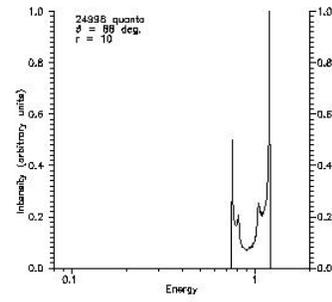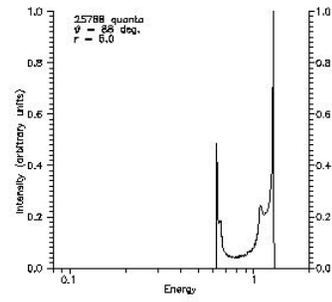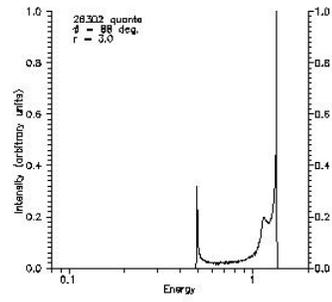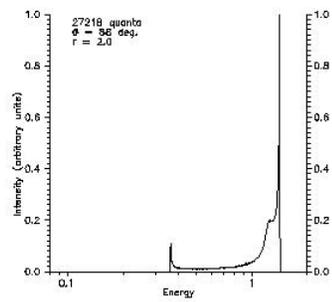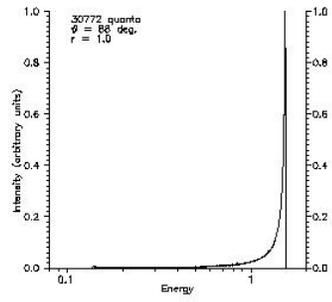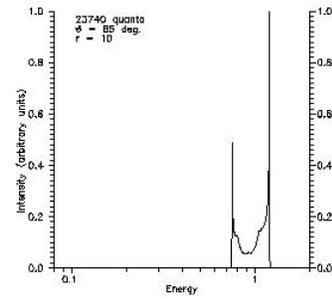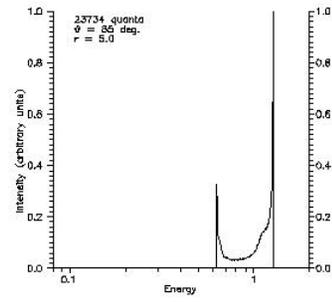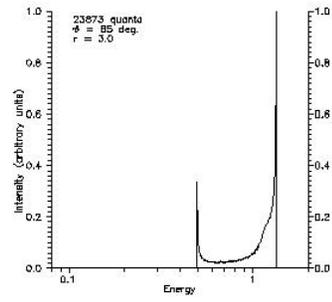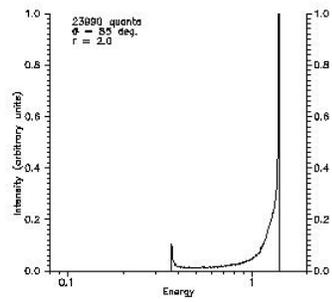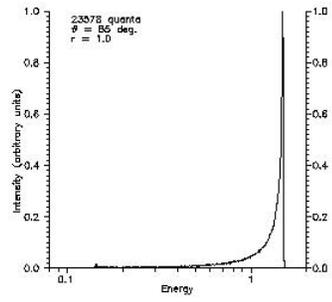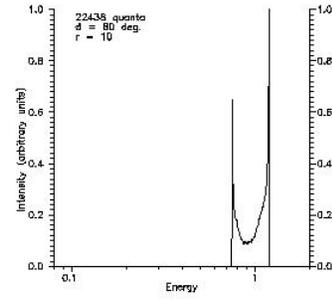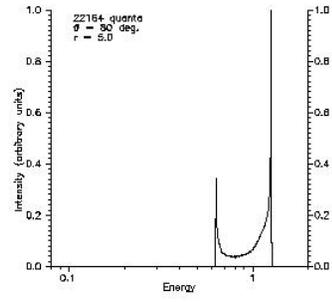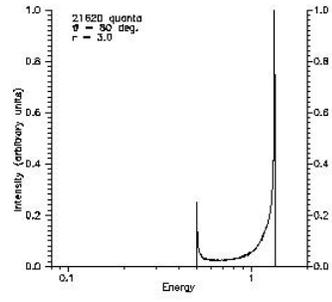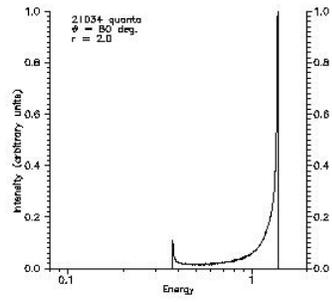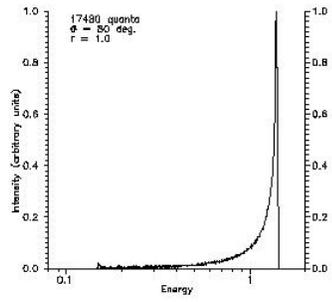
Simulation result
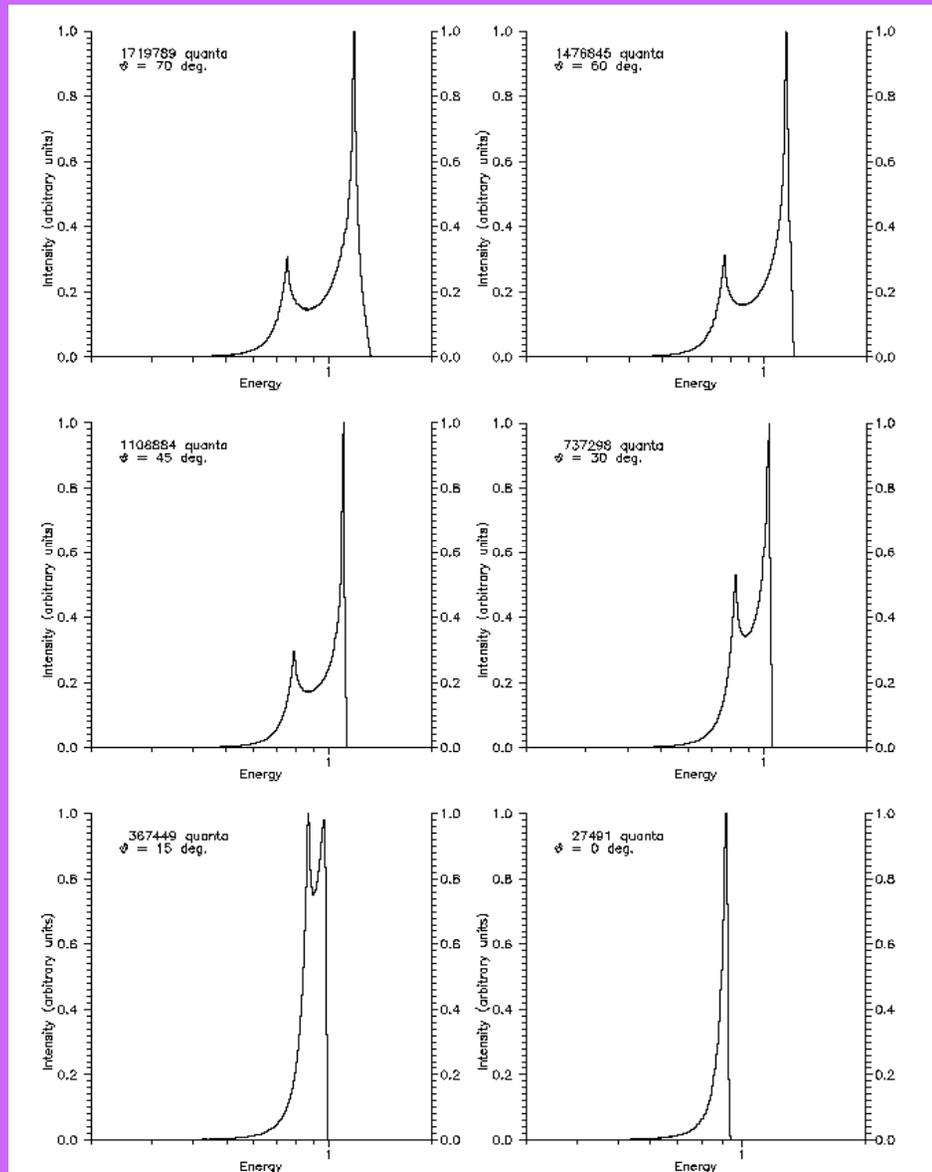
Spectrum of Fe Kα line in isothermal disk with a = 0.9 and emission region between 10 r_g and marginally stable orbit at 1.16 r_g.

The figure presents the dependence on **θ** angle.

Simulation result

Spectrum of Fe Kα line in isothermal disk with a = 0.9 and emission region between 10 r_g and marginally stable orbit at 1.16 r_g.

The figure presents the dependence on θ angle (large θ values).

Simulation result
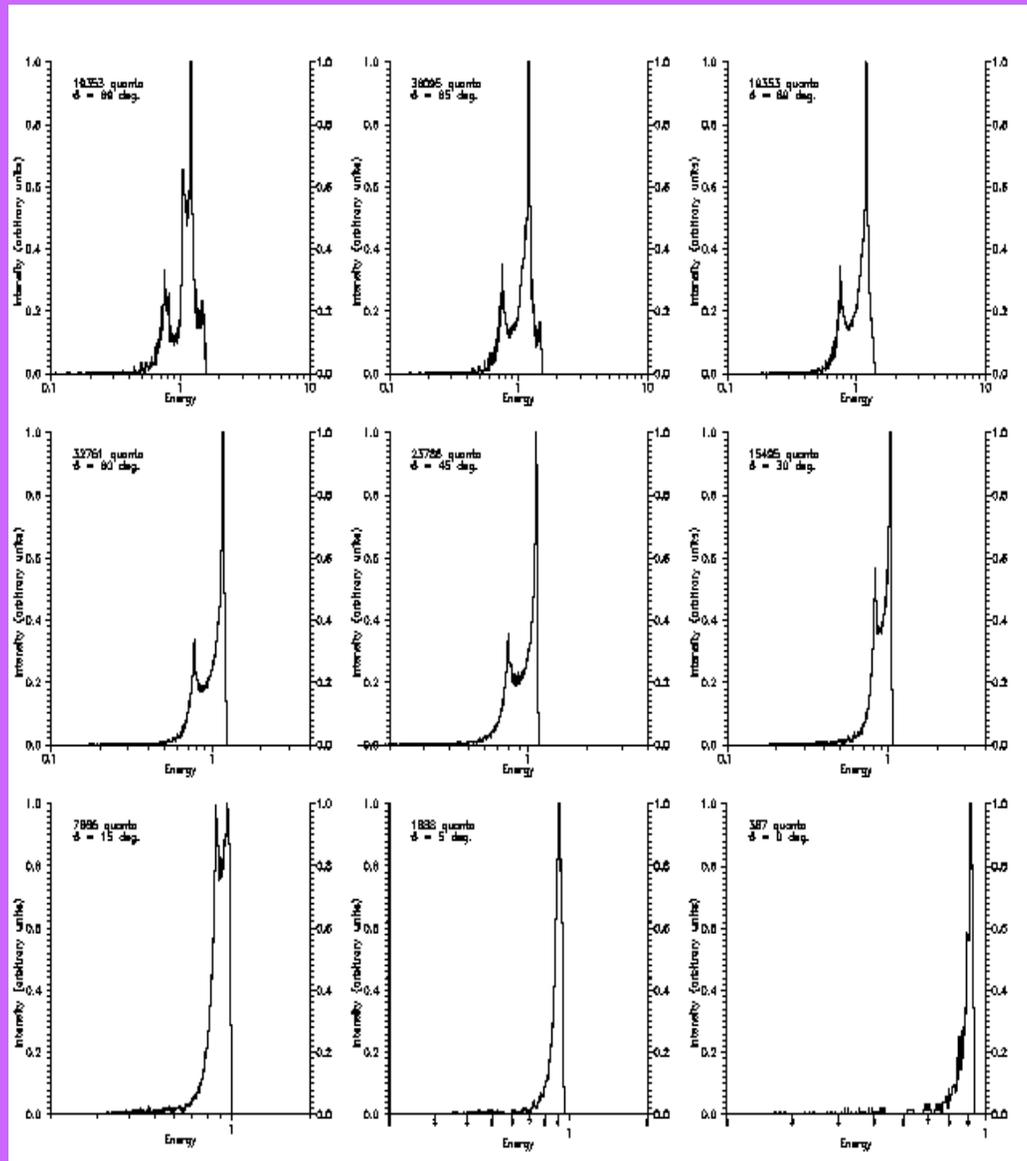
Spectrum of Fe Kα line in isothermal disk with a = 0.99 and emission region between 10 r_g and marginally stable orbit at 0.727 r_g.

At large θ one can see the lensing effect.

Simulation result
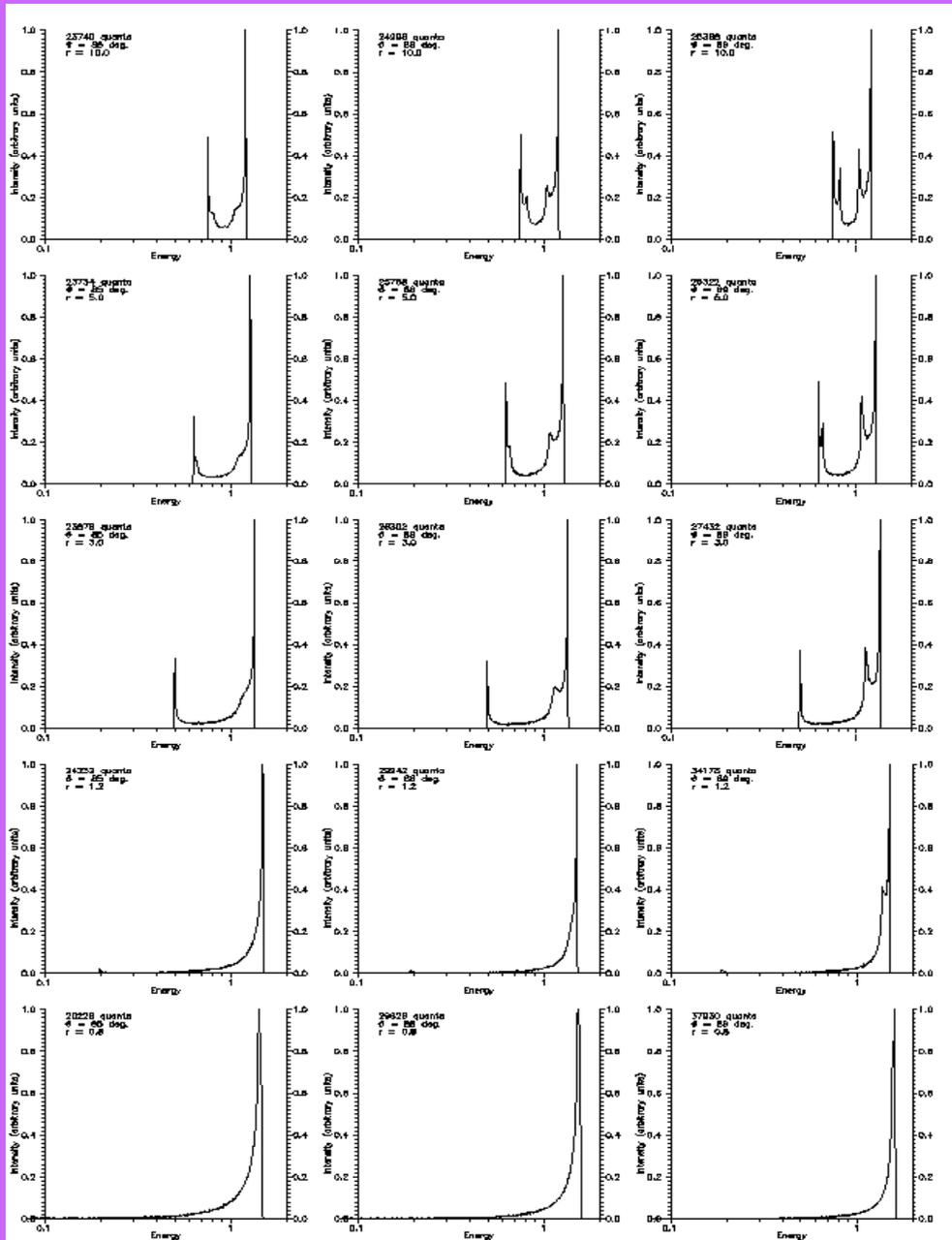
Overview of possible line profiles of a hot spot for different values of radial coordinate and inclination angle.

The radial coordinate decreases from 10 r_g on the top to 0.8 r_g on the bottom. The inclination angle increases from 85 degrees in the left column to 89 degrees in the right.

Zakharov A.F, Repin S.V. A&A, 2003, 406, 7.

Simulation result
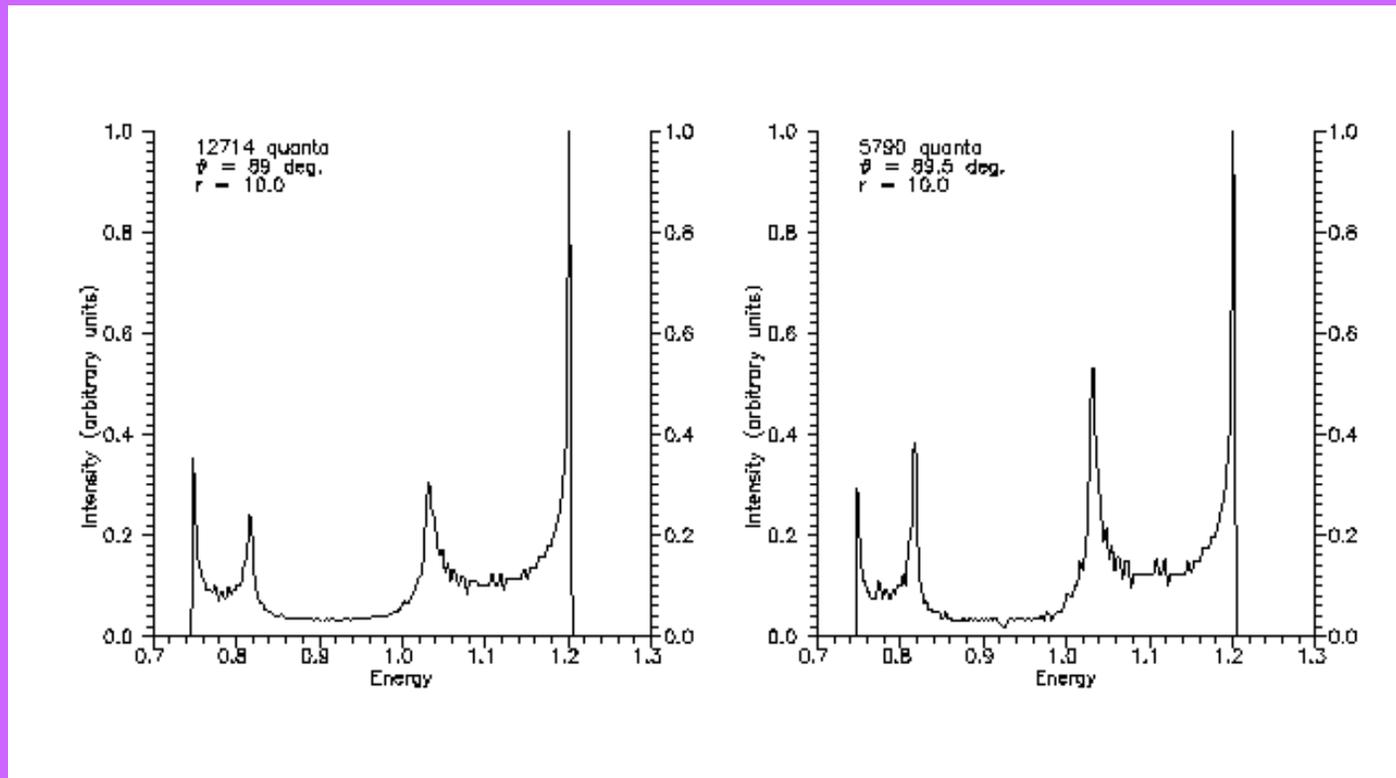
Spectrum of a hot spot rotating at the distance 10 r_g and observed at large inclination angles. Left panel includes all the quanta with $\theta > 89$ degrees. The right one includes the quanta with $\theta > 89.5$ degrees.

Simulation result
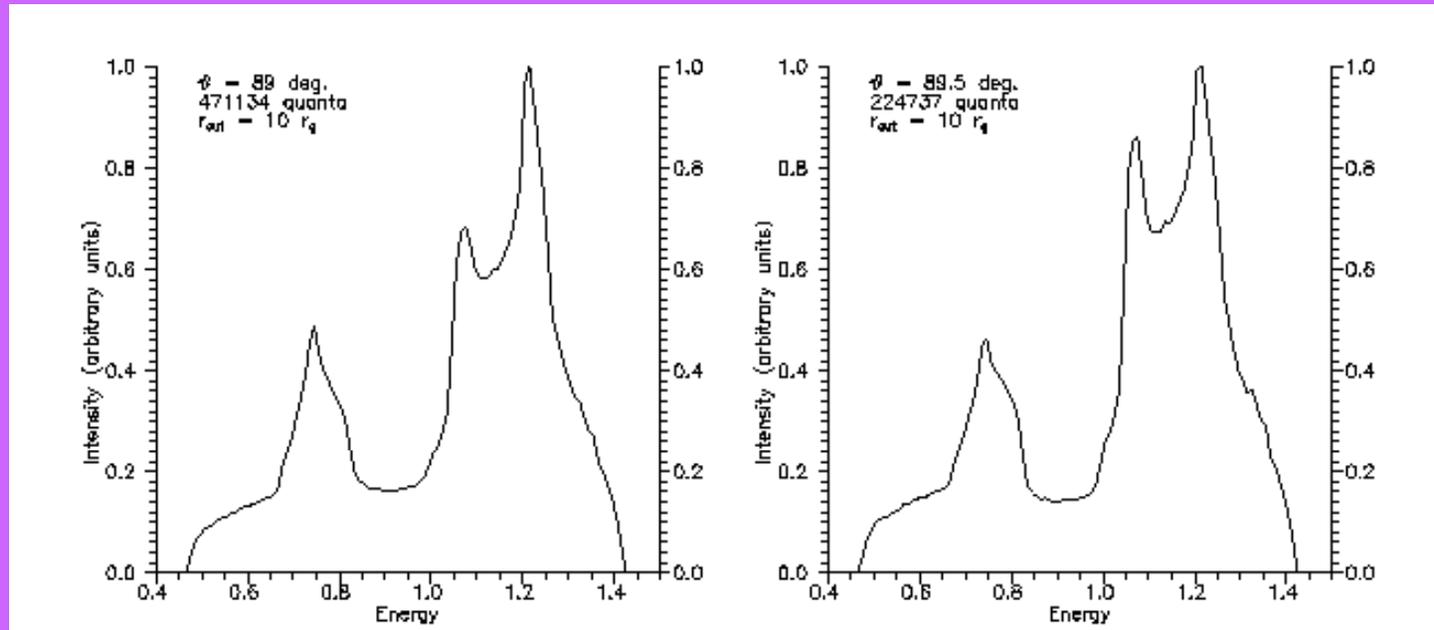
Spectrum of an entire α-disk observed at large inclination angles. Emitting region lies between 3 r_g and 10 r_g. Left panel includes all the quanta with $\theta > 89$ degrees. The right one includes the quanta with $\theta > 89.5$ degrees.

Magnetic field estimations near BH horizon in AGNs and GBHCs
(Zakharov, Kardashev, Lukash, Repin, MNRAS, 342,1325, (2003))

- Zeeman splitting $E_1=E_0-\mu_B H$, $E_2=E_0+ \mu_B H$, $\mu_B=e\hbar/(2m_e c)$, $\mu_B=9.3*10^{-21}$ erg/G
- Figure1
- Figure2
- Figure3
- Figure4
- Figure5
- Figure6
- ASCAdata
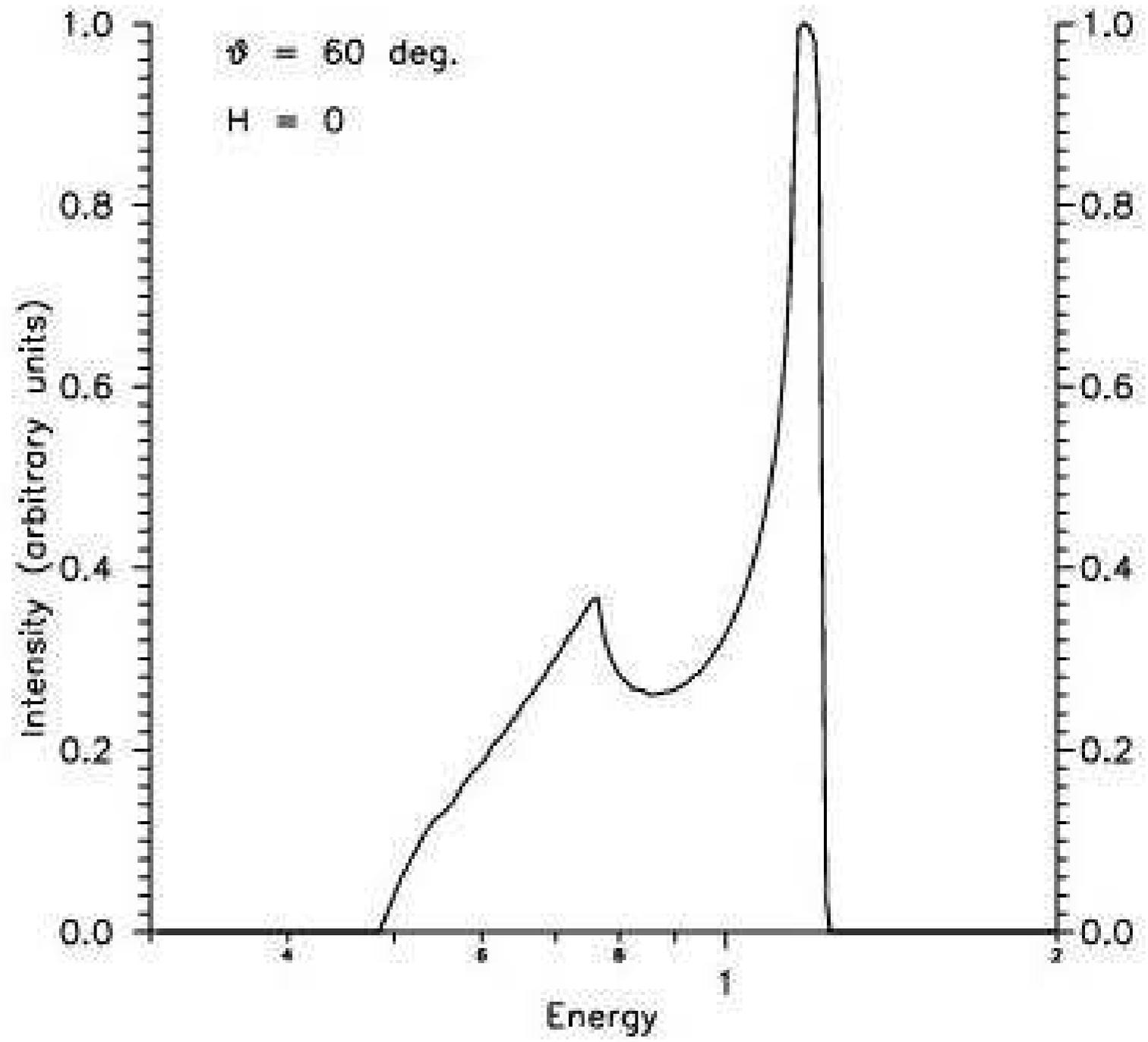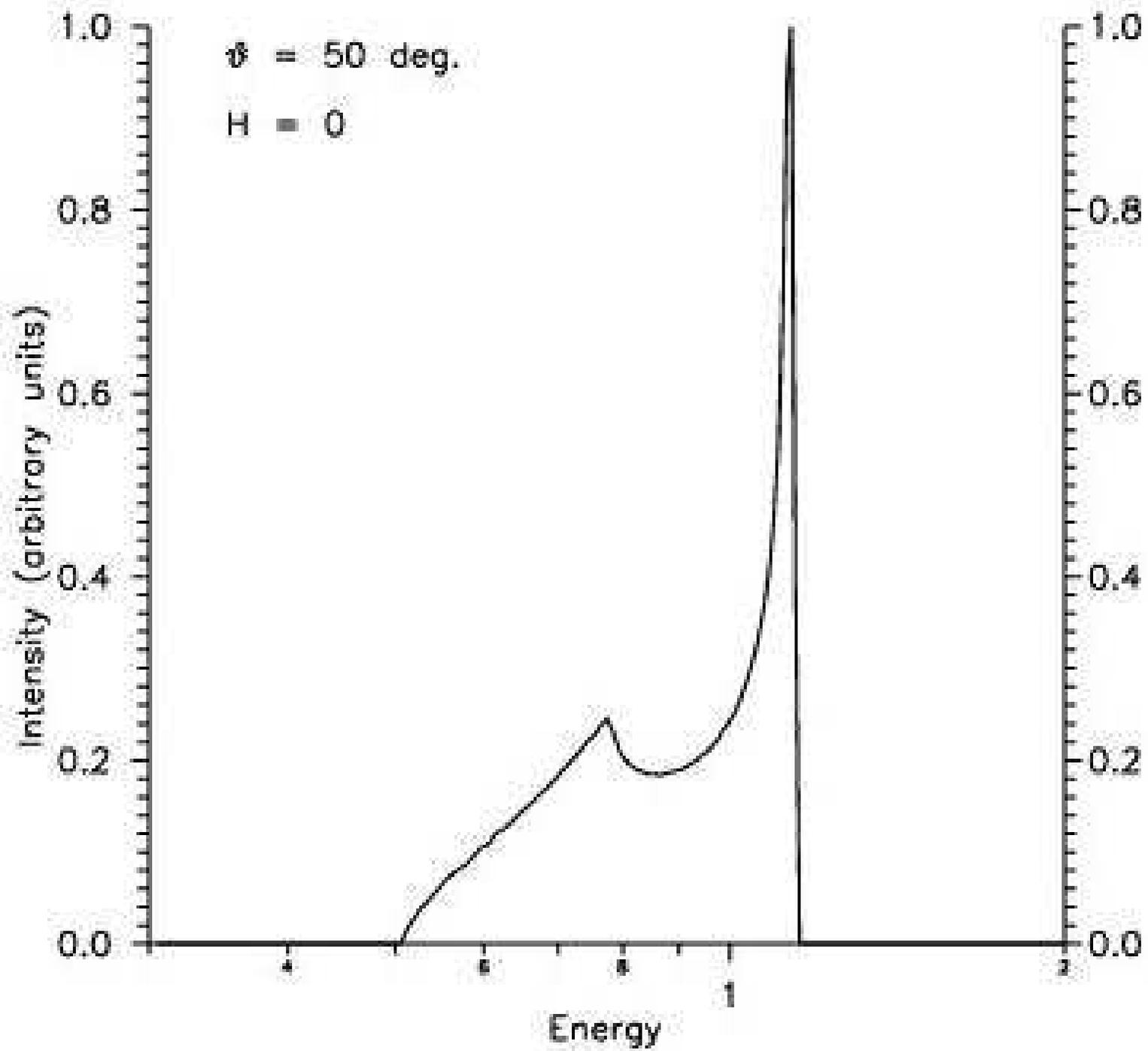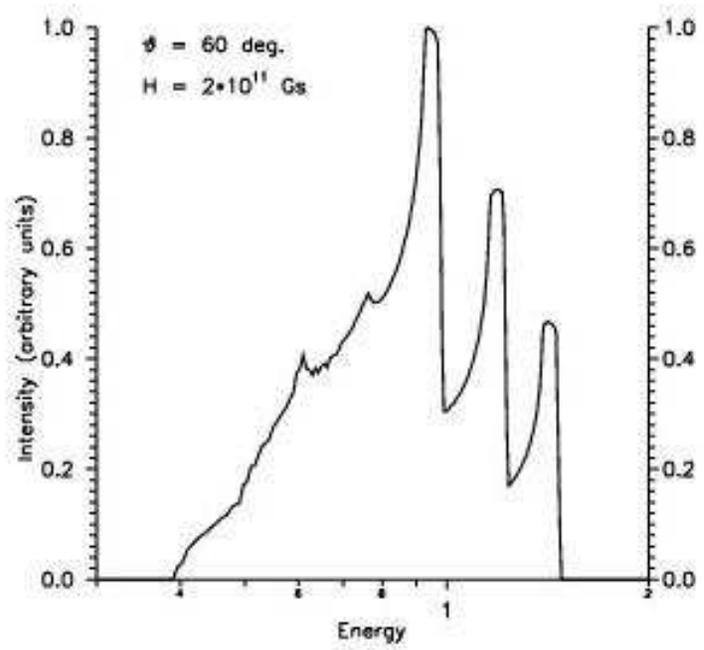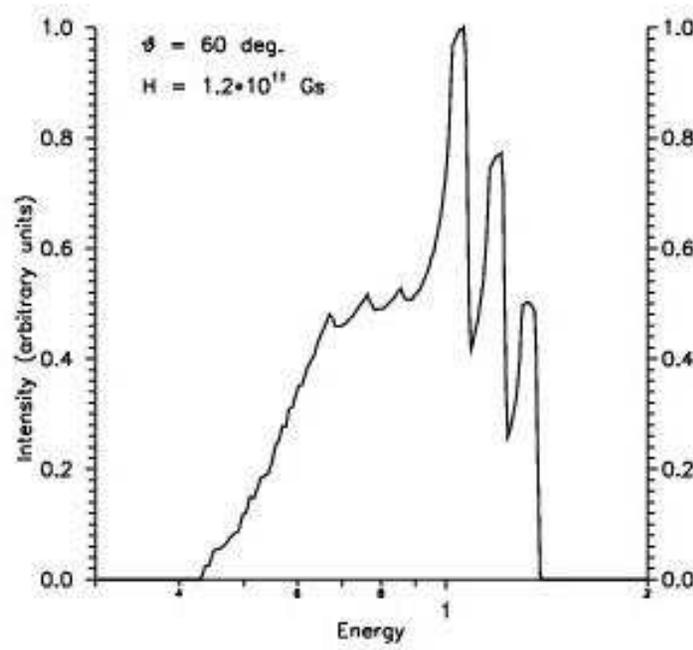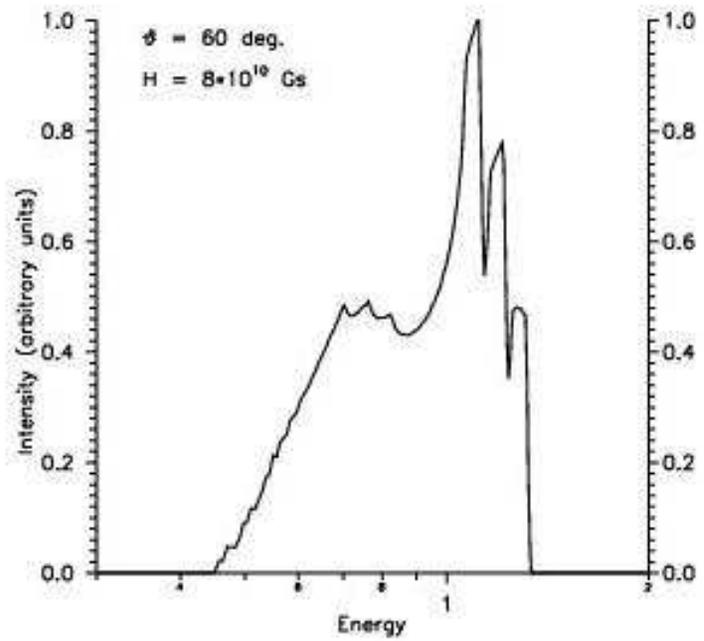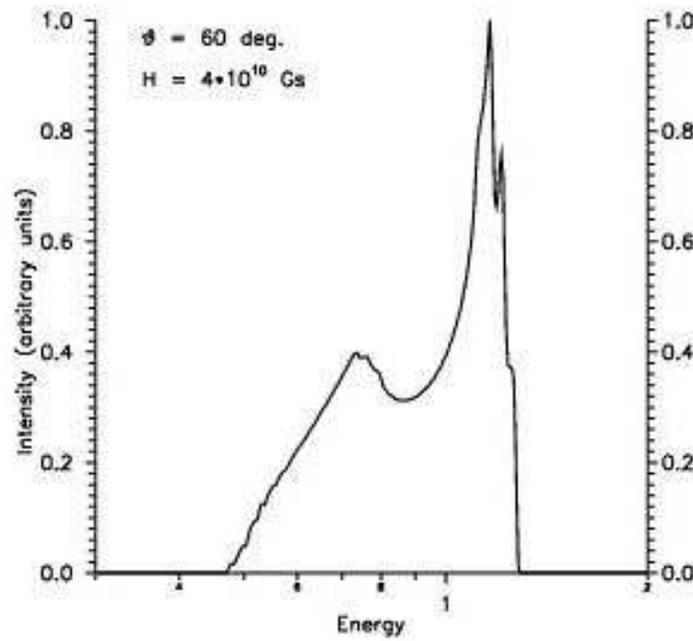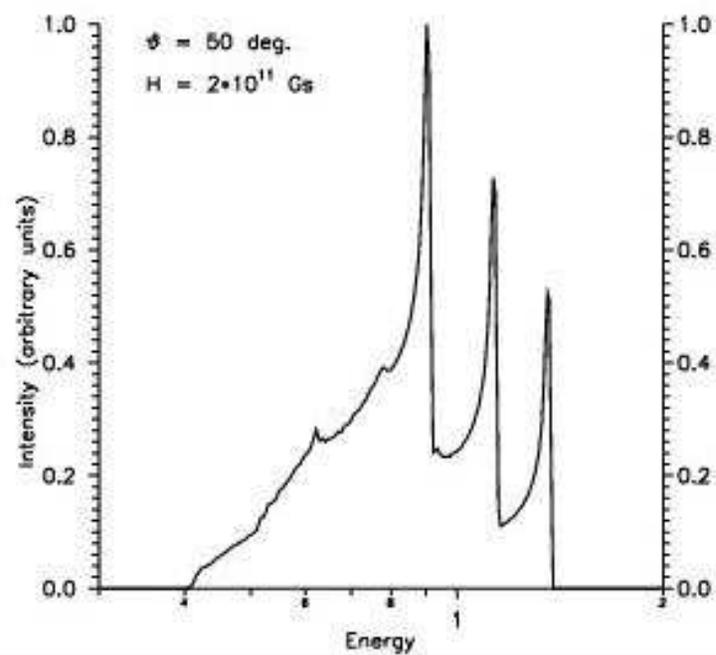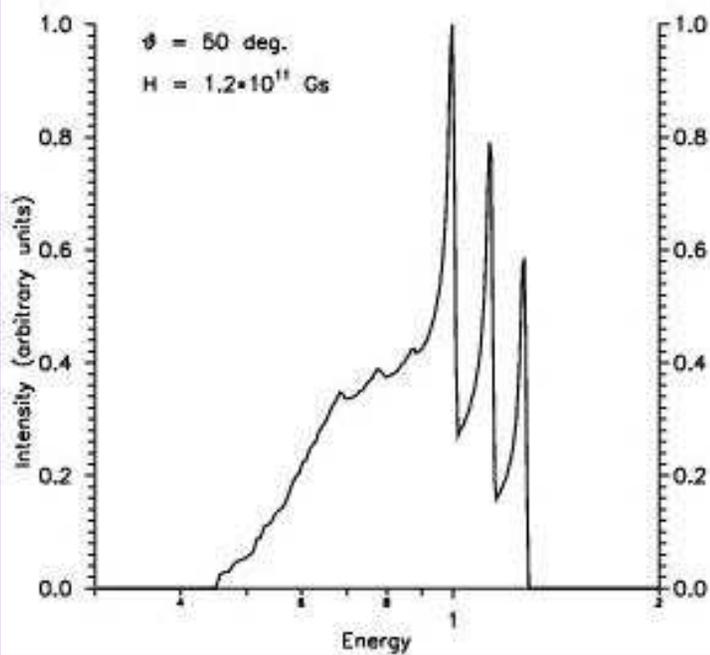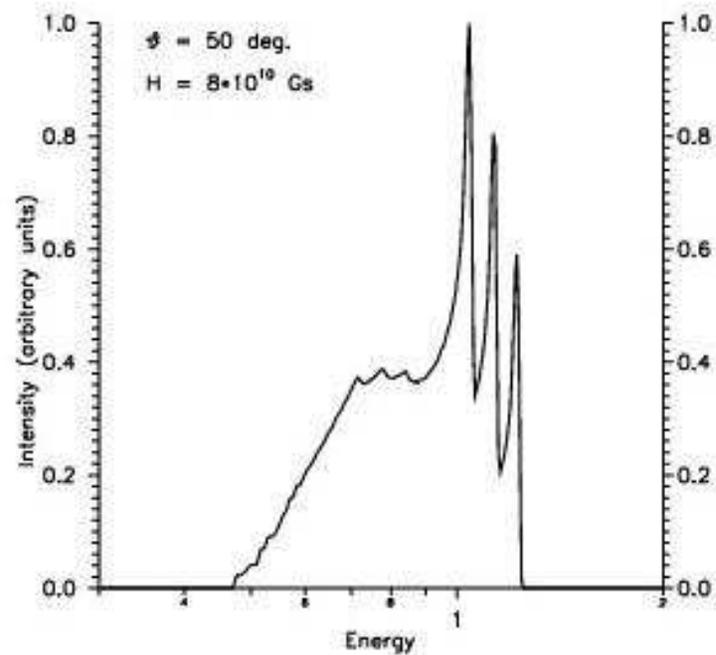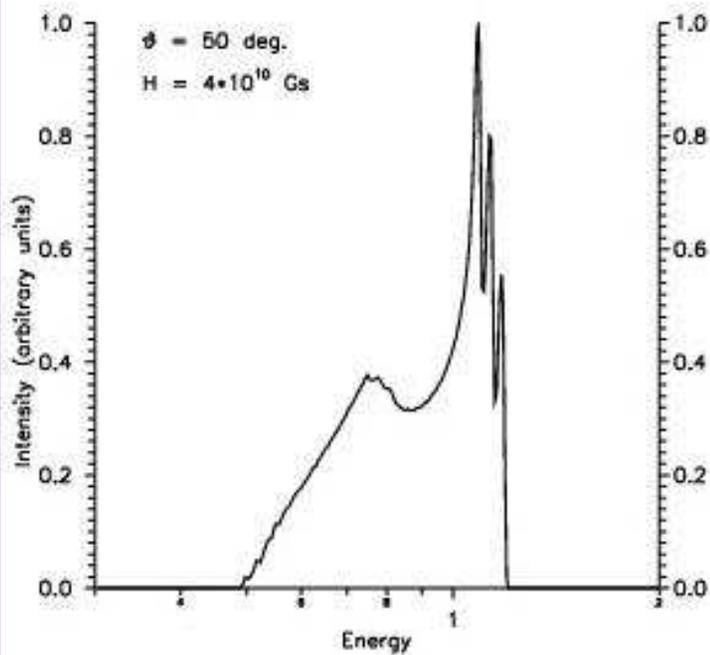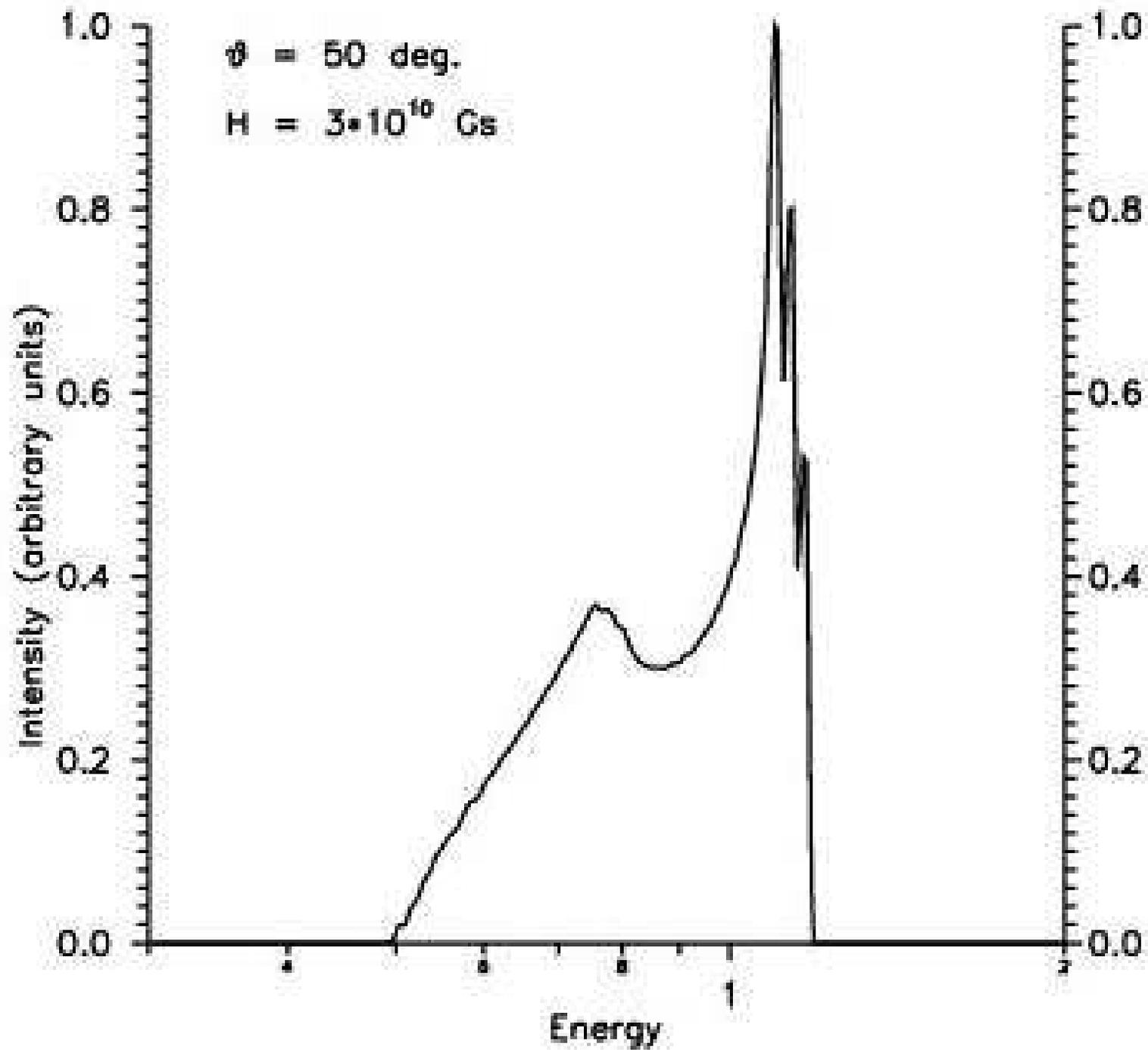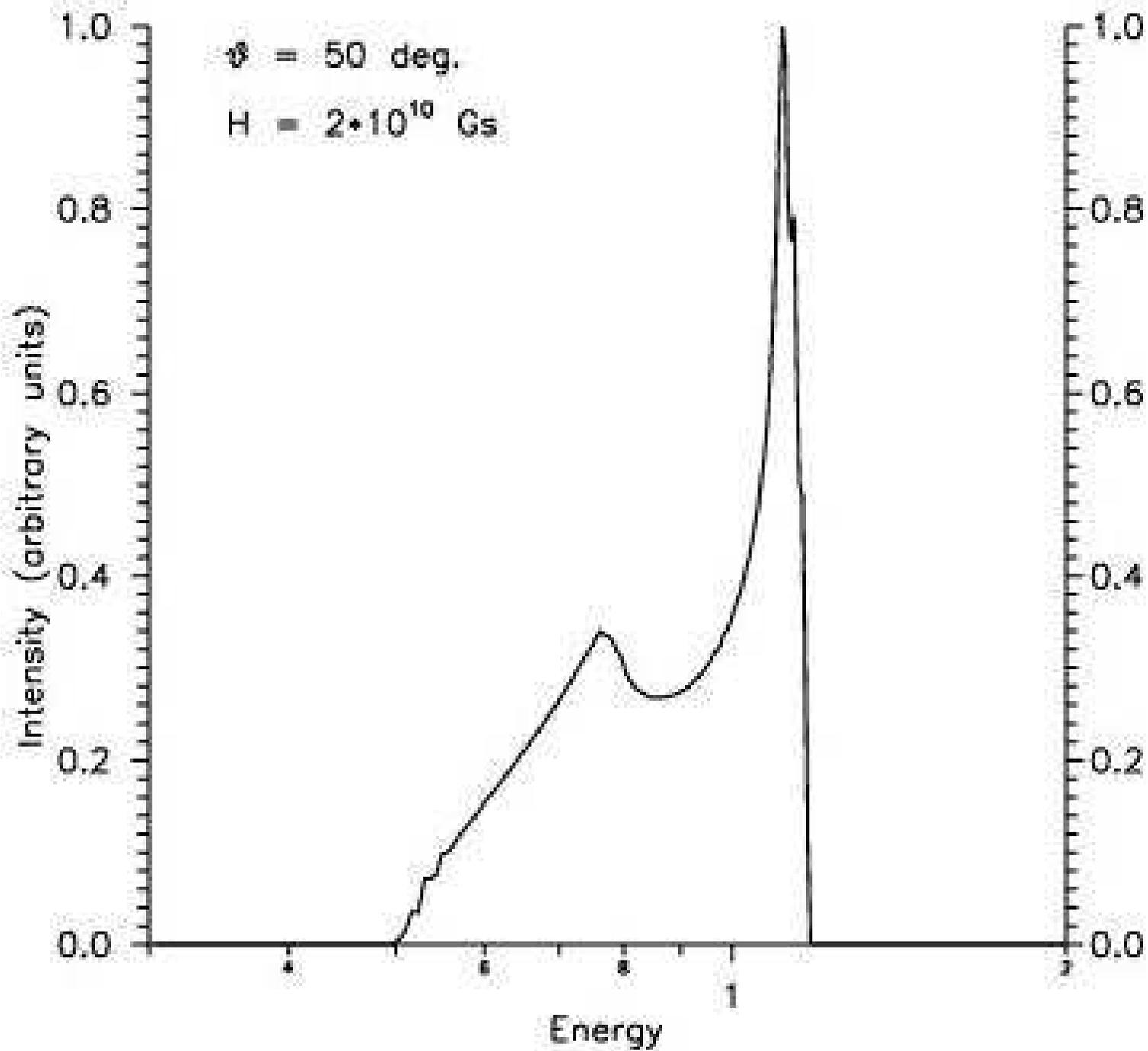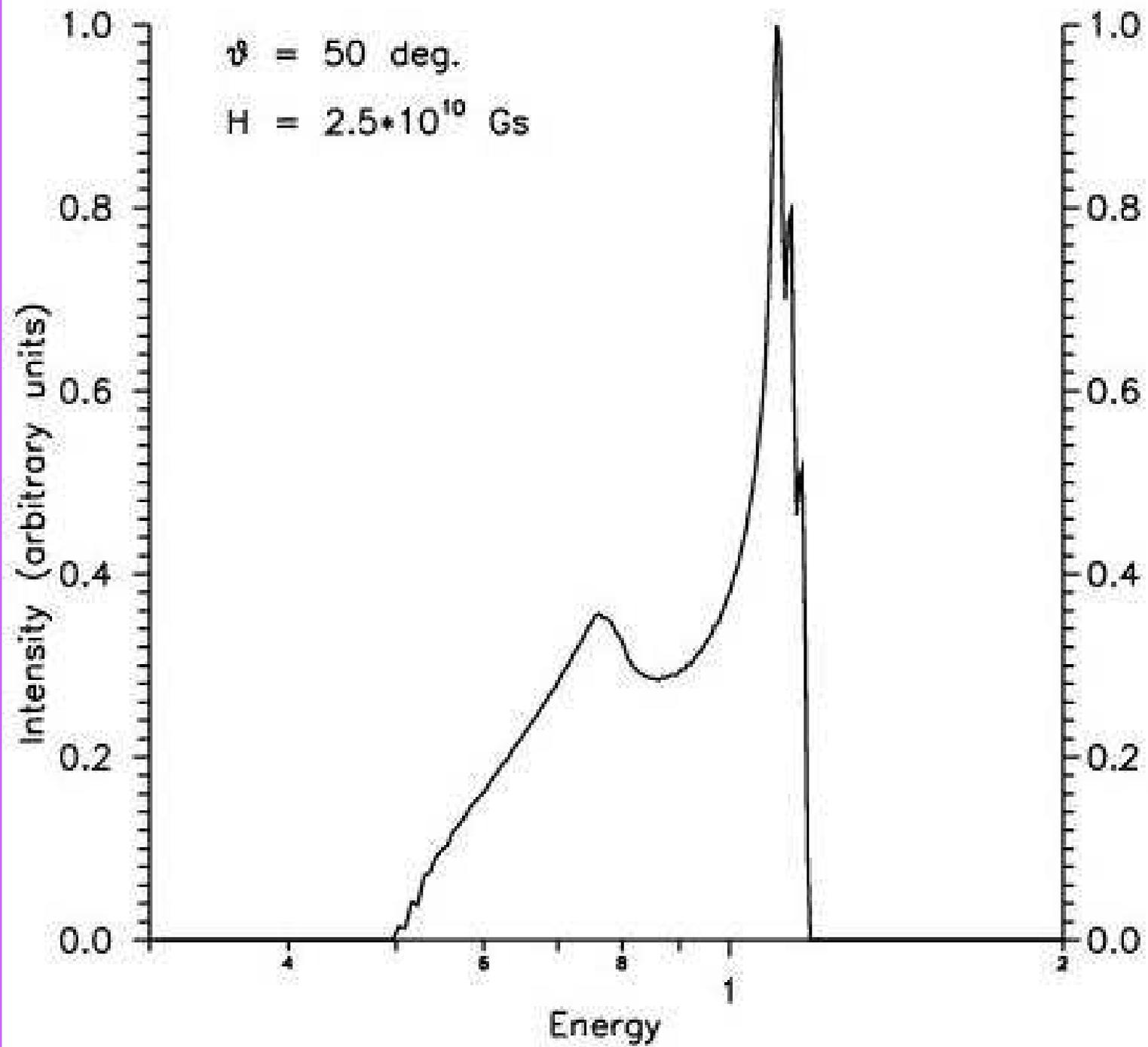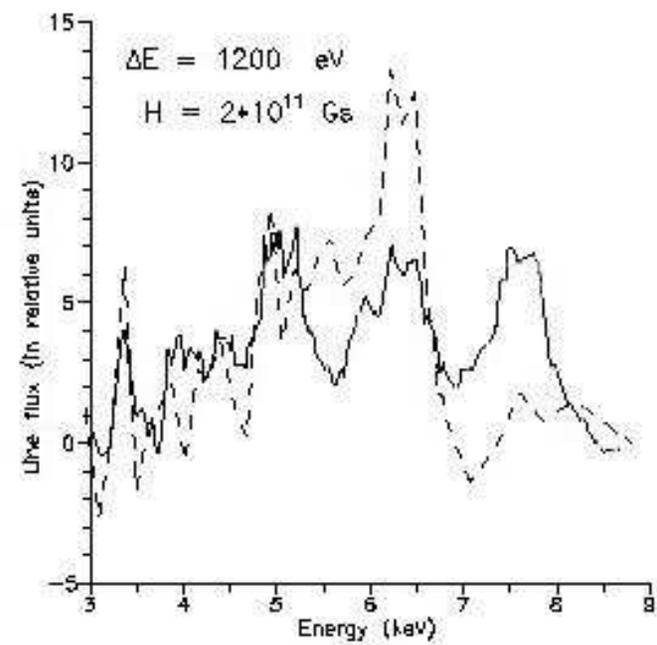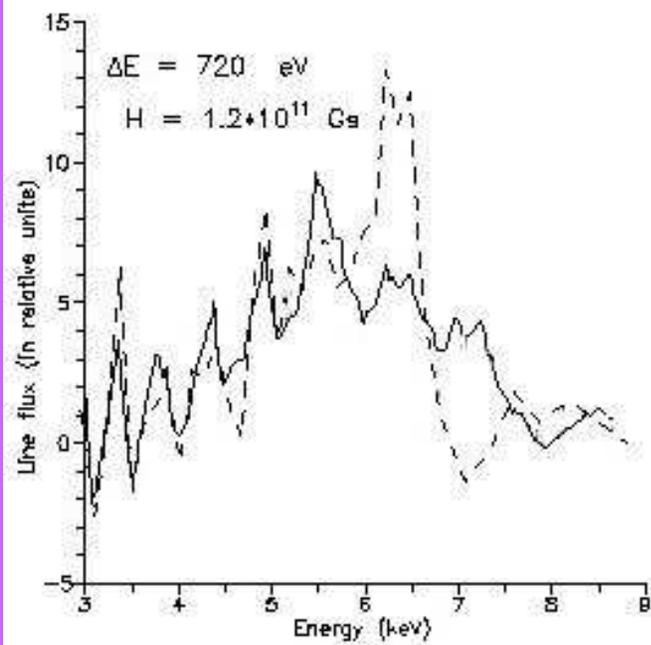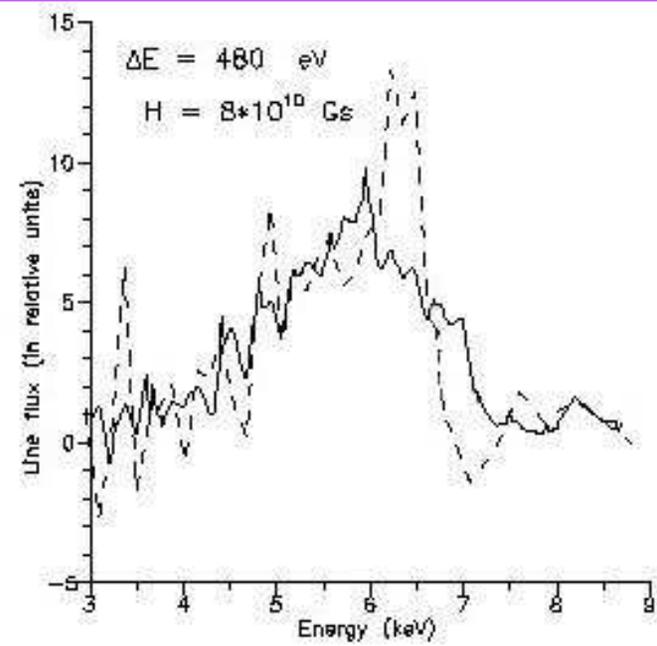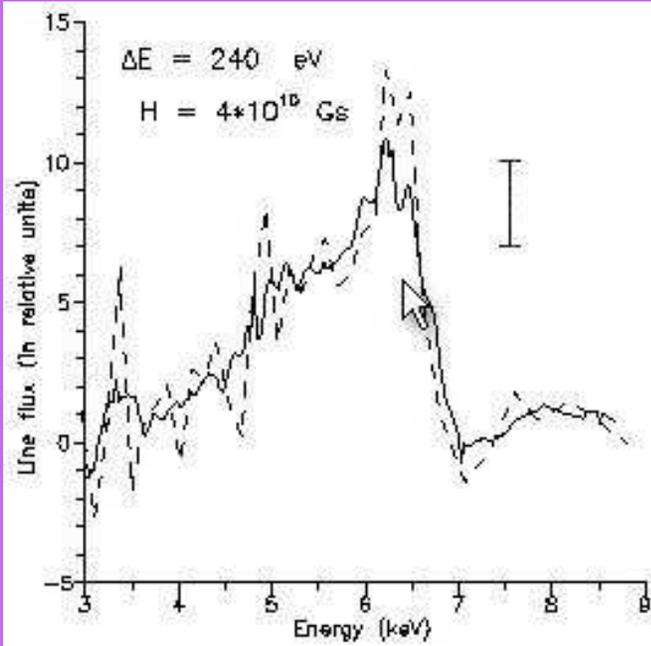
XMM-EPIC observation of MCG−6-30-15: direct evidence for the extraction of energy from a spinning black hole?

Jörn Wilms,[1]★ Christopher S. Reynolds,[2,3]† Mitchell C. Begelman,[3,4] James Reeves,[5] Silvano Molendi,[6] Rüdiger Staubert[1] and Eckhard Kendziorra[1]

[1]*Institut für Astronomie und Astrophysik, Abt. Astronomie, Universität Tübingen, Sand 1, D-72076 Tübingen, Germany*
[2]*Department of Astronomy, University of Maryland, College Park, MD 20742, USA*
[3]*JILA, Campus Box 440, University of Colorado, Boulder, CO 80309, USA*
[4]*Department of Astrophysical and Planetary Sciences, University of Colorado, Boulder, CO 80309, USA*
[5]*X-Ray Astronomy Group, Department of Physics and Astronomy, Leicester University, Leicester LE1 7RH*
[6]*Istituto di Fisica Cosmica, CNR, via Bassini 15, I-20133 Milano, Italy*

ABSTRACT

We present *XMM-Newton* European Photon Imaging Camera (EPIC) observations of the bright Seyfert 1 galaxy MCG−6-30-15, focusing on the broad Fe Kα line at ∼6 keV and the associated reflection continuum, which is believed to originate from the inner accretion disc. We find these reflection features to be *extremely* broad and redshifted, indicating an origin in the very central regions of the accretion disc. It seems likely that we have caught this source in the 'deep minimum' state first observed by Iwasawa et al. The implied central concentration of X-ray illumination is difficult to understand in any pure accretion disc model. We suggest that we are witnessing the extraction and dissipation of rotational energy from a spinning black hole by magnetic fields connecting the black hole or plunging region to the disc.

Key words: accretion, accretion discs – black hole physics – galaxies: individual: MCG−6-30-15 – galaxies: Seyfert – X-rays: galaxies.
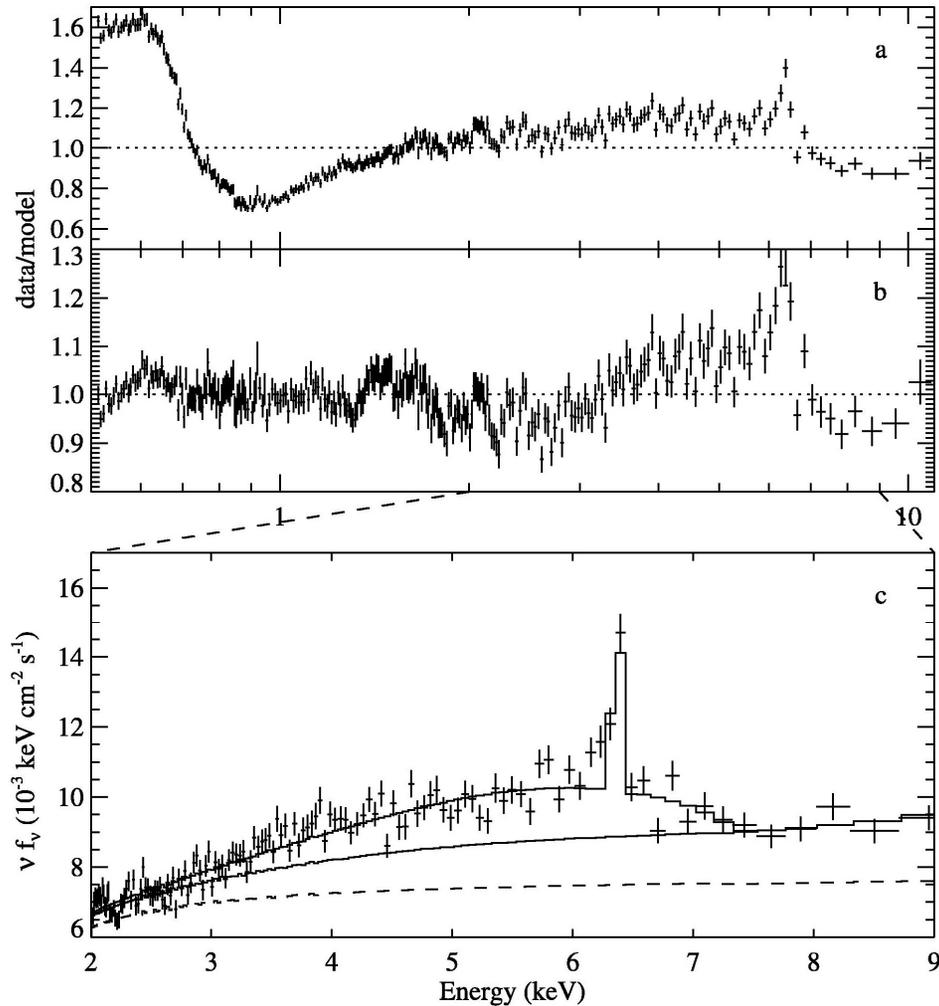
Figure 1. (a) Ratio between data and model from fitting a power law to the $0.5-11$ keV data. (b) Ratio from fitting a power law and the empirical warm absorber model (see text). (c) Deconvolved spectrum of the Fe Kα band, showing the total LAOR model and the continuum with and without (dashed) the reflection component for a model with reflection from an ionized disc. For clarity, the data have been rebinned and only the single-event data points are shown.
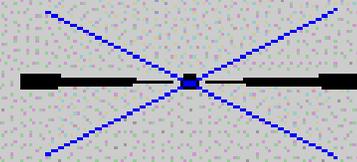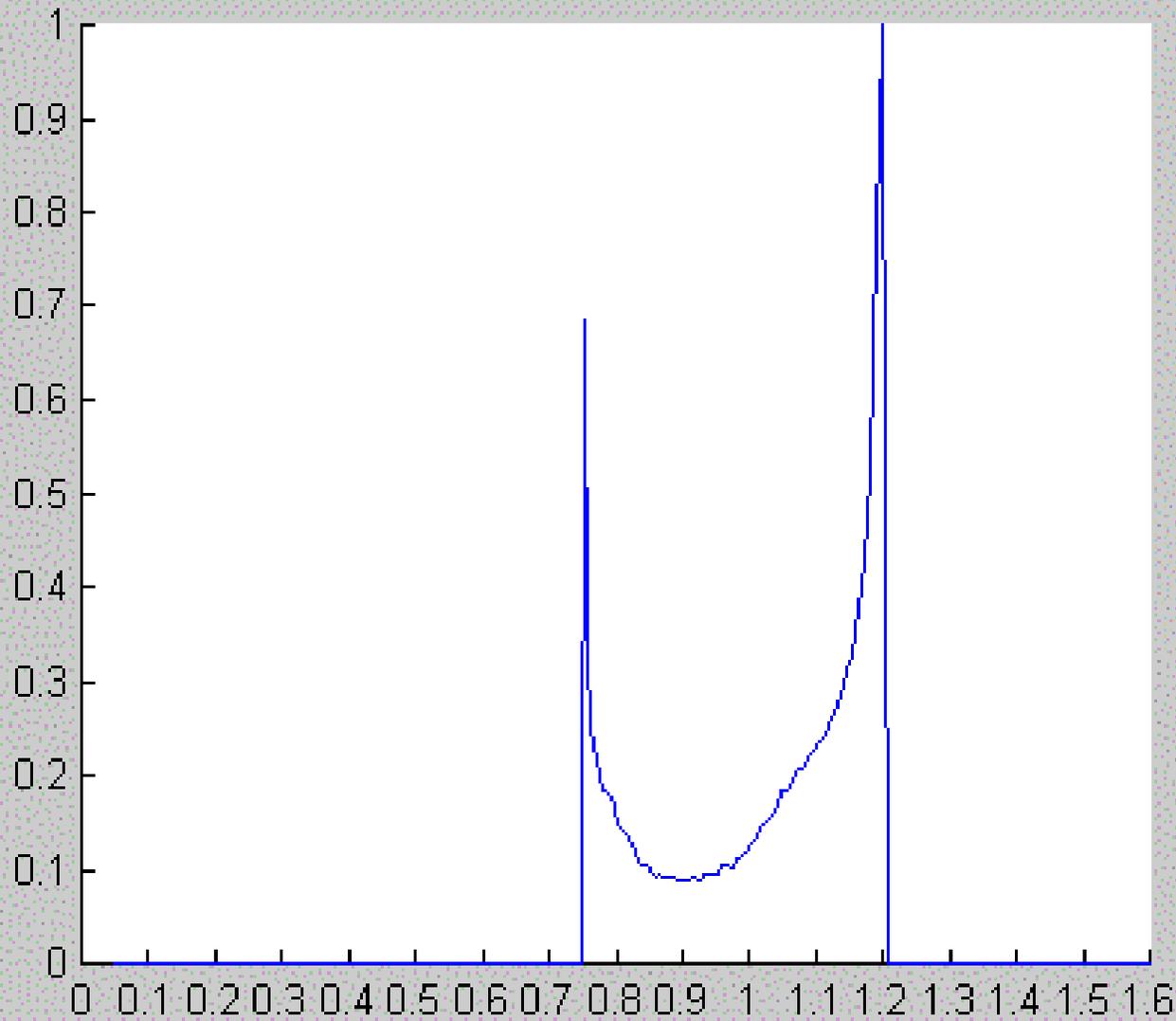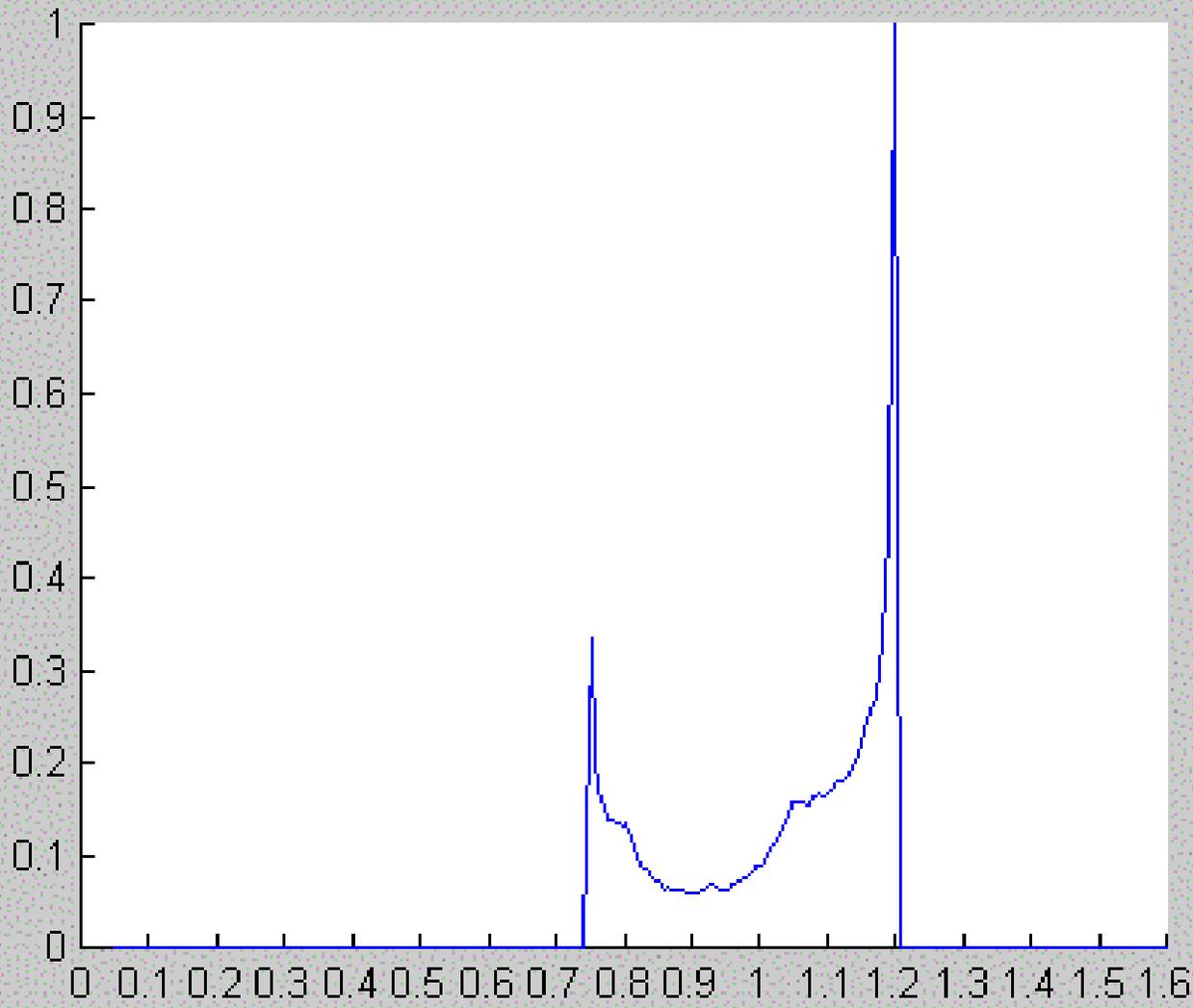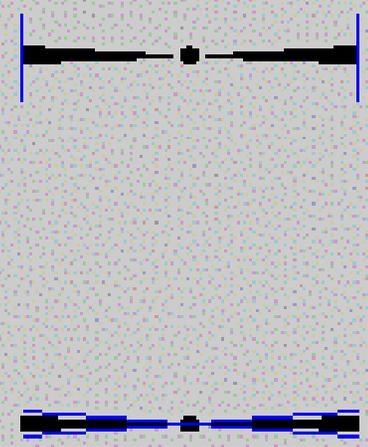
Mirages around Kerr black holes and retro-gravitational lenses

- Let us consider an illumination of black holes. Then retro-photons form caustics around black holes or mirages around black holes or boundaries around shadows.

- (Zakharov, Nucita, DePaolis, Ingrosso,

- New Astronomy 10 (2005) (479-489); astro-ph/0411511)

RETRO-MACHOS: π IN THE SKY?

DANIEL E. HOLZ

Institute for Theoretical Physics, University of California, Santa Barbara, CA 93106

AND

JOHN A. WHEELER

Department of Physics, Princeton University, Princeton, NJ 08544

Draft version September 20, 2004

ABSTRACT

Shine a flashlight on a black hole, and one is greeted with the return of a series of concentric rings of light. For a point source of light, and for perfect alignment of the lens, source, and observer, the rings are of infinite brightness (in the limit of geometric optics). In this manner, distant black holes can be revealed through their reflection of light from the Sun. Such retro-MACHO events involve photons leaving the Sun, making a π rotation about the black hole, and then returning to be detected at the Earth. Our calculations show that, although the light return is quite small, it may nonetheless be detectable for stellar-mass black holes at the edge of our solar system. For example, all (unobscured) black holes of mass M or greater will be observable to a limiting magnitude $\bar{m}$, at a distance given by: $0.02\,\mathrm{pc} \times \sqrt[3]{10^{(\bar{m}-30)/2.5}\,(M/10\,M_\odot)^2}$. Discovery of a Retro-MACHO offers a way to *directly* image the presence of a black hole, and would be a stunning confirmation of strong-field general relativity.

Subject headings: gravitational lensing—black hole physics—relativity
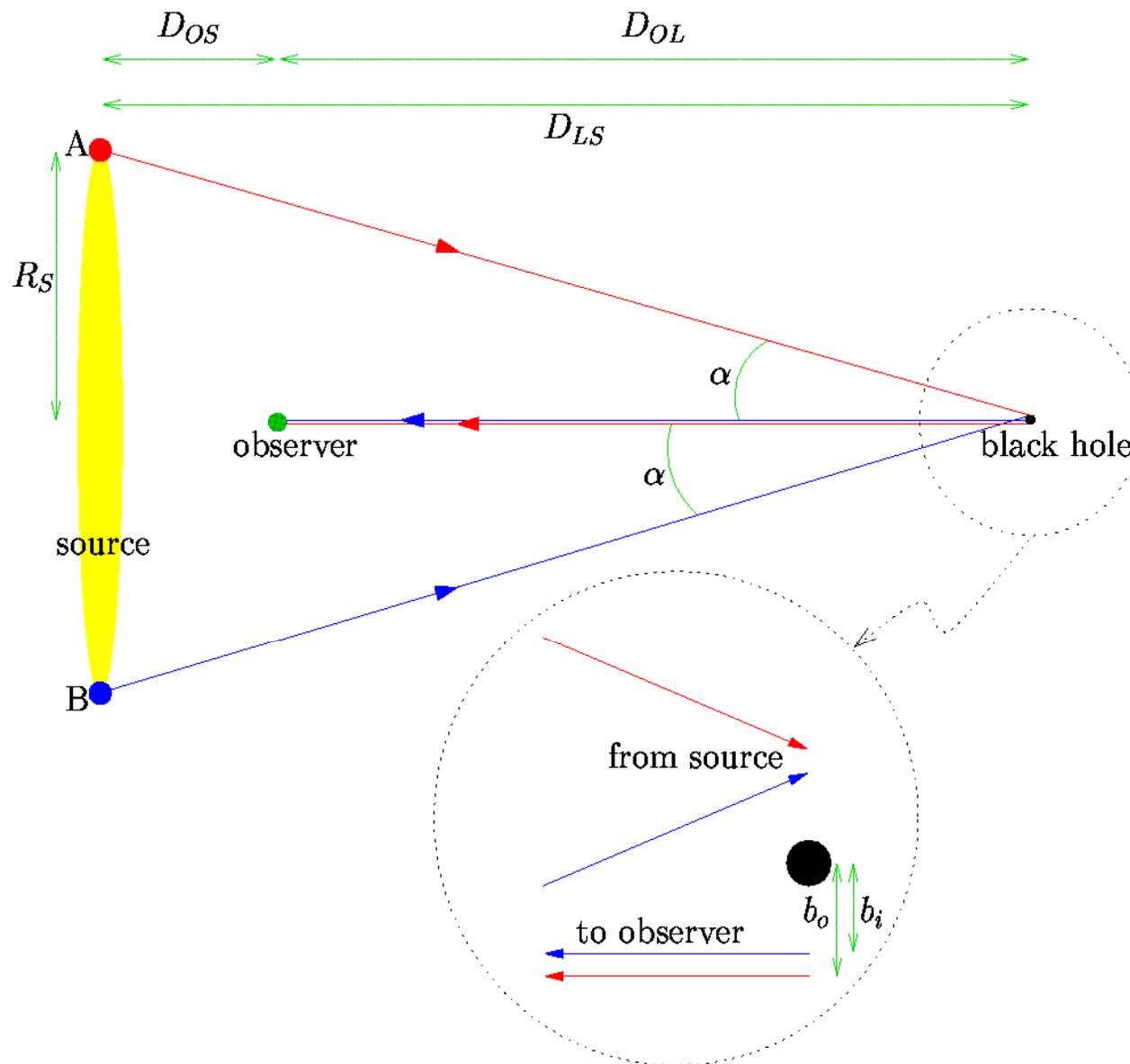
FIG. 1.— Perfect alignment: the (extended) source, observer, and lens are colinear. The resulting image of the source, as lensed by the black hole, is a ring. (The angles in this figure are greatly exaggerated.)
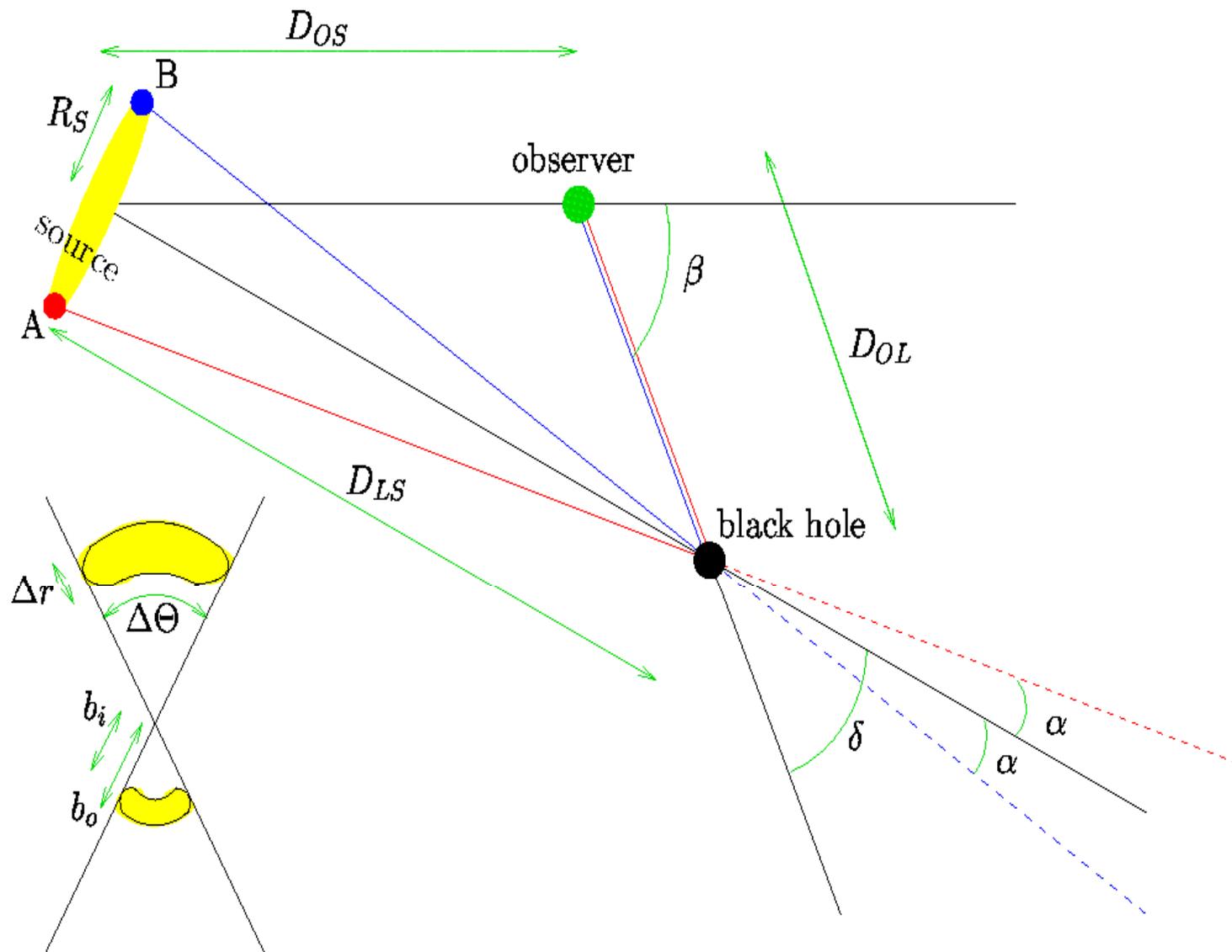
FIG. 2.— Imperfect alignment: the source, observer, and lens are not colinear. Pairs of images are produced, centered on the source–observer–lens plane, on opposite sides of the lens (see inset).
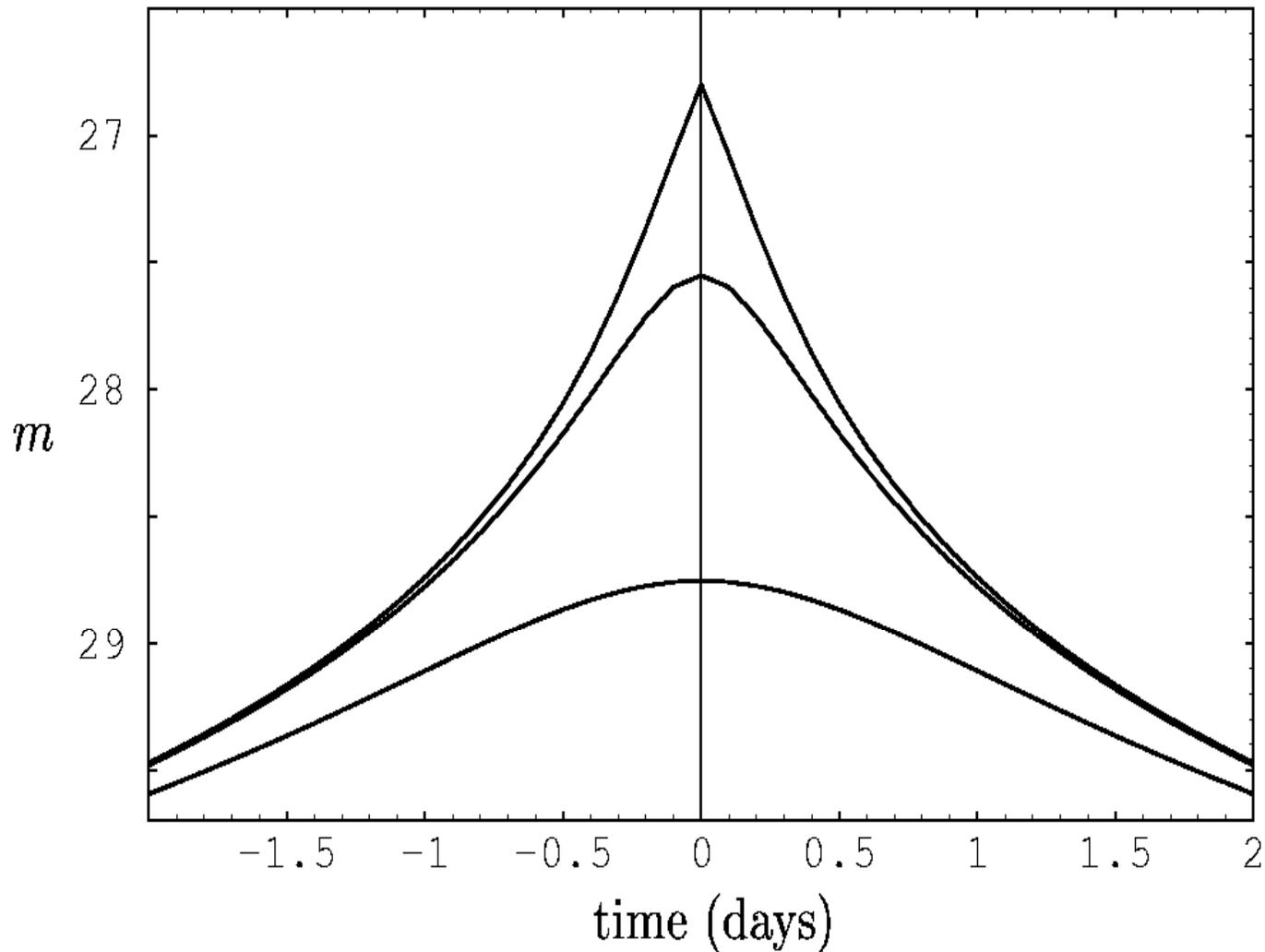
FIG. 3.— Solar retro-MACHO lightcurves: The apparent visual magnitude, m, of the Sun, imaged in a $10\,M_\odot$ black hole at a distance of $0.01\,\mathrm{pc}$. The different curves are for the black hole at angular displacements from the ecliptic plane of 0, $R_\odot/1\,\mathrm{AU}$, and $1°$ respectively (top to bottom).

TABLE 1

RETRO-MACHO BRIGHTNESSES OF THE SUN

BH mass ($M_\odot$)	BH distance (pc)	$\beta = 0$ (perfect alignment)	$\beta = R_\odot/1\,\mathrm{AU}$ (edge alignment)	$\beta = 1°$	$\beta = \pi/4$	$\beta = \pi/2$ (max misalignment)
1	10^{-2}	31.0	32.6	34	38	38
1	10^{-1}	38.6	40.1	41	45	46
10	10^{-2}	26.1	27.6	29	33	33
10	10^{-1}	33.6	35.1	36	40	41
10	1	41.1	42.6	44	48	48

The full classification of geodesic types for Kerr metric is given by Zakharov (1986). As it was shown in this paper, there are three photon geodesic types: capture, scattering and critical curve which separates the first two sets. This classification fully depends only on two parameters $\xi = L_z/E$ and $\eta = Q/E^2$, which are known as Chandrasekhar's constants (Chandrasekhar 1983). Here the Carter constant Q is given by Carter (1968)

$$Q = p_\theta^2 + \cos^2 \theta \left[a^2 \left(m^2 - E^2 \right) + L_z^2/\sin^2 \theta \right],\tag{1}$$

where $E = p_t$ is the particle energy at infinity, $L_z = p_\phi$ is z-component of its angular momentum, $m = p_i p^i$ is the particle mass. Therefore, since photons have $m = 0$

$$\eta = p_\theta^2/E^2 + \cos^2 \theta \left[-a^2 + \xi^2/\sin^2 \theta \right].\tag{2}$$

The first integral for the equation of photon motion (isotropic geodesics) for a radial coordinate in the Kerr metric is described by the following equation (Carter 1968; Chandrasekhar 1983; Zakharov 1986, 1991a)

$$\rho^4 (dr/d\lambda)^2 = R(r),$$

where

$$R(r) = r^4 + (a^2 - \xi^2 - \eta)r^2 + 2[\eta + (\xi - a)^2]r - a^2\eta,\tag{3}$$

and $\rho^2 = r^2 + a^2\cos^2 \theta, \Delta = r^2 - 2r + a^2, a = S/M^2$. The constants M and S are the black hole mass and angular momentum, respectively. Eq. (3) is written in dimensionless variables (all lengths are expressed in black hole mass units M).

If we fix a black hole spin parameter a and consider a plane (ξ, η) and different types of photon trajectories corresponding to (ξ, η), namely, a capture region, a scatter region and the critical curve $\eta_{\text{crit}}(\xi)$ separating the scatter and capture regions. The critical curve is a set of (ξ, η) where the polynomial $R(r)$ has a multiple root (a double root for this case). Thus, the critical curve $\eta_{\text{crit}}(\xi)$ could be determined from the system (Zakharov 1986, 1991a)

$$
\begin{aligned}
R(r) &= 0, \\
\frac{\partial R}{\partial r}(r) &= 0,
\end{aligned}
\tag{4}
$$

for $\eta \geq 0, r \geq r_+ = 1 + \sqrt{1 - a^2}$, because by analysing of trajectories along the θ coordinate we know that for $\eta < 0$ we have $M = \{(\xi, \eta) | \eta \geq -a^2 + 2a|\xi| - \xi^2, -a \leq \xi \leq a\}$ and for each point $(\xi, \eta) \in M$ photons will be captured. If instead $\eta < 0$ and $(\xi, \eta) \bar{\in} M$, photons cannot have such constants of motion, corresponding to the forbidden region (see, (Chandrasekhar 1983; Zakharov 1986) for details).
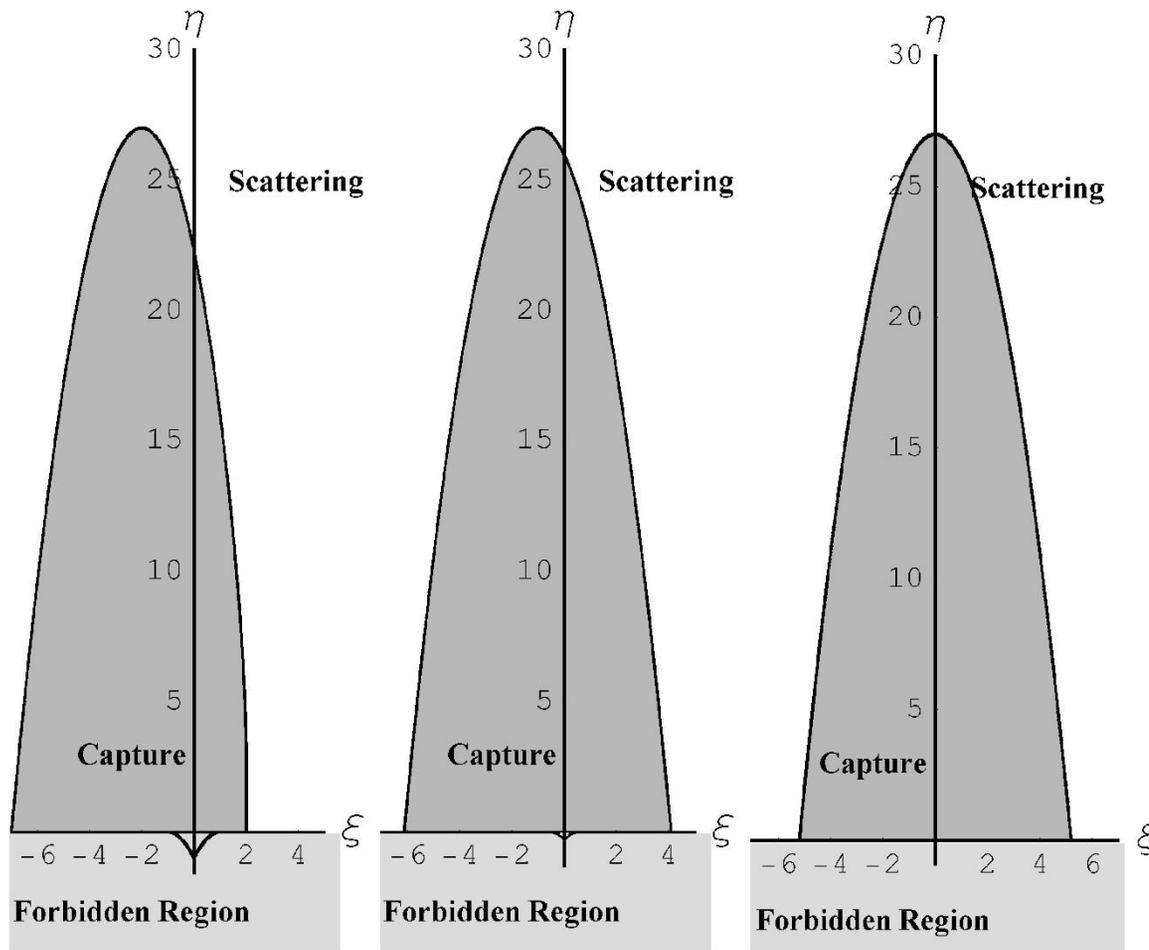
Fig. 1. Different types for photon trajectories and spin parameters ($a = 1., a = 0.5, a = 0.$). Critical curves separate capture and scatter regions. Here we show also the forbidden region corresponding to constants of motion $\eta < 0$ and $(\xi, \eta) \in M$ as it was discussed in the text.
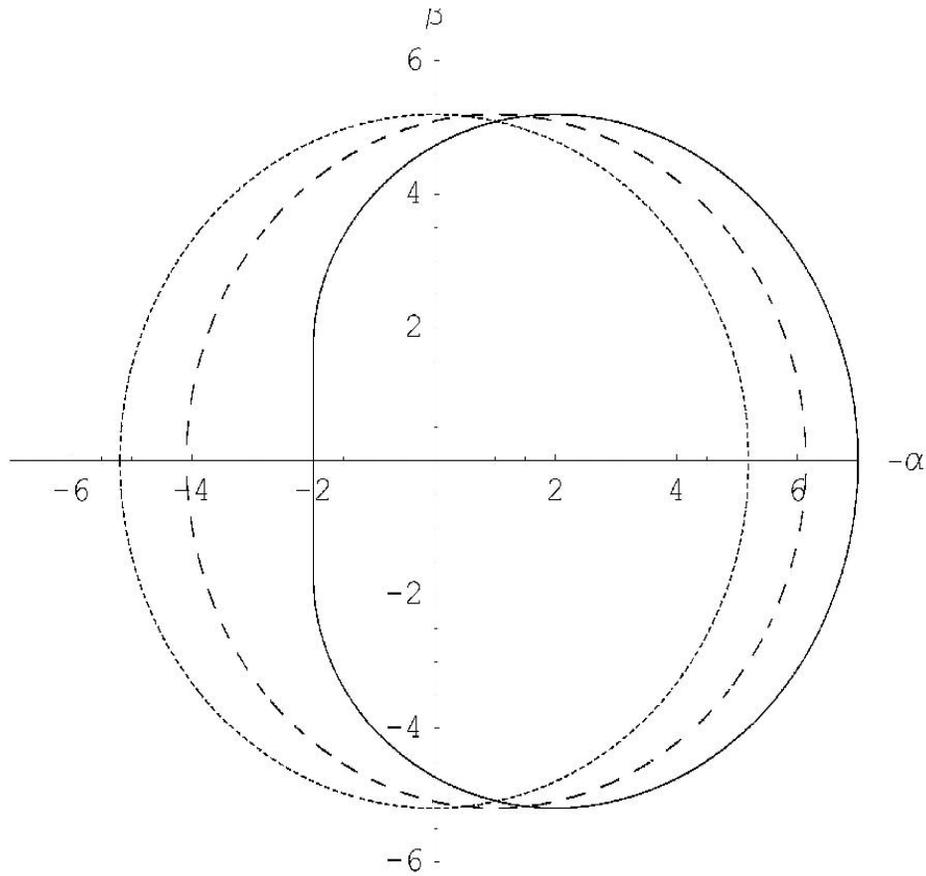
Fig. 2. Mirages around black hole for equatorial position of distant observer and different spin parameters. The solid line, the dashed line and the dotted line correspond to $a = 1, a = 0.5, a = 0$ correspondingly
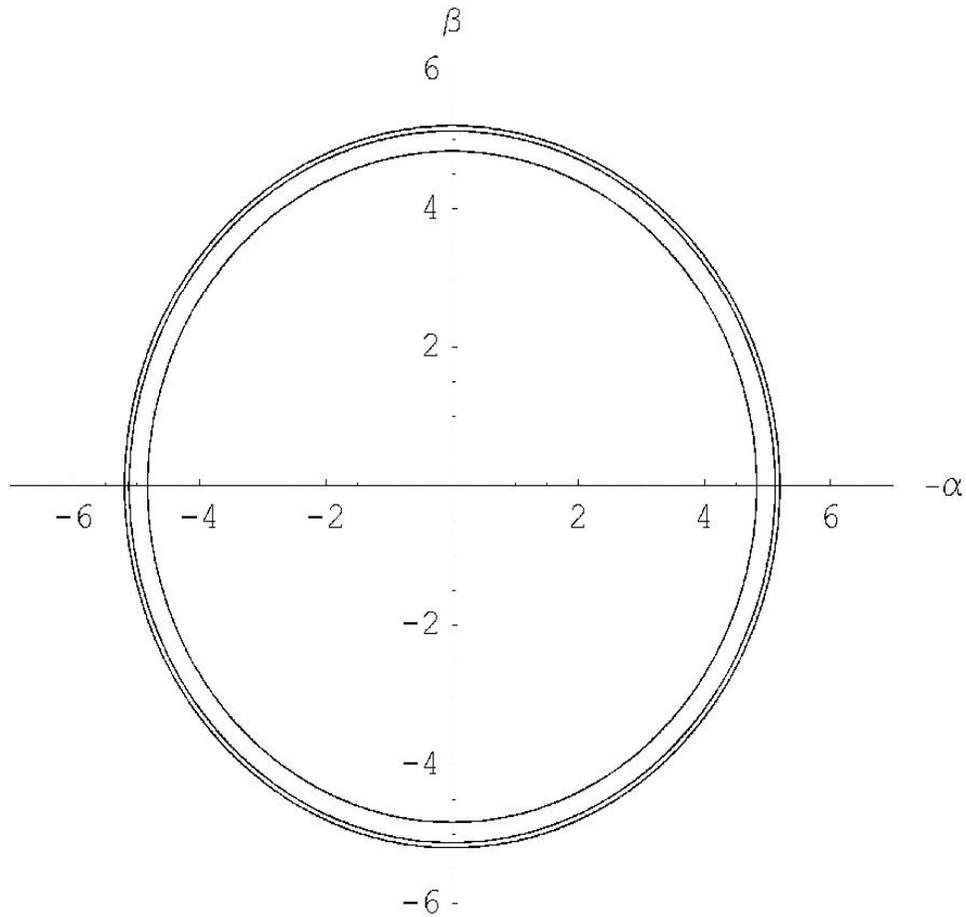
Fig. 3. Mirages around a black hole for the polar axis position of distant observer and different spin parameters ($a = 0, a = 0.5, a = 1$). Smaller radii correspond to greater spin parameters.

Table 1. Dependence of $\eta(0)$ and mirage radii $R_{\mathrm{circ}} = (\eta(0) + a^2)^{1/2}$ on spins.

a	0	0.2	0.4	0.5	0.6	0.8	1.
$\eta(0)$	27	26.839	26.348	25.970	25.495	24.210	22.314
R_{circ}	5.196	5.185	5.14 9	5.121	5.085	4.985	4.828
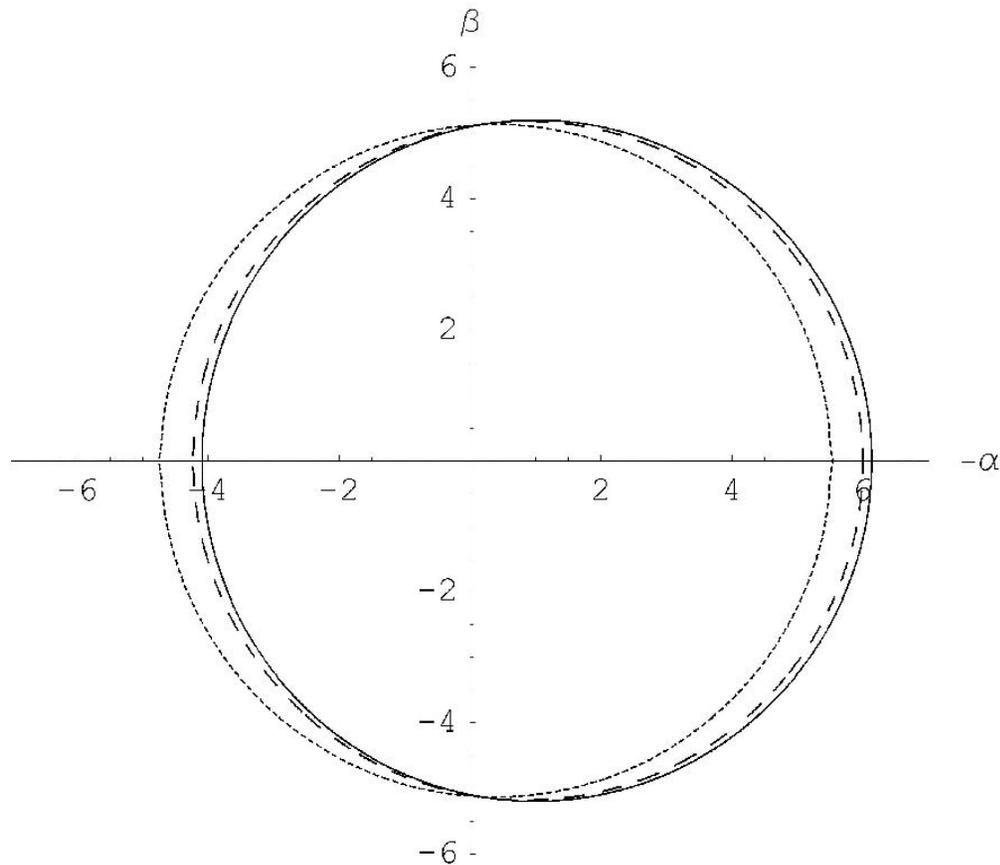
Fig. 4. Mirages around black hole for different angular positions of a distant observer and the spin $a = 0.5$. Solid, dashed and dotted lines correspond to $\theta_0 = \pi/2, \pi/3$ and $\pi/8$, respectively.

- **gr-qc/0604093, April 21, 2006**
  - Title: **Kerr black hole lensing for generic observers in the strong deflection limit**
    Authors: **V. Bozza**, **F. De Luca**, **G. Scarpetta**

found by Carter [9]

$$\pm \int \frac{dx}{\sqrt{R}} = \pm \int \frac{d\vartheta}{\sqrt{\Theta}} \tag{4}$$

$$\phi_f - \phi_i = a \int \frac{x^2 + a^2 - aJ}{\Delta\sqrt{R}} dx - a \int \frac{dx}{\sqrt{R}}$$
$$+ J \int \frac{\csc^2 \vartheta}{\sqrt{\Theta}} d\vartheta, \tag{5}$$

where

$$\Theta = Q + a^2 \cos^2 \vartheta - J^2 \cot^2 \vartheta \tag{6}$$
$$R = x^4 + (a^2 - J^2 - Q)x^2 + (Q + (J-a)^2)x$$
$$- a^2 Q, \tag{7}$$

and ϕ_i is the initial value of the azimuthal coordinate of the photon.

The roots of R represent inversion points in the radial motion. In gravitational lensing we consider photons coming from infinity, grazing the black hole and going back to infinity. For such trajectories there is only one inversion point x_0, representing the closest approach distance. The minimum allowed value of x_0 can be found solving the equations $R(x) = 0$ and $R'(x) = 0$ simultaneously. However, in Kerr black hole, we do not have a unique minimum closest approach x_m, but rather a continuous family of values which depend on the approach trajectory followed by the photon. In particular, it is possible to establish a relation among the minimum closest approach x_m and the corresponding values of the constants of motion J and Q, that we shall indicate by J_m and Q_m (see e.g. Ref. [21])

$$J_m = \frac{x_m^2(2x_m - 3) + a^2(1 + 2x_m)}{a(1 - 2x_m)} \tag{8}$$

$$Q_m = \frac{x_m^3 [2a^2 - x_m(x_m - 3/2)^2]}{a^2(x_m - 1/2)^2}. \tag{9}$$

x_m also represents the radius of the unstable circular photon orbit. This radius is fixed to $3/2$ when $a = 0$ (Schwarzschild black hole). In the case of Kerr black holes, x_m may vary between two limiting values x_{m+}, x_{m-}, depending on the incoming direction of the photon. The two limiting values can be analytically obtained solving the equation $Q_m = 0$. To the third order in a, they read [16]

$$x_{m\pm} = \frac{3}{2} \mp \frac{2}{\sqrt{3}} a - \frac{4}{9} a^2 \mp \frac{20}{27\sqrt{3}} a^3 + O(a^4). \tag{10}$$

For example, photons whose orbit lies on the equatorial plane may turn either in the same sense of the black hole (prograde photons) or in the opposite sense (retrograde photons). Prograde photons are allowed to get closer to the black hole, with a minimum closest approach given by x_{m+}, while retrograde photons must stay farther than x_{m-}, in order to be deflected without falling into the black hole. Photons whose orbit does not lie
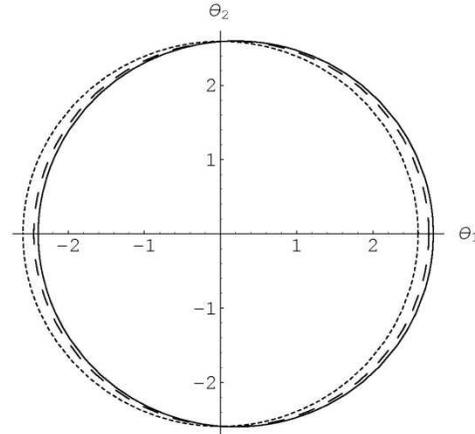
FIG. 2: The shadow of the black hole in the observer sky for $a = 0.1$ and different values of the observer position ϑ_o. The solid line is for $\vartheta_o = \pi/2$ (equatorial observer), the dashed line is for $\vartheta_o = \pi/4$ and the dotted line is for $\vartheta_o = 0$ (polar observer).

on the equatorial plane are characterized by intermediate values of x_m, with $Q_m > 0$. Thus x_m can be used to parametrize the family of unstable photon orbits allowed in Kerr metric or, equivalently, the incoming direction of the photon. The corresponding values of the constants of motion are uniquely determined by Eqs. (8) and (9).

Although exact expressions for x_{m+} and x_{m-} are available, it is convenient to start with a perturbative expansion *ab initio* in order to be prepared to face more complicated quantities in the following [16]. Throughout our treatment, only for x_m we need to push the expansion to the third order, in order to obtain some quantities to the second order in a.

III. THE SHADOW OF A KERR BLACK HOLE

The constants of motion J and Q have an immediate link to the position in the sky where the observer detects the photon. In fact, we can define angular coordinates (θ_1, θ_2) on the observer sky centered on the black hole position. We choose the orientation of these coordinates in such a way that the spin axis of the black hole is projected on the θ_2-axis (see Fig.2).

As shown in Ref. [21], photons detected by the observer at angular coordinates (θ_1, θ_2) are characterized by constants of motion given by

$$J = -\theta_1 D_{OL} \sqrt{1 - \mu_o^2}, \tag{11}$$
$$Q = \theta_2^2 D_{OL}^2 + \mu_o^2(\theta_1^2 D_{OL}^2 - a^2). \tag{12}$$
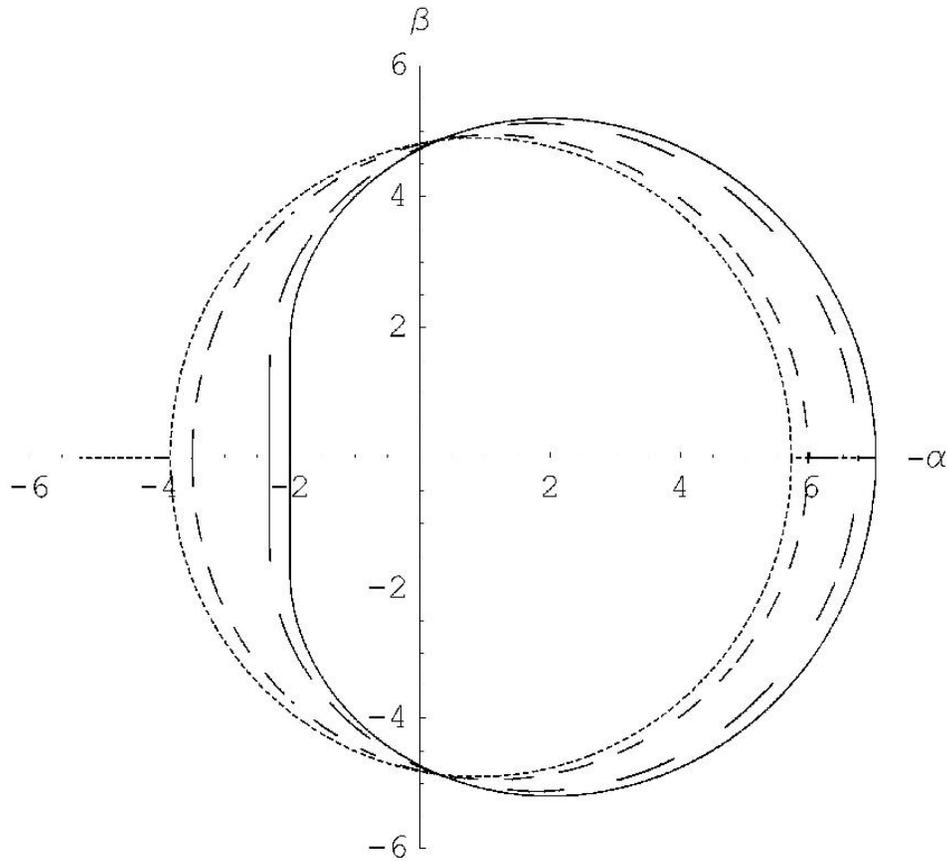
Fig. 5. Mirages around black hole for different angular positions of a distant observer and the spin $a = 1$. Solid, long dashed, short dashed and dotted lines correspond to $\theta_0 = \pi/2, \pi/3, \pi/6$ and $\pi/8$, respectively.

Falcke, Melia, Agol
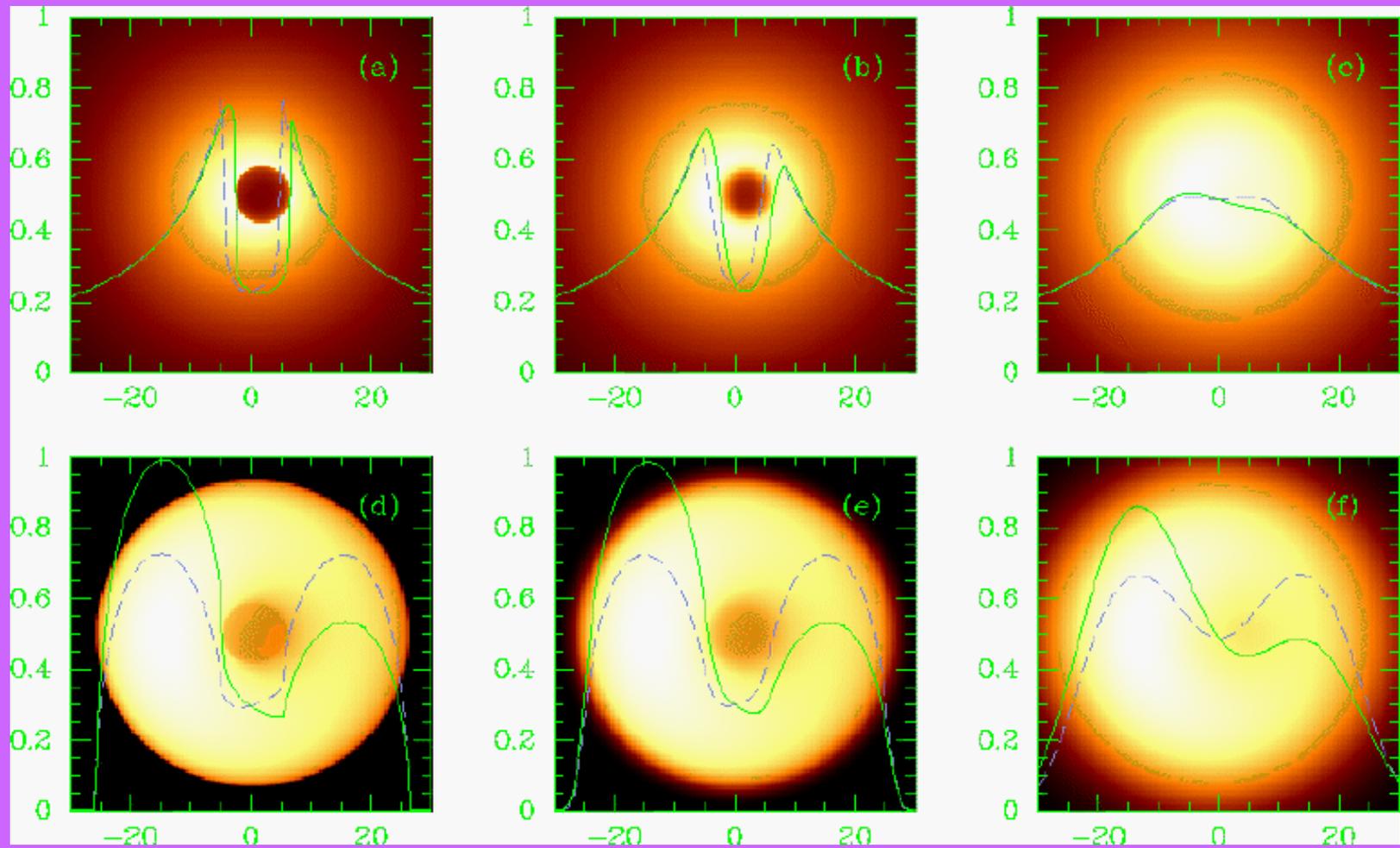
Shadows from Melia

Kevin
Rauch
JHU

R = 8

R = 4

R = 2
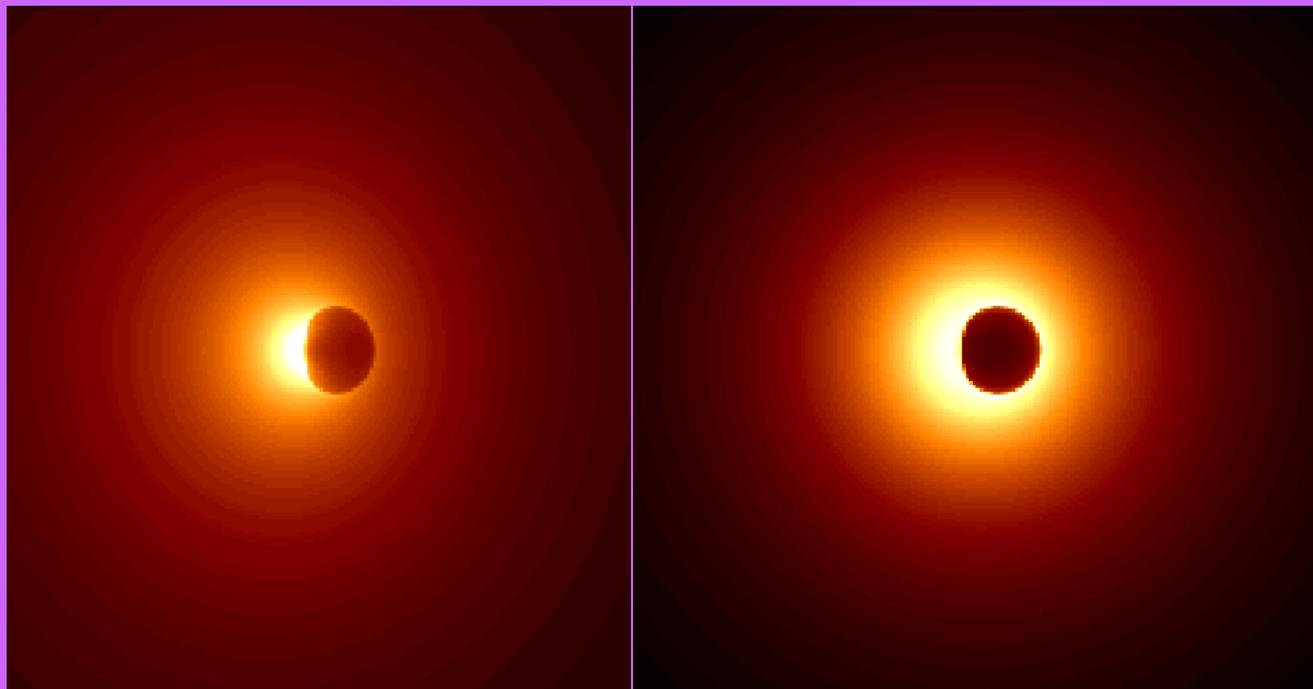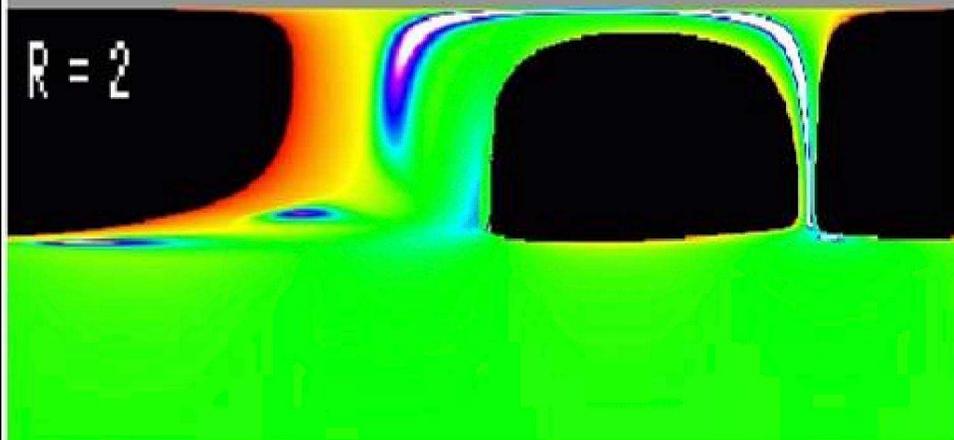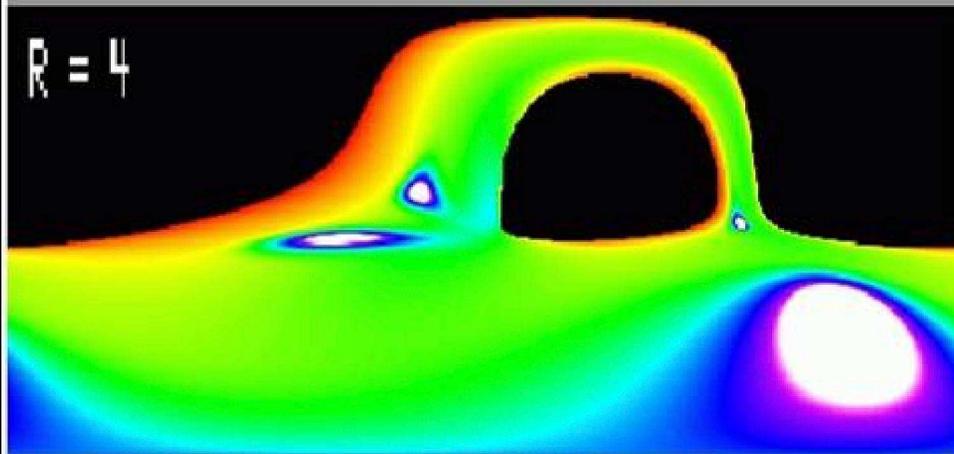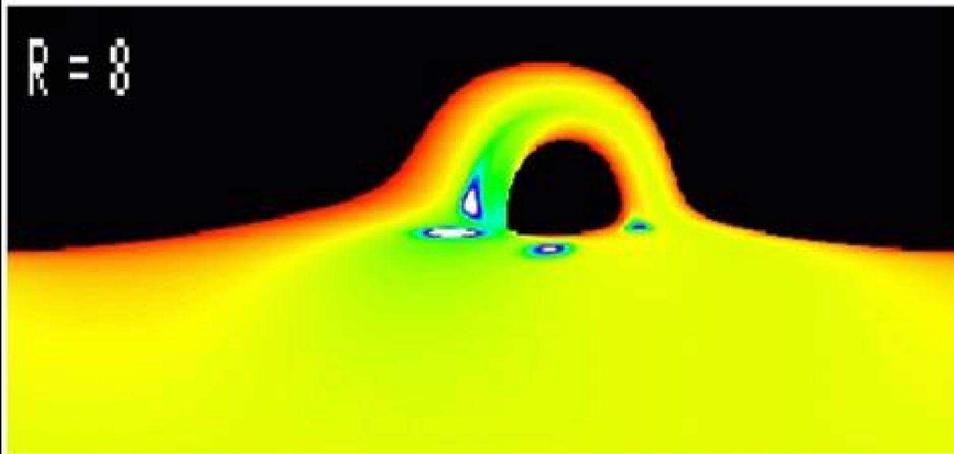
LETTERS

A size of ~1 AU for the radio source Sgr A* at the centre of the Milky Way

Zhi-Qiang Shen[1], K. Y. Lo[2], M.-C. Liang[3], Paul T. P. Ho[4,5] & J.-H. Zhao[4]

Although it is widely accepted that most galaxies have super-massive black holes at their centres[1–3], concrete proof has proved elusive. Sagittarius A* (Sgr A*)[4], an extremely compact radio source at the centre of our Galaxy, is the best candidate for proof[5–7], because it is the closest. Previous very-long-baseline interferometry observations (at 7 mm wavelength) reported that Sgr A* is ~2 astronomical units (AU) in size[8], but this is still larger than the 'shadow' (a remarkably dim inner region encircled by a bright ring) that should arise from general relativistic effects near the event horizon of the black hole[9]. Moreover, the measured size is wavelength dependent[10]. Here we report a radio image of Sgr A* at a wavelength of 3.5 mm, demonstrating that its size is ~1 AU. When combined with the lower limit on its mass[11], the lower limit on the mass density is $6.5 \times 10^{21} M_\odot \, pc^{-3}$ (where $M_\odot$ is the solar mass), which provides strong evidence that Sgr A* is a super-massive black hole. The power-law relationship between wavelength and intrinsic size (size ∝ wavelength$^{1.09}$) explicitly rules out explanations other than those emission models with stratified structure, which predict a smaller emitting region observed at a shorter radio wavelength.

Past very-long-baseline interferometry (VLBI) observations[12–16] of Sgr A* have revealed an east–west elongated structure whose apparent angular size at longer wavelengths is dominated by the interstellar scattering angle, that is, $\Theta_{obs} = \Theta_{obs}^{1\,cm} \lambda^2$, where Θ_{obs} is the observed size in milliarcseconds (mas) at wavelength λ in cm, and equals $\Theta_{obs}^{1\,cm}$ at 1 cm. Thus, VLBI observations at shorter millimetre wavelengths, where the intrinsic structure of Sgr A* could become comparable to the pure scattering size, are expected to show deviations of the observed size from the scattering law. This has been demonstrated by the recent detection of the intrinsic size at 7 mm (ref. 8). On 20 November 2002, we successfully carried out an observation of Sgr A* with the Very Long Baseline Array (VLBA) at its shortest wavelength of 3.5 mm (ref. 10). Our observation, with the steadily improved performance of the VLBA system, has produced the first (to our knowledge) high-resolution image of Sgr A* made at 3.5 mm (Fig. 1), which exhibits an elongated structure too.

To yield a quantitative description of the observed structure, we tried a model fitting procedure[17] in which the amplitude closure relation is applied. Compared to the conventional VLBI
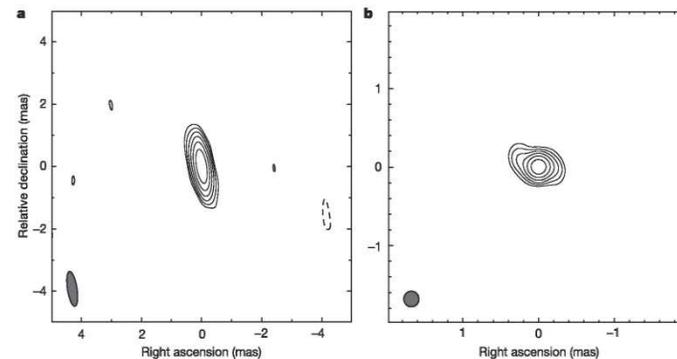
Figure 1 | High-resolution VLBI image of Sgr A* at 3.5 mm obtained with the VLBA on 20 November 2002. The observations were flexibly scheduled to ensure good weather conditions at most sites, and the data were recorded at the highest possible recording rate of 512 Mbit s^{-1}. Standard visibility amplitude calibration including the elevation-dependent opacity correction was done, and the final image was obtained after several iterations of the self-calibration and cleaning procedures. The calibrated total flux density is about 1.2 Jy. **a**, A uniformly weighted image with the restoring beam (indicated at the lower left corner) of 1.13 mas × 0.32 mas at 9°. The peak flux density is 1.08 Jy beam^{-1}. Contour levels are drawn at $3\sigma \times (-1, 1, 2, 4, 8, 16, 32)$; $3\sigma = 17.5$ mJy beam^{-1}. **b**, A super-resolution image with a circular beam of 0.20 mas from which an east–west elongated structure can be seen (see Table 1). Note the different scales. The contour levels are the same as that in **a** with the corresponding peak flux density of 1.01 Jy beam^{-1}.

[1]Shanghai Astronomical Observatory, 80 Nandan Road, Shanghai 200030, China. [2]National Radio Astronomy Observatory, 520 Edgemont Road, Charlottesville, Virginia 22903, USA. [3]Division of Geological and Planetary Sciences, California Institute of Technology, Pasadena, California 91125, USA. [4]Harvard-Smithsonian CfA, 60 Garden Street, Cambridge, Massachusetts 02138, USA. [5]Institute of Astronomy & Astrophysics, Academia Sinica, PO Box 23-141, Taipei 106, Taiwan, China.

Event-horizon-scale structure in the supermassive black hole candidate at the Galactic Centre

Sheperd S. Doeleman[1], Jonathan Weintroub[2], Alan E. E. Rogers[1], Richard Plambeck[3], Robert Freund[4], Remo Tilanus[5,6], Per Friberg[5], Lucy M. Ziurys[4], James Moran[2], Brian Corey[1], Ken H. Young[2], Daniel L Smythe[1], Michael Titus[1], Daniel P. Marrone[7,8], Roger J. Cappallo[1], Douglas C.-J. Bock[9], Geoffrey C. Bower[3], Richard Chamberlin[10], Gary R. Davis[5], Thomas P. Krichbaum[11], James Lamb[12], Holly Maness[3], Arthur E. Niell[1], Alan Roy[11], Peter Strittmatter[4], Daniel Werthimer[13], Alan R. Whitney[1] & David Woody[12]

The cores of most galaxies are thought to harbour supermassive black holes, which power galactic nuclei by converting the gravitational energy of accreting matter into radiation[1]. Sagittarius A*, the compact source of radio, infrared and X-ray emission at the centre of the Milky Way, is the closest example of this phenomenon, with an estimated black hole mass that is 4 million times that of the Sun[2,3]. A long-standing astronomical goal is to resolve structures in the innermost accretion flow surrounding Sgr A* where strong gravitational fields will distort the appearance of radiation emitted near the black hole. Radio observations at wavelengths of 3.5 mm and 7 mm have detected intrinsic structure in Sgr A*, but the spatial resolution of observations at these wavelengths is limited by interstellar scattering[4-7]. Here we report observations at a wavelength of 1.3 mm that set a size of 37^{+16}_{-10} microarcseconds on the intrinsic diameter of Sgr A*. This is less than the expected apparent size of the event horizon of the presumed black hole, suggesting that the bulk of SgrA* emission may not be not centred on the black hole, but arises in the surrounding accretion flow.
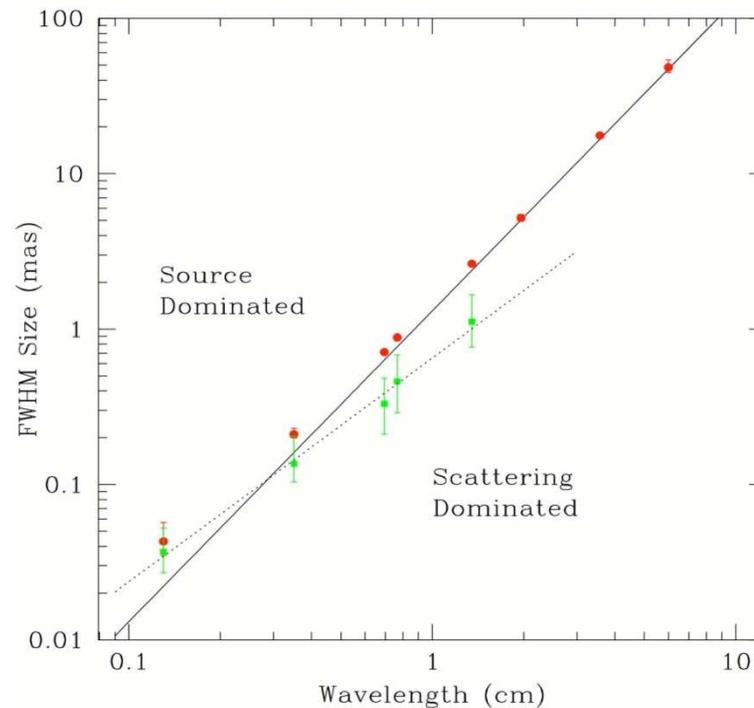
Fig 2

Figure 2 Observed and intrinsic size of Sgr A* as a function of wavelength. Red circles show major-axis observed sizes of Sgr A* from VLBI observations (all errors 3σ). Data from wavelengths of 6 cm to 7 mm are from ref. 13, data at 3.5 mm are from ref. 7, and data at 1.3 mm are from the observations reported here. The solid line is the best-fit λ^2 scattering law from ref. 13, and is derived from measurements made at $\lambda > 17$ cm. Below this line, measurements of the intrinsic size of Sgr A* are dominated by scattering effects, while measurements that fall above the line indicate intrinsic structures that are larger than the scattering size (a 'source-dominated' regime). Green points show derived major-axis intrinsic sizes from 2 cm $< \lambda < 1.3$ mm and are fitted with a λ^α power law ($\alpha = 1.44 \pm 0.07$, 1σ) shown as a dotted line. When the 1.3-mm point is removed from the fit, the power-law exponent becomes $\alpha = 1.56 \pm 0.11$ (1σ).

Direct Measurements of Black Hole Charge with Future Astrometrical Missions

A.F. Zakharov[1,2,3], F. De Paolis[4], G. Ingrosso[4], A.A. Nucita[4]

[1] Institute of Theoretical and Experimental Physics, 25, B.Cheremushkinskaya st., Moscow, 117259, Russia,

[2] Astro Space Centre of Lebedev Physics Institute, 84/32, Profsoyuznaya st., Moscow, 117810, Russia,

[3] Joint Institute for Nuclear Research, Dubna, Russia

[4] Department of Physics, University of Lecce and INFN, Section of Lecce, Via Arnesano, I-73100 Lecce, Italy

Abstract. Recently, Zakharov et al. (2005a) considered the possibility of evaluating the spin parameter and the inclination angle for Kerr black holes in nearby galactic centers by using future advanced astrometrical instruments. A similar approach which uses the characteristic properties of gravitational retro-lensing images can be followed to measure the charge of Reissner-Nordström black hole. Indeed, in spite of the fact that their formation might be problematic, charged black holes are objects of intensive investigations. From the theoretical point of view it is well-known that a black hole is described by only three parameters, namely, its mass M, angular momentum J and charge Q. Therefore, it would be important to have a method for measuring all these parameters, preferably by model independent way. In this paper, we propose a procedure to measure the black hole charge by using the size of the retro-lensing images that can be revealed by future astrometrical missions. A discussion of the Kerr-Newmann black hole case is also offered.

In this paper we focus on the possibility to measure the black hole charge as well and we present an analytical dependence of mirage size on the black hole charge. Indeed, future space missions like Radioastron in radio band or MAXIM in X-ray band have angular resolution close to the shadow size for massive black holes in the center of our and nearby galaxies.

2. Basic Definitions and Equations

The expression for the Reissner - Nordström metric in natural units $(G = c = 1)$ has the form

$$ds^2 = -(1 - 2M/r + Q^2/r^2)dt^2 + (1 - 2M/r + Q^2/r^2)^{-1}dr^2 + r^2(d\theta^2 + sin^2\theta d\phi^2). \quad (1)$$

$$R(r_{max}) = 0, \qquad \frac{\partial R}{\partial r}(r_{max}) = 0, \tag{6}$$

as it was done, for example, by Chandrasekhar (1983) to solve similar problems.

Introducing the notation $\xi^2 = l, Q^2 = q$, we obtain

$$R(r) = r^4 - lr^2 + 2lr - qr. \tag{7}$$

The discriminant Δ of the polynomial $R(r)$ has the form (as it was shown by Zakharov (1991a,b, 1994a)):

$$\Delta = 16l^3[l^2(1-q) + l(-8q^2 + 36q - 27) - 16q^3]. \tag{8}$$

The polynomial $R(r)$ thus has a multiple root if and only if

$$l^3[l^2(1-q) + l(-8q^2 + 36q - 27) - 16q^3] = 0. \tag{9}$$

Excluding the case $l = 0$, which corresponds to a multiple root at $r = 0$, we find that the polynomial $R(r)$ has a multiple root for $r \geq r_+$ if and only if

$$l^2(1-q) + l(-8q^2 + 36q - 27) - 16q^3 = 0. \tag{10}$$

If $q = 0$, we obtain the well-known result for a Schwarzschild black hole (Misner, Thorne and Wheeler 1973; Wald 1984; Lightman et al. 1975), $l = 27$, or $L_{cr} = 3\sqrt{3}$. If $q = 1$, then $l = 16$, or $L_{cr} = 4$, which also corresponds to numerical results given by Young (1976).

The photon capture cross section for an extreme charged black hole turns out to be considerably smaller than the capture cross section of a Schwarzschild black hole. The critical value of the impact parameter, characterizing the capture cross section for a Reissner - Nordström black hole, is determined by the equation (Zakharov 1991a,b, 1994a)

$$l = \frac{(8q^2 - 36q + 27) + \sqrt{(8q^2 - 36q + 27)^2 + 64q^3(1-q)}}{2(1-q)}. \tag{11}$$

As it was explained by Zakharov et al. (2005a,b) this leads to the formation of shadows described by the critical value of L_{cr} or, in other words, in the spherically symmetric case, shadows are circles with radii L_{cr}. Therefore, measuring the shadow size, one could evaluate the black hole charge in black hole mass units M.
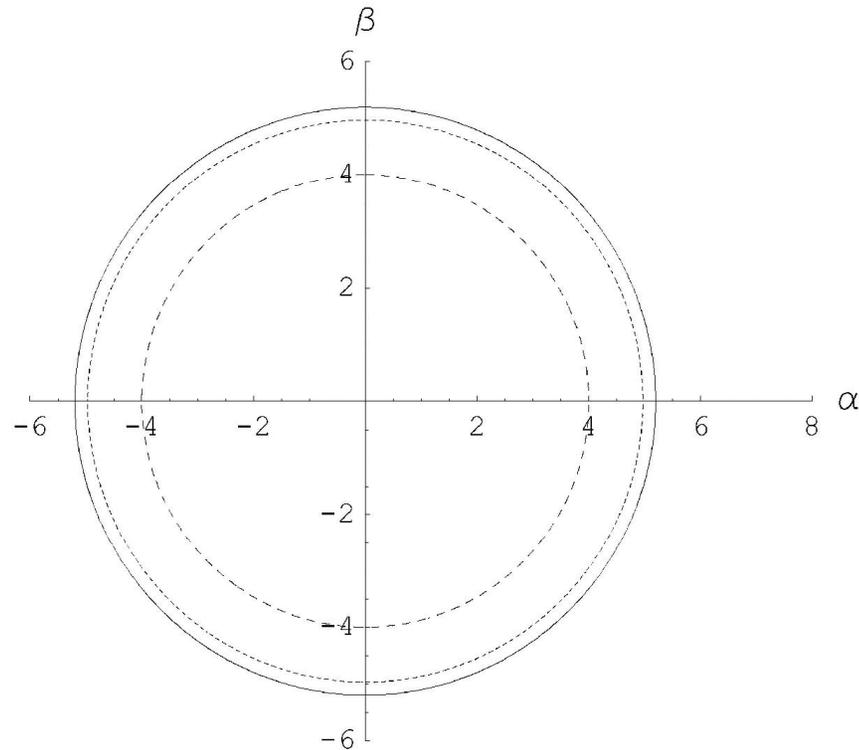
Fig. 1. Shadow (mirage) sizes are shown for selected charges of black holes $Q = 0$ (solid line), $Q = 0.5$ (short dashed line) and $Q = 1$ (long dashed line).
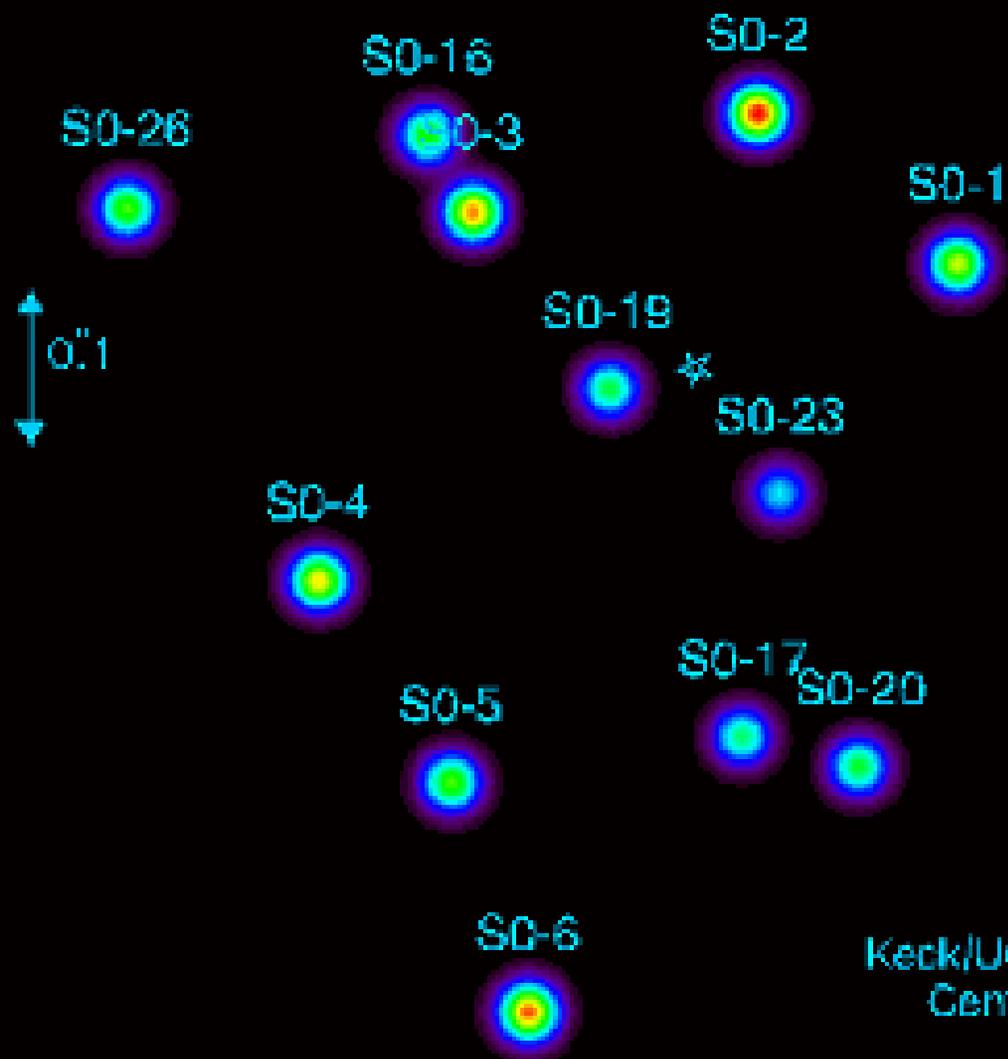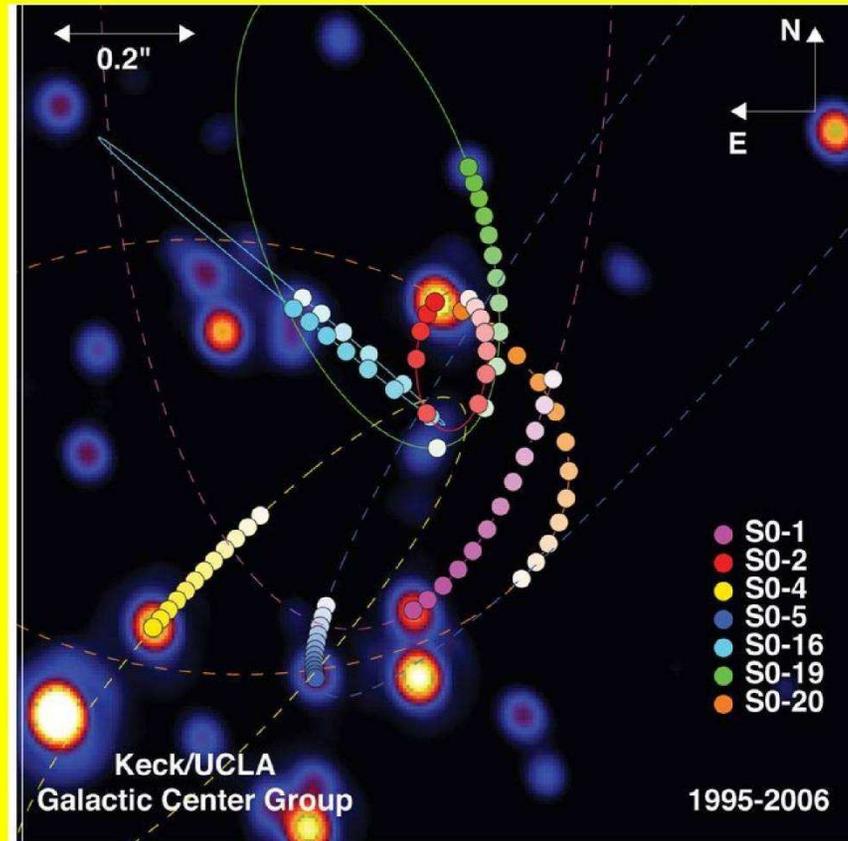
Figure 19: Bright stars near the Galactic Centre.

MONITORING STELLAR ORBITS AROUND THE MASSIVE BLACK HOLE IN THE GALACTIC CENTER

S. Gillessen[1], F. Eisenhauer[1], S. Trippe[1], T. Alexander[3], R. Genzel[1,2], F. Martins[4], T. Ott[1]

Draft version October 26, 2008

ABSTRACT

We present the results of 16 years of monitoring stellar orbits around the massive black hole in center of the Milky Way using high resolution near-infrared techniques. This work refines our previous analysis mainly by greatly improving the definition of the coordinate system, which reaches a long-term astrometric accuracy of $\approx 300\,\mu$as, and by investigating in detail the individual systematic error contributions. The combination of a long time baseline and the excellent astrometric accuracy of adaptive optics data allow us to determine orbits of 28 stars, including the star S2, which has completed a full revolution since our monitoring began. Our main results are: all stellar orbits are fit extremely well by a single point mass potential to within the astrometric uncertainties, which are now $\approx 6\times$ better than in previous studies. The central object mass is $(4.31 \pm 0.06|_{\mathrm{stat}} \pm 0.36|_{R_0}) \times 10^6 M_\odot$ where the fractional statistical error of 1.5% is nearly independent from R_0 and the main uncertainty is due to the uncertainty in R_0. Our current best estimate for the distance to the Galactic Center is $R_0 = 8.33 \pm 0.35$ kpc. The dominant errors in this value is systematic. The mass scales with distance as $(3.95 \pm 0.06) \times 10^6 (R_0/8\,\mathrm{kpc})^{2.19} M_\odot$. The orientations of orbital angular momenta for stars in the central arcsecond are random. We identify six of the stars with orbital solutions as late type stars, and six early-type stars as members of the clockwise rotating disk system, as was previously proposed. We constrain the extended dark mass enclosed between the pericenter and apocenter of S2 at less than 0.066, at the 99% confidence level, of the mass of Sgr A*. This is two orders of magnitudes larger than what one would expect from other theoretical and observational estimates.

Subject headings: blackhole physics — astrometry — Galaxy: center — infrared: stars
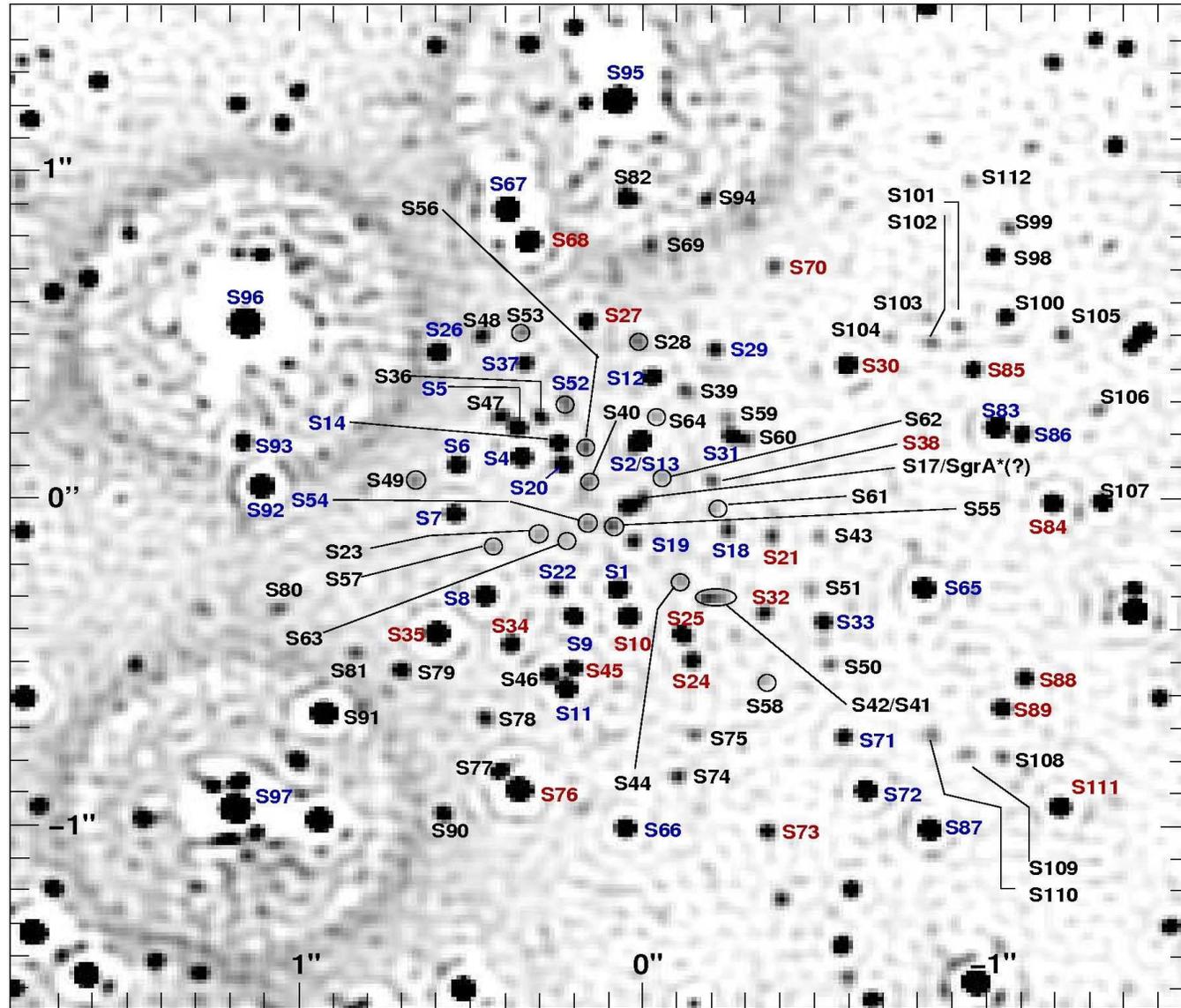
FIG. 1.— Finding chart of the S-star cluster. This figure is based on a natural guide star adaptive optics image obtained as part of this study, using NACO at UT4 (Yepun) of the VLT on July 20, 2007 in the H-band. The original image with a FWHM of ≈ 75 mas was deconvolved with the Lucy-Richardson algorithm and beam restored with a Gaussian beam with FWHM $= 2$ pix$=26.5$ mas. Stars as faint as $m_H = 19.2$ (corresponding roughly to $m_K = 17.7$) are detected at the 5σ level. Only stars that are unambiguously identified in several images have designated names, ranging from S1 to S112. Blue labels indicate early-type stars, red labels late-type stars. Stars with unknown spectral type are labelled in black. At the position of Sgr A* some light is seen, which could be either due to Sgr A* itself or due to a faint, so far unrecognized star being confused with Sgr A*.

FIG. 14.— Fitted value of R_0 for various scaling factors of the S2 2002 data, using a fit with the coordinate system priors. The factor by which the 2002 astrometric errors of the S2 data is scaled up strongly influences the distance. The mean factor determined in Figure 9 is ≈ 7, corresponding to $R_0 \approx 8.1\,\mathrm{kpc}$.

FIG. 15.— Contour plot of χ^2 as function of R_0 and central point mass. The two parameters are strongly correlated. The contours are generated from the S2 data including the 2002 data; fitting at each point all other parameters both of the potential and the orbital elements. The black dots indicate the position and errors of the best fit values of the mass for the respective distance; the blue line is a power law fit to these points; the corresponding function is given in the upper row of the text box. The central point is chosen at the best fitting distance. The red points and the red dashed line are the respective data and fit for the S2 data excluding the 2002 data; the fit is reported in the lower row of the text box. The contour levels are drawn at confidence levels corresponding to 1σ, 3σ, 5σ, 7σ, 9σ.

From the numbers it seems that the fit excluding the

FIG. 13.— Top: The S2 orbital data plotted in the combined coordinate system and fitted with a Keplerian model in which the velocity of the central point mass and its position were free fit parameters. The non-zero velocity of the central point mass is the reason why the orbit figure does not close exactly in the overlap region 1992/2008 close to apocenter. The fitted position of the central point mass is indicated by the elongated dot inside the orbit near the origin; its shape is determined from the uncertainty in the position and the fitted velocity, which leads to the elongation. Bottom: The measured radial velocities of S2 and the radial velocity as calculated from the orbit fit.

In the last years intensive searches for dark matter (DM), especially its non-baryonic component, both in galactic halos and at galaxy centers have been undertaken (see for example Bertone et al. (2005,2005a) for recent results). It is generally accepted that the most promising candidate for the DM non-baryonic component is neutralino. In this case, the γ-flux from galactic halos (and from our Galactic halo in particular) could be explained by neutralino annihilation (Gurevich et al. 1997,Bergstrom et al. 1998, Tasitsiomi et al. 2002, Stoehr et al. 2003, Prada et al. 2004,Profumo et al. 2005, Mambrini et al. 2005). Since γ-rays are detected not only from high galactic latitude, but also from the Galactic Center, there is a wide spread hypothesis (see, Evans (2004) for a discussion) that a DM concentration might be present at the Galactic Center. In this case the Galactic Center could be a strong source of γ-rays and neutrinos (Bouquet 1989, Stecker 1988, Berezinsky et al. 1994, Bergstrom et al. 1998, Bertone et al. 2004, Gnedin et al. 2004,Bergstrom et al. 2005, Horns 2005, Bertone et al. 2005) due to DM annihilation. Since it is also expected that DM forms spikes at

galaxy centers (Gondolo & Silk 1999, Ullio et al. 2001, Merritt et al. 2003) the γ-ray flux from the Galactic Center should increase significantly in that case.

At the same time, progress in monitoring bright stars near the Galactic Center have been reached recently (Genzel et al. 2003, Ghez et al. 2003, Ghez et al. 2005). The astrometric limit for bright stellar sources near the Galactic Center with 10 meter telescopes is today $\delta\theta_{10} \sim 1$ mas and the Next Generation Large Telescope (NGLT) will be able to improve this number at least down to $\delta\theta_{30} \sim 0.5$ mas (Weinberg et al. 2005) or even to $\delta\theta_{30} \sim 0.1$ mas (Weinberg et al. 2005) in the K-band. Therefore, it will be possible to measure the proper motion for about ~ 100 stars with astrometric errors several times smaller than errors in current observations.

The aim of this talk is to constrain the parameters of the DM distribution possible present around the Galactic Center by considering the induced apoastron shift due to the presence of this DM sphere and either available

data obtained with the present generation of telescopes (the so called *conservative* limit) and also expectations from future NGLT observations or with other advanced observational facilities.

Celestial mechanics of S2 like stars for BH+cluster (A.A. Nucita, F. De Paolis, G. Ingrosso, A. Qadir, AFZ, PASP, v. 119, p. 349 (2007))

GR predicts that orbits about a massive central body suffer periastron shifts yielding *rosette* shapes. However, the classical perturbing effects of other objects on inner orbits give an opposite shift. Since the periastron advance depends strongly on the compactness of the central body, the detection of such an effect may give information about the nature of the central body itself. This would apply for stars orbiting close to the GC, where there is a "dark object", the black hole hypothesis being the most natural explanation of the observational data. A cluster of stars in the vicinity of the GC (at a distance < 1 arcsec) has been monitored by ESO and Keck teams for several years.

For a test particle orbiting a Schwarzschild black hole of mass M_{BH}, the periastron shift is given by (see e.g. Weinberg, 1972)

$$\Delta\phi_S \simeq \frac{6\pi G M_{BH}}{d(1-e^2)c^2} + \frac{3(18+e^2)\pi G^2 M_{BH}^2}{2d^2(1-e^2)^2 c^4} \,, \tag{9}$$

d and e being the semi-major axis and eccentricity of the test particle orbit, respectively. For a rotating black hole with spin parameter $a = |\mathbf{a}| = J/GM_{\mathrm{BH}}$, the space-time is described by the Kerr metric and, in the most favorable case of equatorial plane motion ($(\mathbf{a,v}) = 0$), the shift is given by (Boyer and Price (1965))

$$\Delta\phi_K \simeq \Delta\phi_S + \frac{8a\pi M_{BH}^{1/2} G^{3/2}}{d^{3/2}(1-e^2)^{3/2} c^3} + \frac{3a^2\pi G^2}{d^2(1-e^2)^2 c^4} \,, \tag{10}$$

which reduces to eq. (9) for $a \to 0$. In the more general case, $\mathbf{a.v} \neq 0$, the

expected periastron shift has to be evaluated numerically.

The expected periastron shifts (mas/revolution), $\Delta\phi$ (as seen from the center) and $\Delta\phi_E$ (as seen from Earth at the distance $R_0 \simeq 8$ kpc from the GC), for the Schwarzschild and the extreme Kerr black holes, for the S2 and S16 stars turn out to be $\Delta\phi^{S2} = 6.3329 \times 10^5$ and 6.4410×10^5 and $\Delta\phi_E^{S2} = 0.661$ and 0.672 respectively, and $\Delta\phi^{S16} = 1.6428 \times 10^6$ and 1.6881×10^6 and $\Delta\phi_E^{S16} = 3.307$ and 3.399 respectively. Recall that

$$\Delta\phi_E = \frac{d(1+e)}{R_0}\Delta\phi_{S,K} \ . \tag{11}$$

Notice that the differences between the periastron shifts for the Schwarzschild and the maximally rotating Kerr black hole is at most 0.01 mas for the S2 star and 0.009 mas for the S16 star. In order to make these measurements with the required accuracy, one needs to know the S2 orbit with a precision of at least 10 μas.

The star cluster surrounding the central black hole in the GC could be sizable. At least 17 members have been observed within 15 mpc up to now (Ghez et al. (2005)). However, the cluster mass and density distribution, that is to say its mass and core radius, is still unknown. The presence of this cluster affects the periastron shift of stars orbiting the central black hole. The periastron advance depends strongly on the mass density profile and especially on the central density and typical length scale.

We model the stellar cluster by a Plummer model density profile (Binney & Tremaine (1987))

$$\rho_{CL}(r) = \rho_0 f(r) \,, \qquad \text{with} \qquad f(r) = \left[1 + \left(\frac{r}{r_c}\right)^2\right]^{-\alpha/2} \,, \quad (12)$$

where the cluster central density ρ_0 is given by

$$\rho_0 = \frac{M_{CL}}{\int_0^{R_{CL}} 4\pi r^2 f(r) \, dr} \, , \qquad (13)$$

R_{CL} and M_{CL} being the cluster radius and mass, respectively. According to dynamical observations towards the GC, we require that the total mass $M(r) = M_{BH} + M_{CL}(r)$ contained within $r \simeq 5 \times 10^{-3}$ pc is $M \simeq 3.67 \times 10^6 \, M_\odot$. Useful information is provided by the cluster mass fraction, $\lambda_{CL} = M_{CL}/M$, and its complement, $\lambda_{BH} = 1 - \lambda_{CL}$. As one can see, the requirement given in eq. (13) implies that $M(r) \to M_{BH}$ for $r \to 0$. The total mass density profile $\rho(r)$ is given by

$$\rho(r) = \lambda_{BH} M \delta^{(3)}(\overrightarrow{r}) + \rho_0 f(r) \qquad (14)$$

and the mass contained within r is

$$M(r) = \lambda_{BH} M + \int_0^r 4\pi r'^2 \rho_0 f(r') \, dr' . \tag{15}$$

According to GR, the motion of a test particle can be fully described by solving the geodesic equations. Under the assumption that the matter distribution is static and pressureless, the equation of motion of the test particle becomes (see e.g. Weinberg 1972))

$$\frac{d\mathbf{v}}{dt} \simeq -\nabla(\Phi_N + 2\Phi_N^2) + 4\mathbf{v}(\mathbf{v} \cdot \nabla)\Phi_N - v^2 \nabla \Phi_N . \tag{16}$$

For the S2 star, d and e given in the literature are 919 AU and 0.87 respectively. They yield the orbits of the S2 star for different values of the

black hole mass fraction λ_{BH} shown in Figure 20. The Plummer model parameters are $\alpha = 5$, core radius $r_c \simeq 5.8$ mpc. Note that in the case of $\lambda_{BH} = 1$, the expected (prograde) periastron shift is that given by eq. (9), while the presence of the stellar cluster leads to a retrograde periastron shift. For comparison, the expected periastron shift for the S16 star is given in Figure 31. In the latter case, the binary system orbital parameters were taken from Schödel et al. (2003)) assuming also for the S16 mass a conservative value of $\simeq 10$ M$_\odot$.
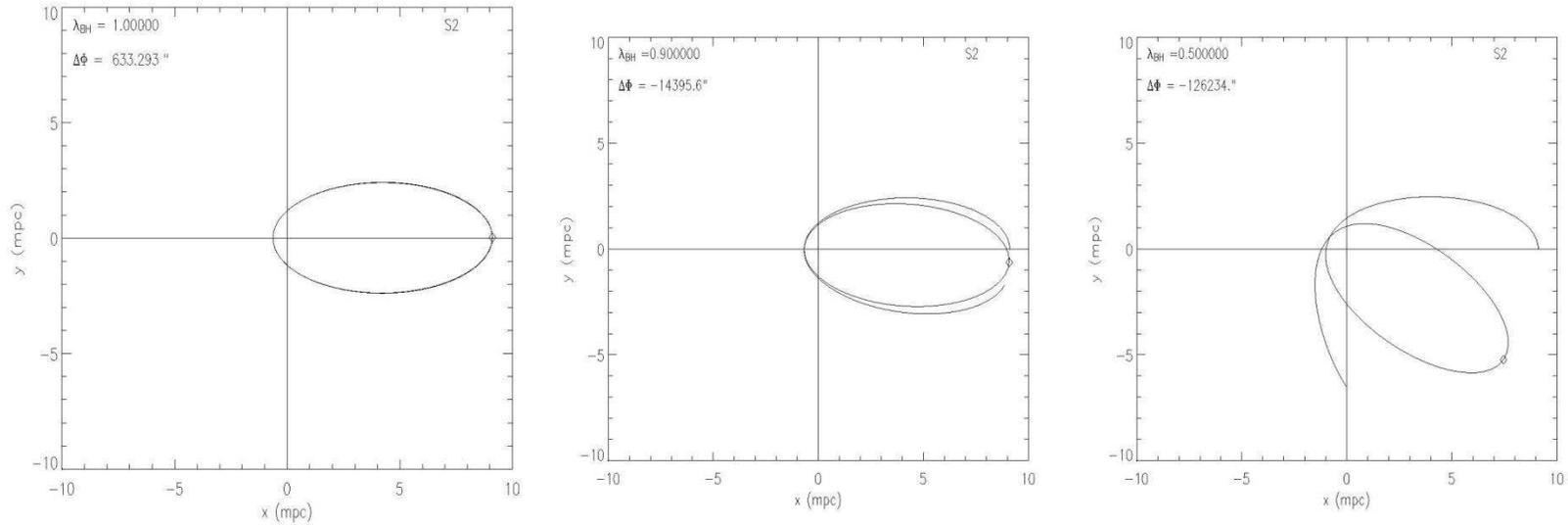
Figure 20: Post Newtonian orbits for different values of the black hole mass fraction λ_{BH} are shown for the S2 star (upper panels). Here, we have assumed that the Galactic central black hole is surrounded by a stellar cluster whose density profile follows a Plummer model with $\alpha = 5$ and a core radius $r_c \simeq 5.8$ mpc. The periastron shift values in each panel is given in arcseconds.
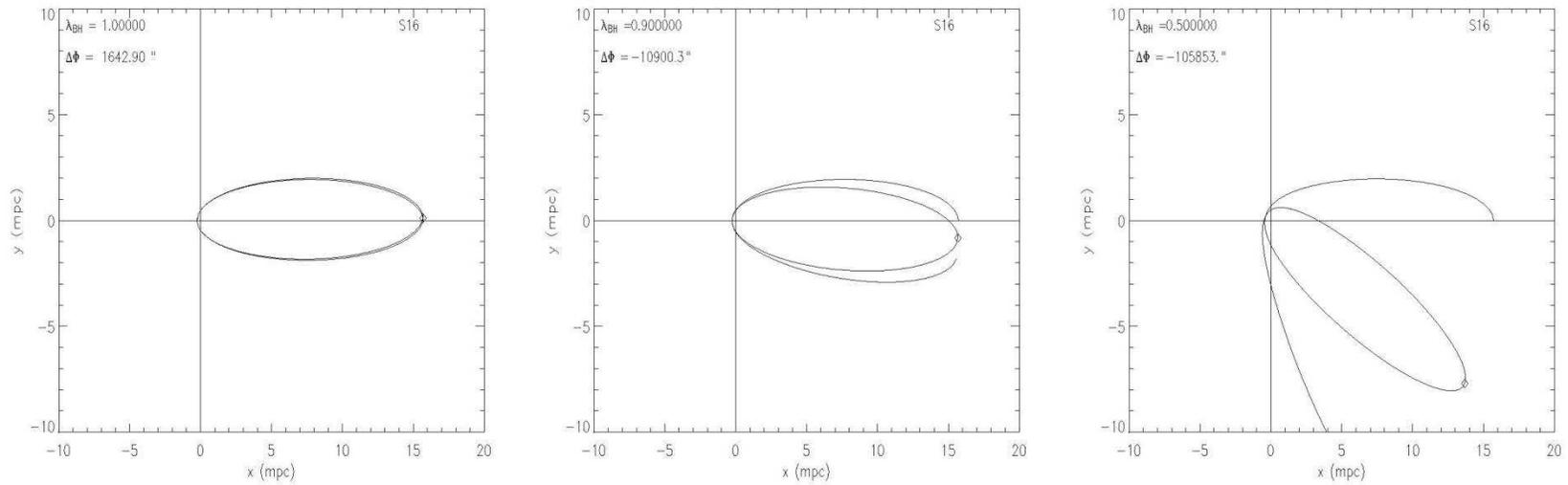
Figure 21: The same as in Figure 20 but for the S16–Sgr A* binary system. In this case, the binary system orbital parameters were taken from Ghez et al. (2005) assuming for the S16 mass a conservative value of $\simeq 10$ M$_\odot$.

The mass concentration at the Galactic Center

Recent advancements in infrared astronomy are allowing to test the scale of the mass profile at the center of our galaxy down to tens of AU. With the Keck 10 m telescope, the proper motion of several stars orbiting the Galactic Center black hole have been monitored and almost entire orbits, as for example that of the S2 star, have been measured allowing an unprecedent description of the Galactic Center region. Measurements of the amount of mass $M(< r)$ contained within a distance r from the Galactic Center are continuously improved as more precise data are collected. Recent observations (Ghez et al. (2003)) extend down to the periastron distance ($\simeq 3 \times 10^{-4}$ pc) of the S16 star and they correspond to a value of the enclosed mass within $\simeq 3 \times 10^{-4}$ pc of $\simeq 3.67 \times 10^6$ M$_\odot$. Several authors have used these observations to model the Galactic Center mass concentration. Here and in the following, we use the three component

model for the central region of our galaxy based on estimates of enclosed mass given by Ghez et al (2003, 2005) recently proposed by Hall and Gondolo (2006). This model is constituted by the central black hole, the central stellar cluster and the DM sphere (made of WIMPs), i.e.

$$M(<r) = M_{BH} + M_*(<r) + M_{DM}(<r) \ , \qquad (17)$$

where M_{BH} is the mass of the central black hole Sagittarius A*. For the central stellar cluster, the empirical mass profile is

$$M_*(<r) = \begin{cases} M_* \left(\frac{r}{R_*}\right)^{1.6} \ , & r \leq R_* \\ \\ M_* \left(\frac{r}{R_*}\right)^{1.0} \ , & r > R_* \end{cases} \qquad (18)$$

with a total stellar mass $M_* = 0.88 \times 10^6$ M$_\odot$ and a size $R_* = 0.3878$ pc.

As far as the mass profile of the DM concentration is concerned, Hall & Gondolo (2006) have assumed a mass distribution of the form

$$
M_{DM}(<r) = \begin{cases} M_{DM} \left(\dfrac{r}{R_{DM}}\right)^{3-\alpha}, & r \leq R_{DM} \\[2em] M_{DM}, & r > R_{DM} \end{cases} \tag{19}
$$

M_{DM} and R_{DM} being the total amount of DM in the form of WIMPs and the radius of the spherical mass distribution, respectively.

Hall and Gondolo (2006) discussed limits on DM mass around the black hole at the Galactic Center. It is clear that present observations of stars around the Galactic Center do not exclude the existence of a DM sphere with mass $\simeq 4 \times 10^6 M_\odot$, well contained within the orbits of the known stars, if its radius R_{DM} is $\lesssim 2 \times 10^{-4}$ pc (the periastron distance of the S16 star in the more recent analysis (Ghez et al. 2005)). However, if one

considers a DM sphere with larger radius, the corresponding upper value for M_{DM} decreases (although it tends again to increase for extremely extended DM configurations with $R_{DM} \gg 10$ pc). In the following, we will assume for definiteness a DM mass $M_{DM} \sim 2 \times 10^5 M_\odot$, that is the upper value for the DM sphere (Hall & Gondolo (2006)) within an acceptable confidence level in the range $10^{-3} - 10^{-2}$ pc for R_{DM}. As it will be clear in the following, we emphasize that even a such small value for the DM mass (that is about only 5% of the standard estimate $3.67 \pm 0.19 \times 10^6 \ M_\odot$ for the dark mass at the Galactic Center (Ghez et al. 2005)) may give some observational signatures.

Evaluating the S2 apoastron shift [1] as a function of R_{DM}, one can further constrain the DM sphere radius since even now we can say that there is no evidence for negative apoastron shift for the S2 star orbit at the

---

[1] We want to note that the periastron and apoastron shifts $\Delta\Phi$ as seen from the orbit center have the same value whereas they have different values as seen from Earth (see Eq. (23)). When we are comparing our results with orbit reconstruction from observations we refer to the apoastron shift as seen from Earth.

level of about 10 mas (Genzel et al. 2003). In addition, since at present the precision of the S2 orbit reconstruction is about 1 mas, we can say that even without future upgrades of the observational facilities and simply monitoring the S2 orbit, it will be possible within about 15 years to get much more severe constraints on R_{DM}.

Moreover, observational facilities will allow in the next future to monitor faint infrared objects at the astrometric precision of about 10 μas (Eisenhauer et al. 2005) and, in this case, previous estimates will be sensibly improved since it is naturally expected to monitor eccentric orbits for faint infrared stars closer to the Galactic Center with respect to the S2 star.

In Fig. 30, the mass profile $M(< r)$ (Ghez et al. 2003) obtained by using observations of stars nearby the Galactic Center is shown (solid line). The dotted line represents the stellar mass profile as given in Eq. (18), while the dashed lines are for DM spheres with mass $M_{DM} \simeq 2 \times 10^5$ M$_\odot$ and

radii $R_{DM} = 10^{-3}$ and 10^{-2} pc, respectively.

Apoastron Shift Constraints

According to GR, the motion of a test particle can be fully described by solving the geodesic equations. Under the assumption that the matter distribution is static and pressureless, the equations of motion at the first post-Newtonian (PN) approximation become (see e.g. (Fock 1961, Weinberg 1972, Rubilar & Eckart 2001))

$$
\frac{d\mathbf{v}}{dt} \simeq -\nabla(\Phi_N + 2\Phi_N^2) + 4\mathbf{v}(\mathbf{v} \cdot \nabla)\Phi_N - v^2 \nabla \Phi_N \ . \tag{21}
$$

We note that the PN-approximation is the first relativistic correction from which the apoastron advance phenomenon arises. In the case of the S2 star, the apoastron shift as seen from Earth (from Eq. (23)) due to the presence of a central black hole is about 1 mas, therefore not directly

detectable at present since the available precision in the apoastron shift is about 10 mas (but it will become about 1 mas in 10–15 years even without considering possible technological improvements). It is also evident that higher order relativistic corrections to the S2 apoastron shift are even smaller and therefore may be neglected at present, although they may become important in the future.

As it will be discussed below, the Newtonian effect due to the existence of a sufficiently extended DM sphere around the black hole may cause a apoastron shift in the opposite direction with respect to the relativistic advance due to the black hole. Therefore, we have considered the two effects comparing only the leading terms.

For the DM distribution at the Galactic Center we follow Eq. (19) as done in Hall & Gondolo (2006). Clearly, if in the future faint infrared stars (or spots) closer to the black hole with respect to the S2 star will be monitored (Eisenhauer, (2005)), this simplified model might well not hold

and higher order relativistic corrections may become necessary.

For a spherically symmetric mass distribution (such as that described above) and for a gravitational potential given by Eq. (20), Eq. (21) may be rewritten in the form (see for details Rubilar & Eckart (2001))

$$\frac{d\mathbf{v}}{dt} \simeq -\frac{GM(r)}{r^3}\left[\left(1 + \frac{4\Phi_N}{c^2} + \frac{v^2}{c^2}\right)\mathbf{r} - \frac{4\mathbf{v}(\mathbf{v}\cdot\mathbf{r})}{c^2}\right] \, , \qquad (22)$$

$\mathbf{r}$ and $\mathbf{v}$ being the vector radius of the test particle with respect to the center of the stellar cluster and the velocity vector, respectively. Once the initial conditions for the star distance and velocity are given, the rosetta shaped orbit followed by a test particle can be found by numerically solving the set of ordinary differential equations in eq. (22).

In Fig. 20, as an example, assuming that the test particle orbiting the Galactic Center region is the S2 star, we show the Post Newtonian orbits

detectable at present since the available precision in the apoastron shift is about 10 mas (but it will become about 1 mas in 10–15 years even without considering possible technological improvements). It is also evident that higher order relativistic corrections to the S2 apoastron shift are even smaller and therefore may be neglected at present, although they may become important in the future.

As it will be discussed below, the Newtonian effect due to the existence of a sufficiently extended DM sphere around the black hole may cause a apoastron shift in the opposite direction with respect to the relativistic advance due to the black hole. Therefore, we have considered the two effects comparing only the leading terms.

For the DM distribution at the Galactic Center we follow Eq. (19) as done in Hall & Gondolo (2006). Clearly, if in the future faint infrared stars (or spots) closer to the black hole with respect to the S2 star will be monitored (Eisenhauer, (2005)), this simplified model might well not hold

and higher order relativistic corrections may become necessary.

For a spherically symmetric mass distribution (such as that described above) and for a gravitational potential given by Eq. (20), Eq. (21) may be rewritten in the form (see for details Rubilar & Eckart (2001))

$$\frac{d\mathbf{v}}{dt} \simeq -\frac{GM(r)}{r^3}\left[\left(1 + \frac{4\Phi_N}{c^2} + \frac{v^2}{c^2}\right)\mathbf{r} - \frac{4\mathbf{v}(\mathbf{v}\cdot\mathbf{r})}{c^2}\right]\,, \qquad (22)$$

$\mathbf{r}$ and $\mathbf{v}$ being the vector radius of the test particle with respect to the center of the stellar cluster and the velocity vector, respectively. Once the initial conditions for the star distance and velocity are given, the rosetta shaped orbit followed by a test particle can be found by numerically solving the set of ordinary differential equations in eq. (22).

In Fig. 20, as an example, assuming that the test particle orbiting the Galactic Center region is the S2 star, we show the Post Newtonian orbits

obtained by the black hole only, the black hole plus the stellar cluster and the contribution of two different DM mass density profiles. In each case the S2 orbit apoastron shift is given. As one can see, for selected parameters for DM and stellar cluster masses and radii the effect of the stellar cluster is almost negligible while the effect of the DM distribution is crucial since it enormously overcome the shift due to the relativistic precession. Moreover, as expected, its contribution is opposite in sign with respect to that of the black hole (Nucita et al. (2007)).

We note that the expected apoastron (or, equivalently, periastron) shifts (mas/revolution), $\Delta\Phi$ (as seen from the center) and the corresponding values $\Delta\phi_E^{\pm}$ as seen from Earth (at the distance $R_0 \simeq 8$ kpc from the GC) are related by

$$\Delta\phi_E^{\pm} = \frac{d(1 \pm e)}{R_0}\Delta\Phi, \tag{23}$$

where with the sign $\pm$ are indicated the shift angles of the apoastron $(+)$

and periastron (-), respectively. The S2 star semi-major axis and eccentricity are $d = 919$ AU and $e = 0.87$ (Ghez et al. 2005).

In Fig. 32, the S2 apoastron shift as a function of the DM distribution size R_{DM} is given for $\alpha = 0$ and $M_{DM} \simeq 2 \times 10^5$ M$_\odot$. Taking into account that the present day precision for the apoastron shift measurements is of about 10 mas, one can say that the S2 apoastron shift cannot be larger than 10 mas. Therefore, any DM configuration that gives a total S2 apoastron shift larger than 10 mas (in the opposite direction due to the DM sphere) is excluded. The same analysis is shown in Figs. 33 and 34 for two different values of the DM mass distribution slope, i.e. $\alpha = 1$ and $\alpha = 2$, respectively. In any case, we have calculated the apoastron shift for the S2 star orbit assuming a total DM mass $M_{DM} \simeq 2 \times 10^5$ M$_\odot$. As one can see by inspecting Figs. 32-34, the upper limit of about 10 mas on the S2 apoastron shift may allow to conclude that DM radii in the range about $10^{-3} - 10^{-2}$ pc are excluded by present observations.

We notice that the results of the present analysis allows to further constrain the results (Hall and Gondolo 2006) who have concluded that if the DM sphere radius is in the range $10^{-3} - 1$ pc, configurations with DM mass up to $M_{DM} = 2 \times 10^5 \, M_\odot$ are acceptable. The present analysis shows that DM configurations of the same mass are acceptable only for R_{DM} out the range between $10^{-3} - 10^{-2}$ pc, almost irrespectively of the α value.
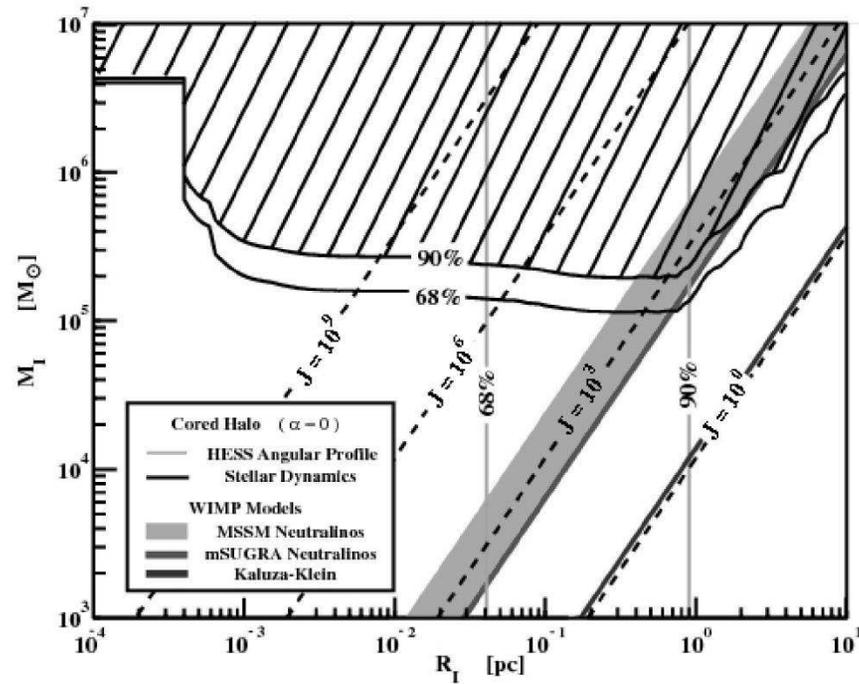
Figure 28: An allowed region for DM distribution from S2 like star trajectories near the Black Hole at the Galactic Center (Hall and Gondolo (2006)).
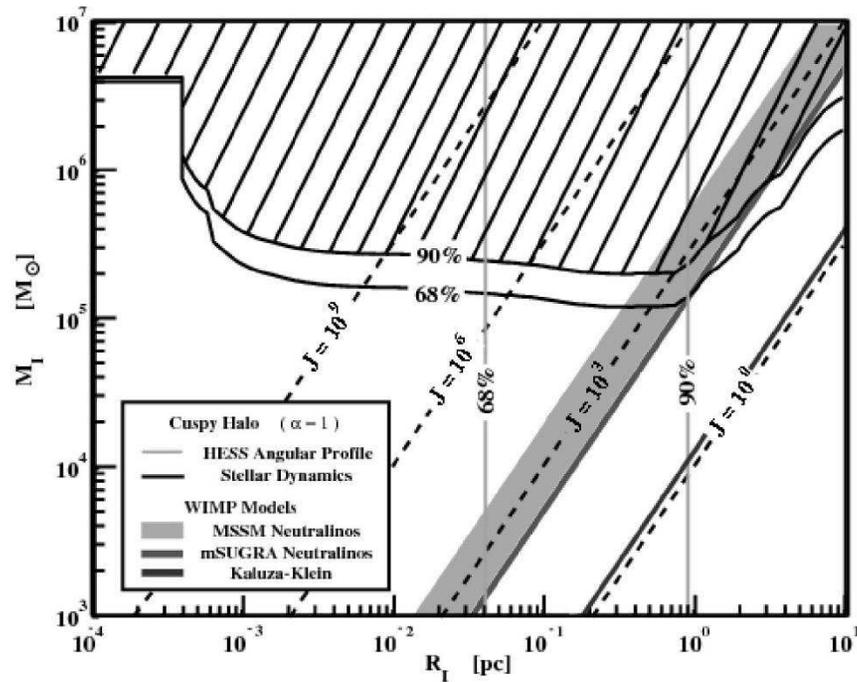
Figure 29: An allowed region for DM distribution from S2 like star trajectories near the Black Hole at the Galactic Center (Hall and Gondolo (2006).
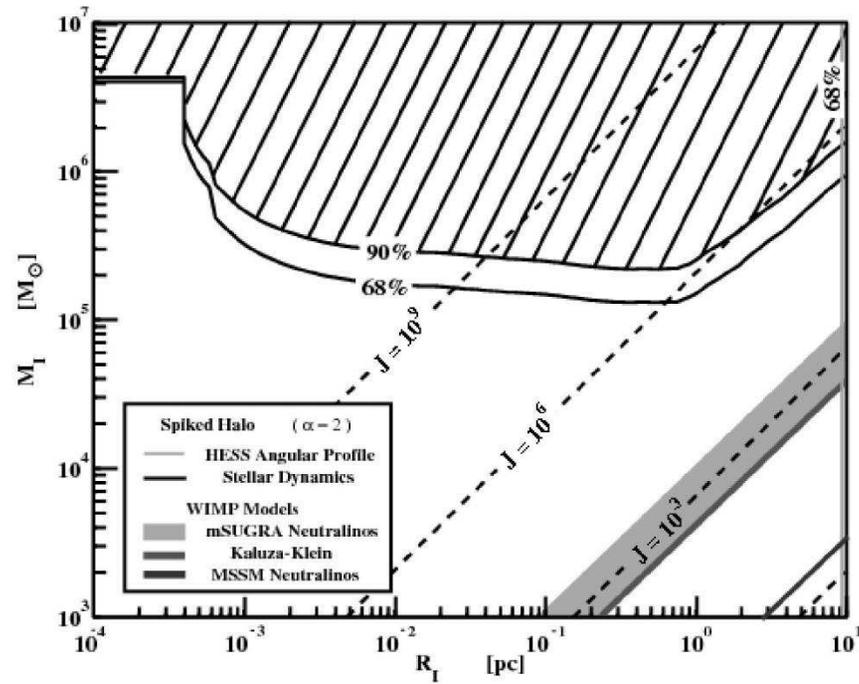
Figure 30: An allowed region for DM distribution from S2 like star trajectories near the Black Hole at the Galactic Center (Hall and Gondolo (2006).
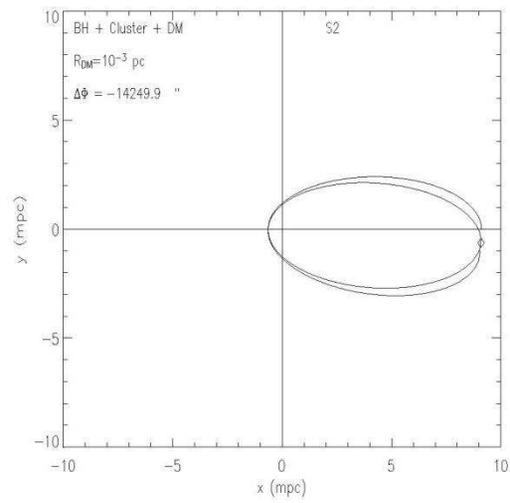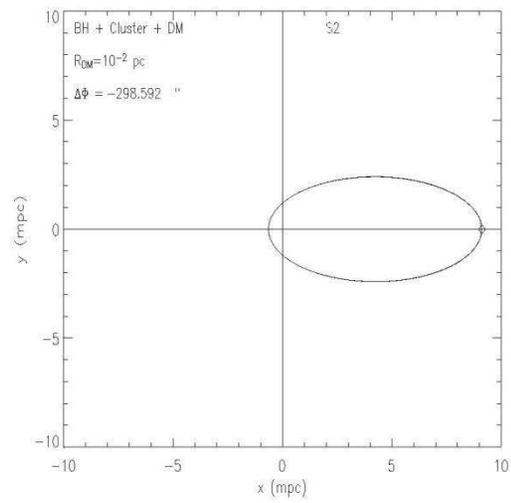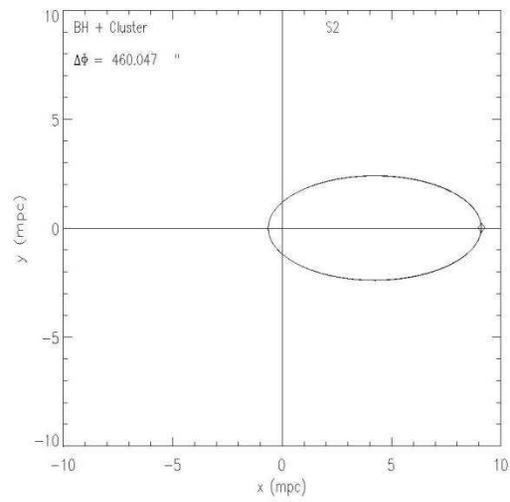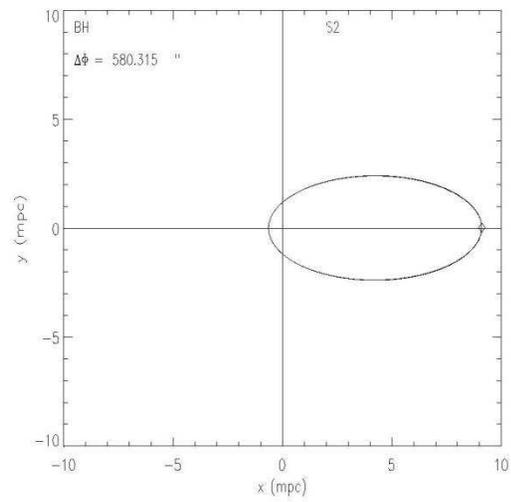
Figure 31: PN-orbits for different mass configurations at the Galactic Center. The S2 star has been considered as a test particle and its apoastron shift is indicated in each panel as $\Delta\Phi$ (in arcsec). The top-left panel shows the central black hole contribution to the S2 shift that amounts to about 580 arcsec. The top-right panels shows the combined contribution of the black hole and the stellar cluster (taken following eq. 18) to the S2 apoastron shift. In the two bottom panels the contribution due to two different DM mass-density profiles is added (as derived in eq. 19). We assume that DM mass $M_{DM} \simeq 2 \times 10^5$ M$_\odot$.
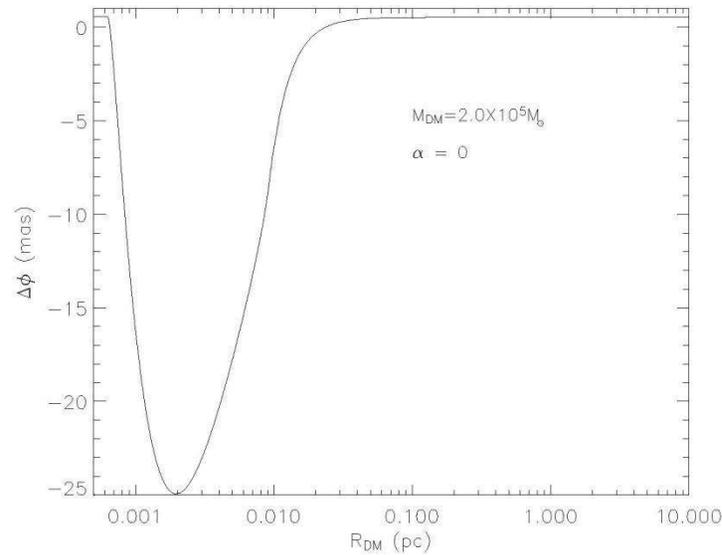
Figure 32: Apoastron shift as a function of the DM radius R_{DM} for $\alpha = 0$ and $M_{DM} \simeq 2 \times 10^5$ M$_\odot$. Taking into account present day precision for the apoastron shift measurements (about 10 mas) one can say that DM radii R_{DM} in the range $8 \times 10^{-4} - 10^{-2}$ pc are not acceptable.
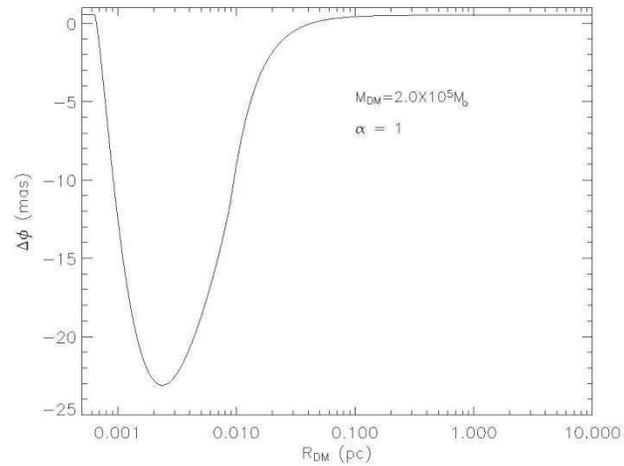
Figure 33: The same as in Fig. 32 for $\alpha = 1$ and $M_{DM} \simeq 2 \times 10^5$ M$_\odot$. As in the previous case one can say that the S2 apoastron shift put severe limits on the DM mass radii that are not acceptable in the range $9 \times 10^{-4} - 10^{-2}$ pc.
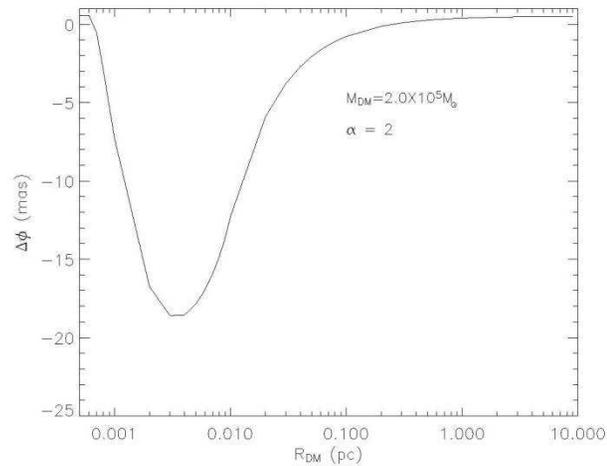
Figure 34: The same as in Fig. 32 for $\alpha = 2$ and $M_{DM} \simeq 2 \times 10^5$ M$_\odot$. As in the previous case one can say that the upper limit to the S2 apoastron shift allows to constrain the DM radius to be out the range $1.0 \times 10^{-3} - 1.1 \times 10^{-2}$ pc.

- **Conclusions**

- VLBI systems in mm and sub-mm bands or MAXIM could detect mirages ("faces") around black holes.

- Shapes of images give an important information about BH parameter

- Trajectories of bright stars or bright spots around massive BHs are very important tool for an evaluation of BH parameters

- Thanks for your kind attention!

- [Macho_96_5_light_curve](#)
- [Macho_96_6_light_curve](#)
- [Likelihood functions for BH microlenses](#)
- [Probable masses and distances for BH microlenses](#)
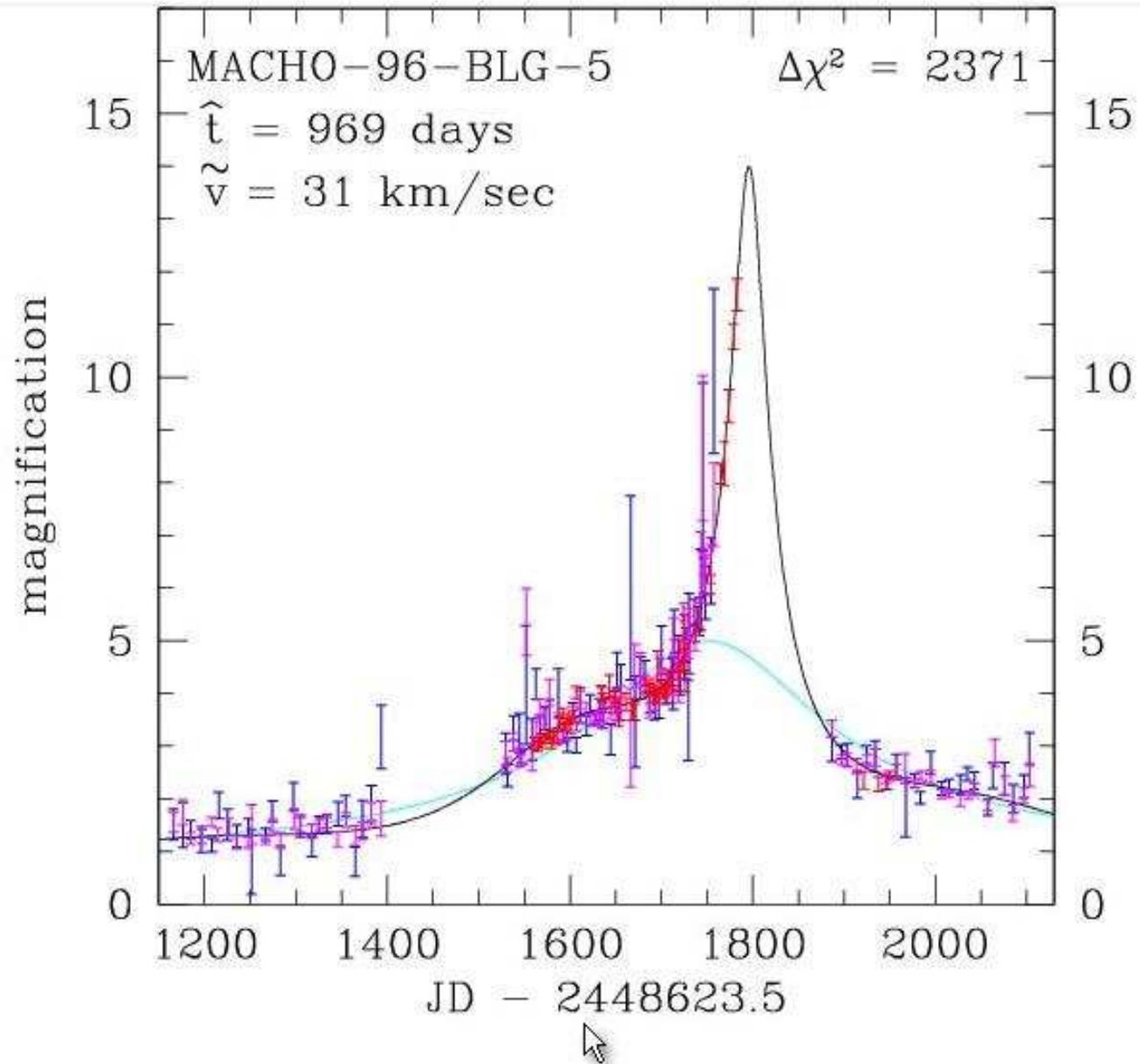
Fig. 7.— MACHO-96-BLG-5 lightcurves normalized to the unlensed flux of the lensed star. The MACHO red and blue data are plotted in magenta and blue, respectively, and the CTIO data are shown in red. The black curve is the parallax fit while the cyan curve is the best fit standard microlensing lightcurve. An additional 4 years of data showing very little photometric variation are not shown.
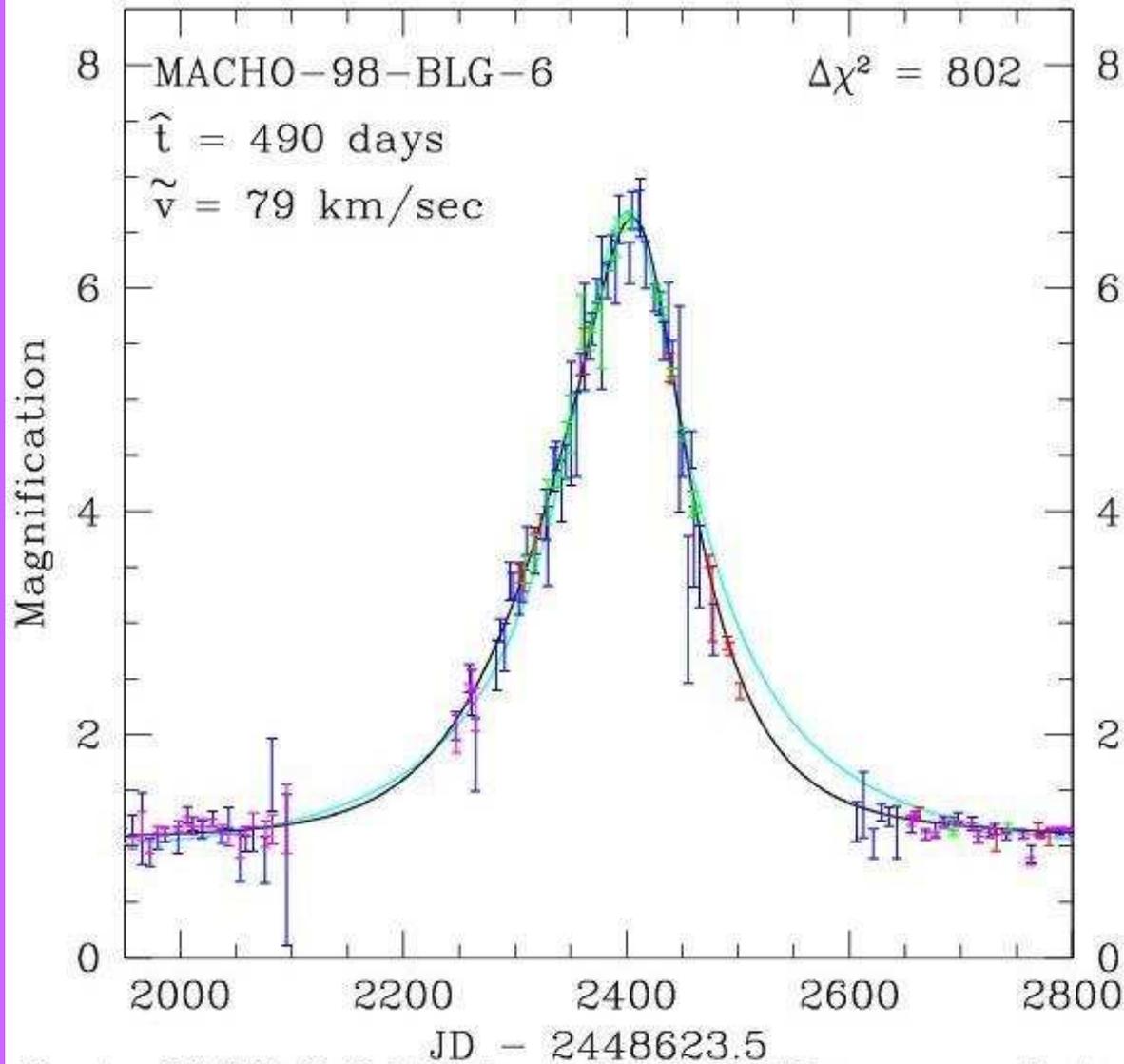
Fig. 4.— MACHO-98-BLG-6 lightcurve closeup with lightcurves normalized to the unlensed flux of the lensed star. The MACHO red and blue data are plotted in magenta and blue, respectively, the CTIO data are shown in red, and the MPS data are shown in green. The black curve is the parallax fit while the cyan curve is the best fit standard microlensing lightcurve. The gap in the MACHO red data during the day 2280-2650 interval is due to a CCD failure. An additional year of data showing no photometric variation is not shown.
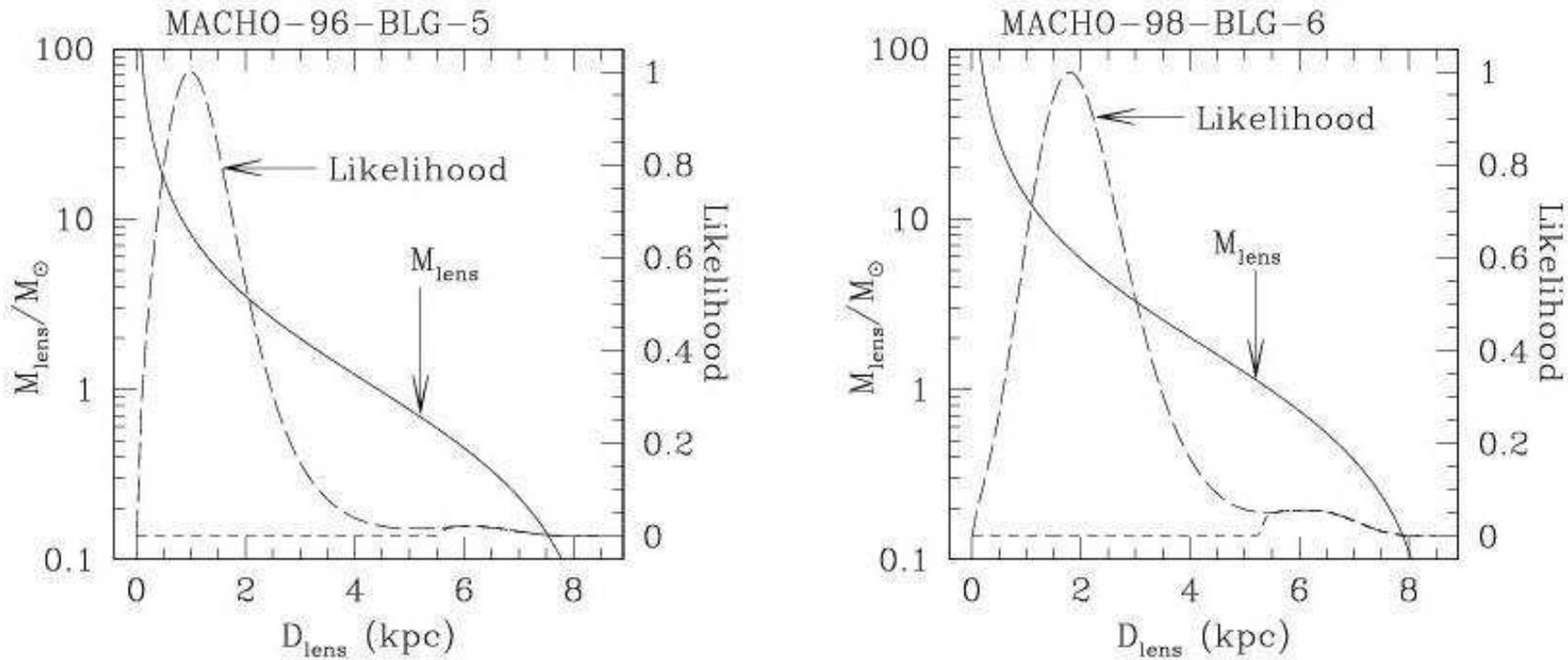
Fig. 11.— The mass vs. distance relations (solid curves) for our candidate black hole lenses are shown along with the likelihood functions (long dashed curves) computed assuming a standard model for the Galactic phase space distribution. The source star is assumed to reside in the bulge for both events. The implied best fit masses are $M = 6^{+10}_{-3} M_\odot$ for the MACHO-96-BLG-5 lens and $M = 6^{+7}_{-3} M_\odot$ for the MACHO-98-BLG-6. The 95% confidence level lower limits on the masses are $1.6 M_\odot$ and $0.94 M_\odot$ respectively. The short dashed curves delineate the portion of the likelihood functions that is allowed when the lens is assumed to be a main sequence star. The ratio of the area below this portion to the entire area below the likelihood curve gives a probability that a lens is a main sequence star. For MACHO-96-BLG-5, the upper limit on the lens brightness is very stringent because of the HST images, and a main sequence lens is ruled out.

Table 7. Mass & Magnitude Estimates for the MACHO Microlensing Parallax Events

Event	$M/M_\odot$	$M_{MS}/M_\odot$	$D_{\ell-MS}$	sep-MS	V_s	$\Delta I_{\ell s}$	$\Delta V_{\ell s}$	$\Delta B_{\ell s}$	$\Delta U_{\ell s}$
104-C	$1.1^{+1.1}_{-0.5}$	0.74	2.7 kpc	40 mas	17.3	3.5	3.5	3.5	3.2
96-BLG-5	6^{+10}_{-3}	-	-	-	-	-	-	-	-
96-BLG-12	$1.3^{+1.8}_{-0.7}$	0.75	2.0 kpc	28 mas	18.0	2.1	2.2	2.2	2.3
98-BLG-6	$2.5^{+1.7}_{-0.9}$	0.88	5.7 kpc	5 mas	20.1	2.2	1.9	1.6	1.1
99-BLG-1	$0.7^{+1.2}_{-0.4}$	0.40	1.7 kpc	17 mas	18.9	1.8	3.2	3.6	3.9
99-BLG-8	$1.2^{+1.6}_{-0.6}$	1.2	1.6 kpc	25 mas	16.3	1.3	0.7	−0.3	−1.1

Note. — These are the parameters of the "most likely" main sequence star lenses for our best microlensing parallax events. For MACHO-96-BLG-5, a main sequence lens is ruled out.

SYSTEMATIC ANALYSIS OF 22 MICROLENSING PARALLAX CANDIDATES

SHAWN POINDEXTER,[1] CRISTINA AFONSO,[2] DAVID P. BENNETT,[3] JEAN-FRANCOIS GLICENSTEIN,[4]
ANDREW GOULD,[1] MICHAŁ K. SZYMAŃSKI,[5] AND ANDRZEJ UDALSKI[5]

ABSTRACT

We attempt to identify all microlensing parallax events for which the parallax fit improves $\Delta\chi^2 > 100$ relative to a standard microlensing model. We outline a procedure to identify three types of discrete degeneracies (including a new one that we dub the "ecliptic degeneracy") and find many new degenerate solutions in 16 previously published and six unpublished events. Only four events have one unique solution, and the other 18 events have a total of 44 solutions. Our sample includes three previously identified black hole (BH) candidates. We consider the newly discovered degenerate solutions and determine the relative likelihood that each of these is a BH. We find that the lens of event MACHO-99-BLG-22 is a strong BH candidate (78%), event MACHO-96-BLG-5 is a marginal BH candidate (37%), and MACHO-98-BLG-6 is a weak BH candidate (2.2%). The lens of event OGLE-2003-BLG-84 may be a Jupiter-mass free-floating planet candidate based on a weak 3 σ detection of finite-source effects. We find that event MACHO-179-A is a brown dwarf candidate within $\sim$100 pc of the Sun, mostly due to its very small projected Einstein radius, $\tilde{r}_{\mathrm{E}} = 0.23 \pm 0.05$ AU. As expected, these microlensing parallax events are biased toward lenses that are heavier and closer than average. These events were examined for xallarap (or binary-source motion), which can mimic parallax. We find that 23% of these events are strongly affected by xallarap.

What is a black hole?

Everyone already seems to know!
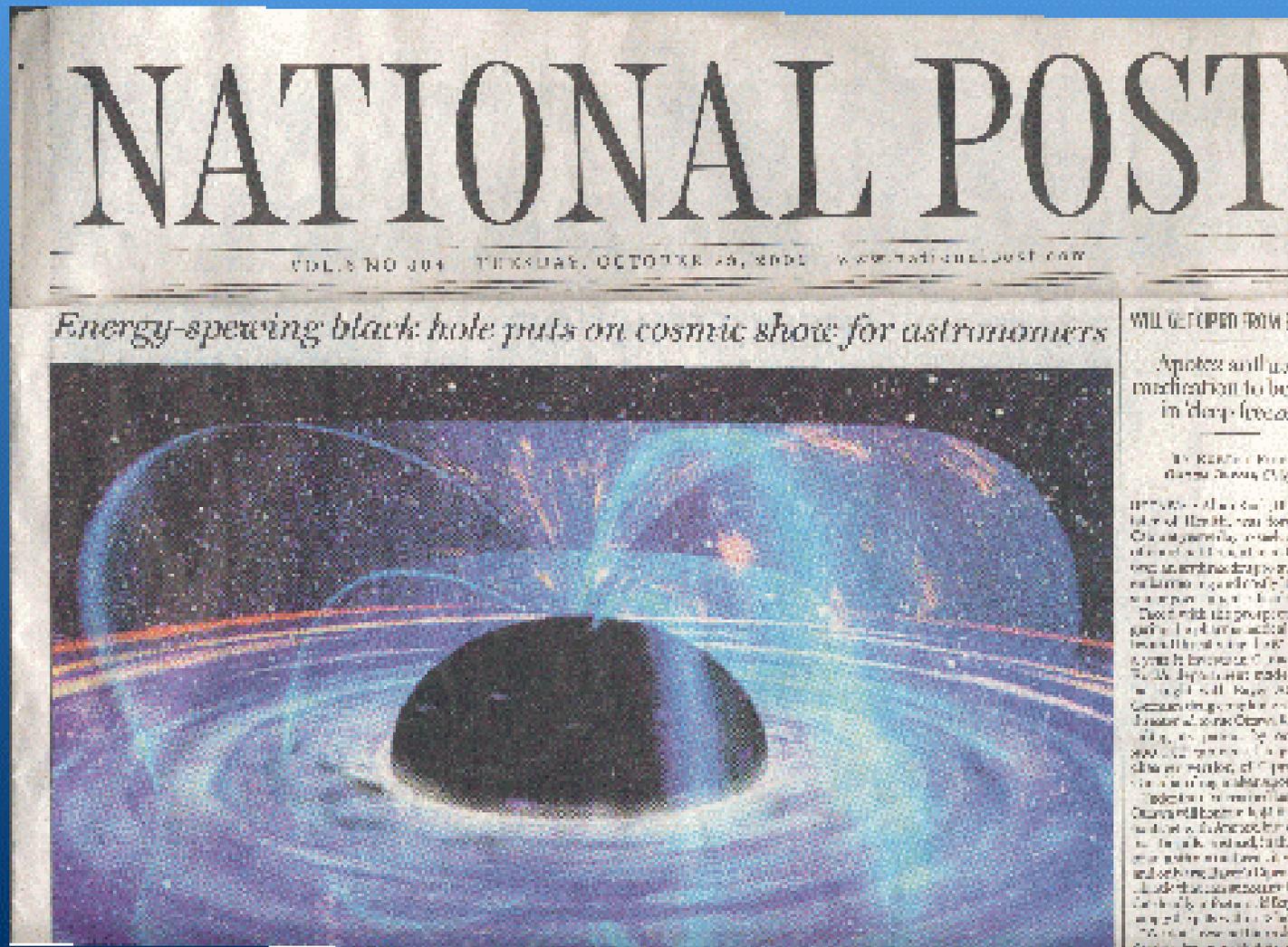
Relativistic Fe Kα Lines with *XMM-Newton*

Jörn Wilms
(University of Warwick)

http://astro.uni-tuebingen.de/~wilms
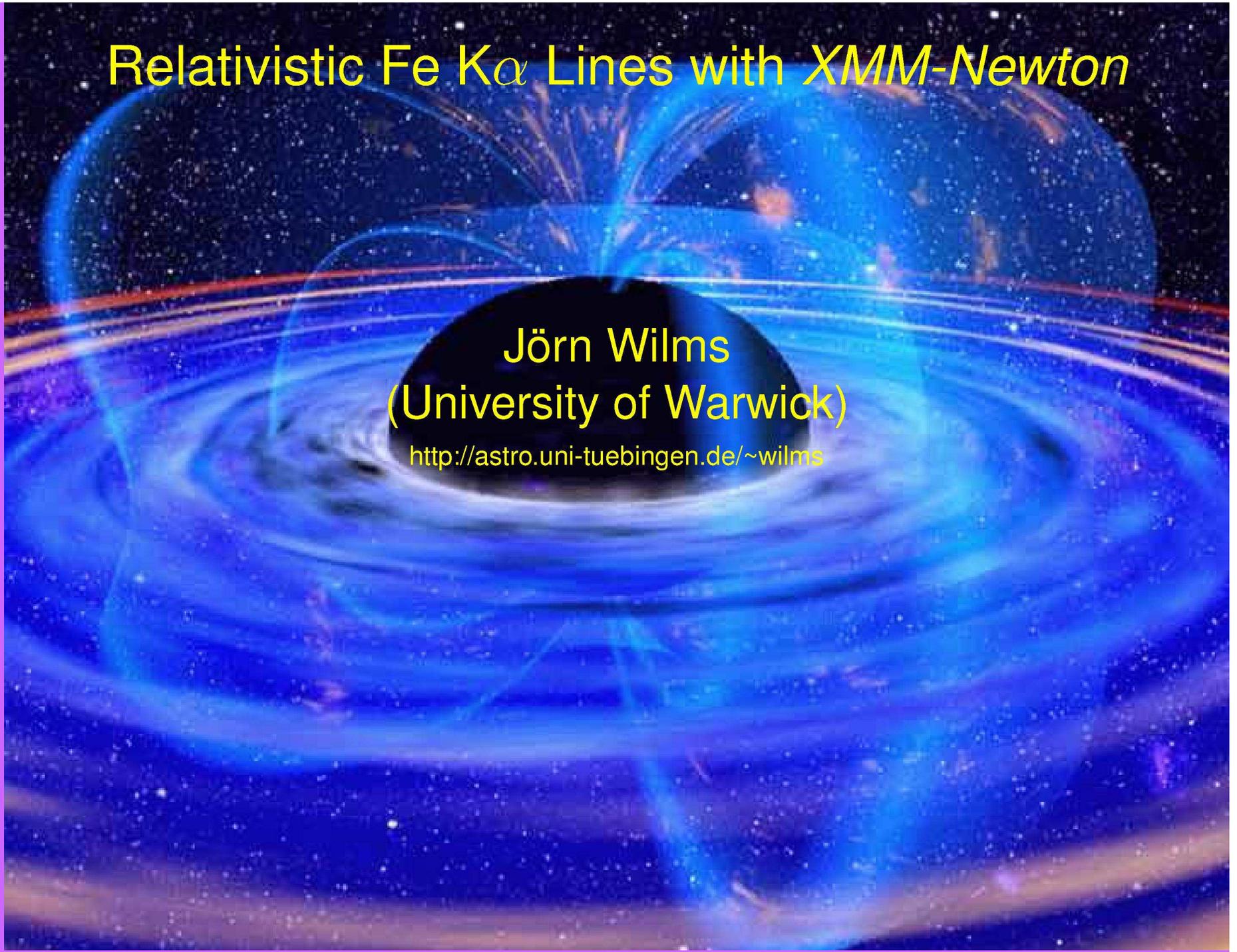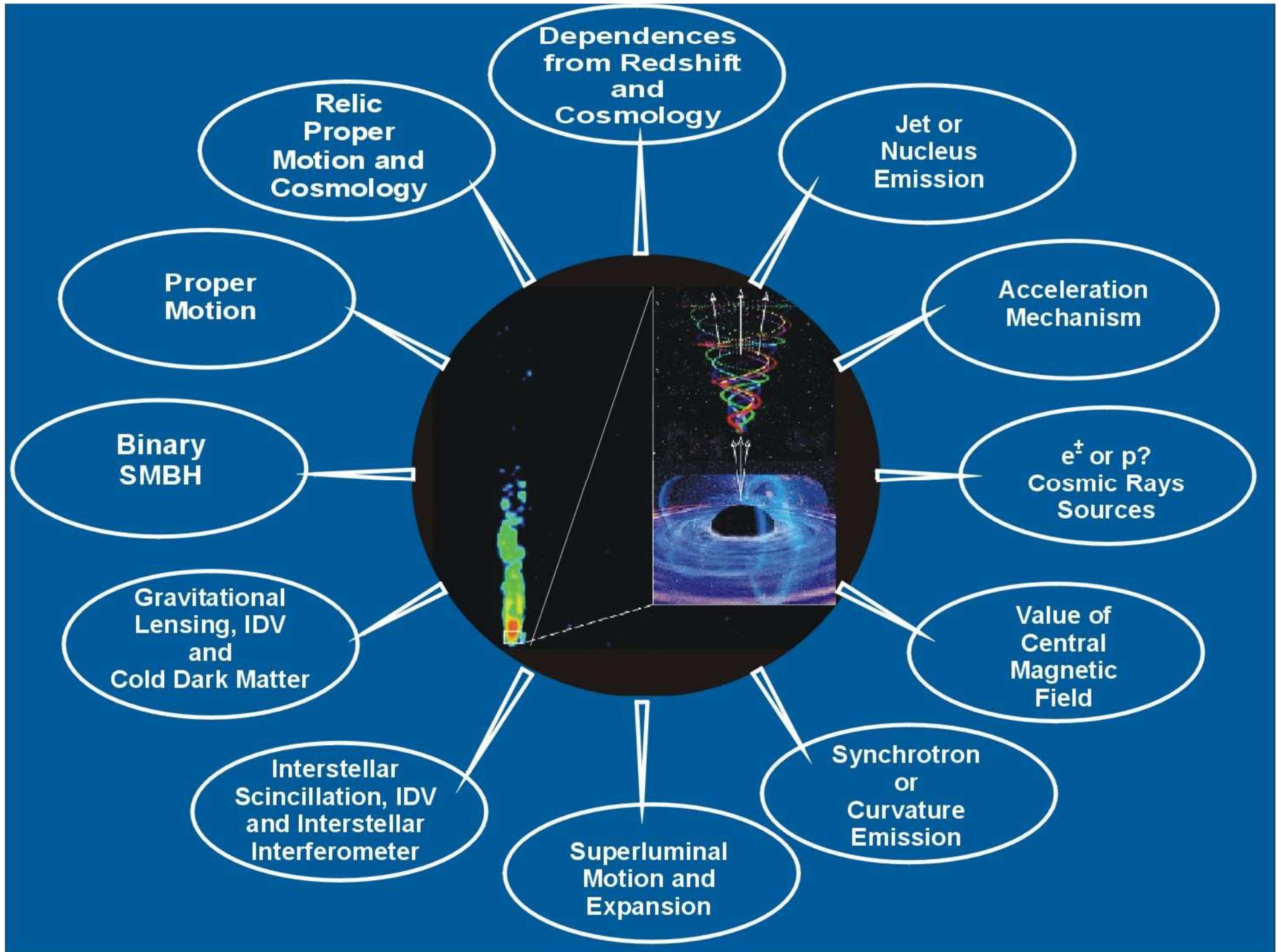
Conclusion

Scientific Questions

subdivided into topics where important progress can be expected in the Cosmic Vision 2015-2025 timeframe

3. What are the fundamental physical laws of the Universe?

3.3 Matter under extreme conditions

Probe gravity theory in the very strong field environment of black holes and other compact objects, and the state of matter at supra-nuclear energies in neutron stars

**4. How did the Universe originate and what is it made of?**

4.2 The Universe taking shape

Find the very first gravitationally-bound structures that were assembled in the Universe – precursors to today's galaxies, groups and clusters of galaxies – and trace their evolution to the current epoch

4.3 The evolving violent Universe

Trace the formation and evolution of the supermassive black holes at galaxy centres – in relation to galaxy and star formation – and trace the life cycles of matter in the Universe along its history

Large-Aperture X-ray Observatory

$Z = 2$

$Z = 0$
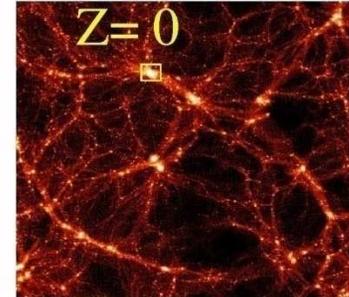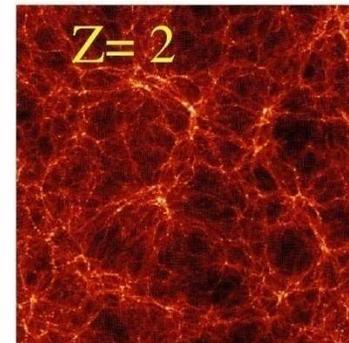
# XMM-Newton observations of MCG-6-30-15 in the 2-10 keV band
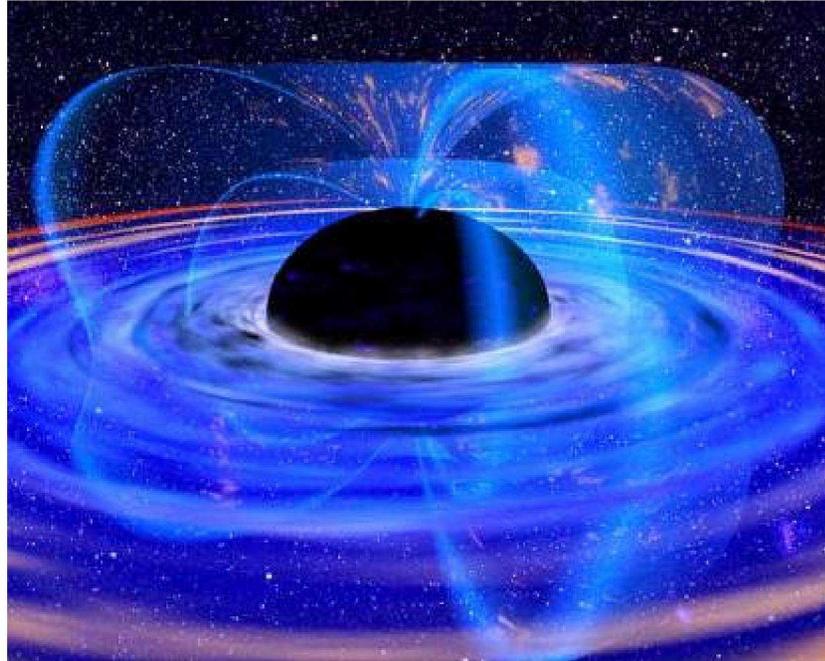
Wilms et al 2002; Fabian et al 2002; Vaughan et al 2002; Fabian & Vaughan 2002; Ballantyne et al 2003; Reynolds et al 2003; Vaughan & Fabian 2004

Understanding the spectral behaviour
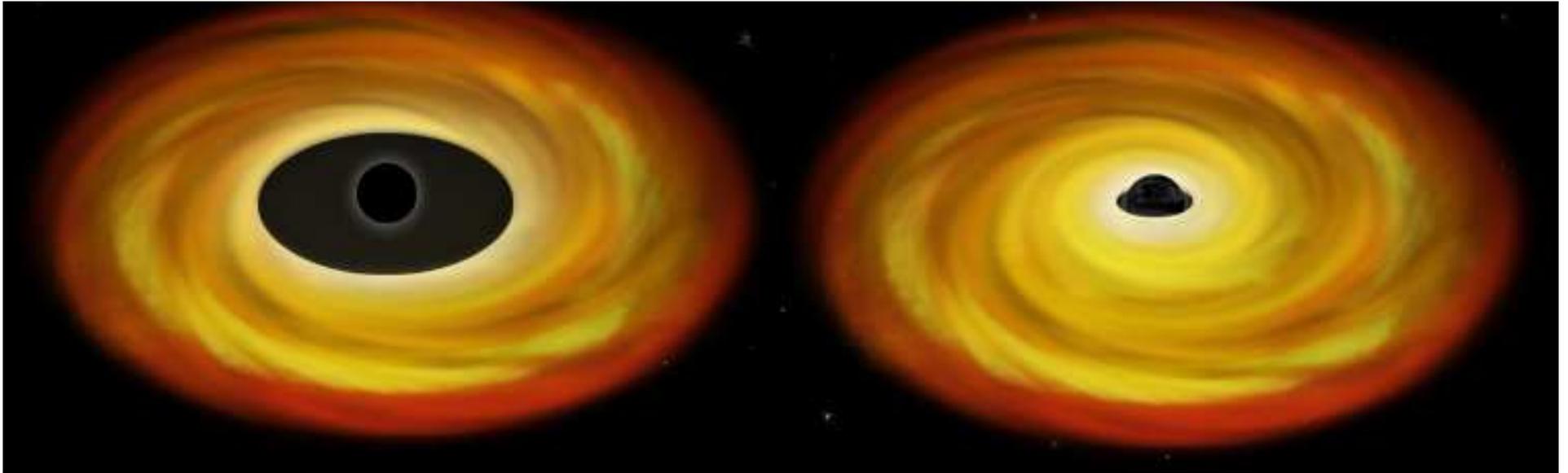
SPIN
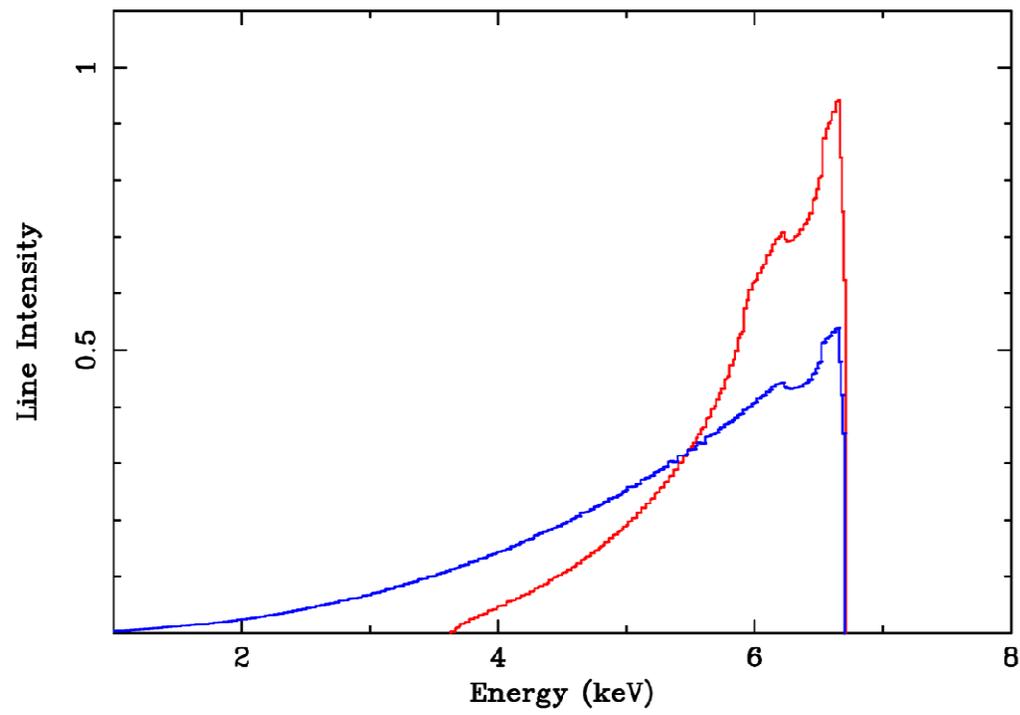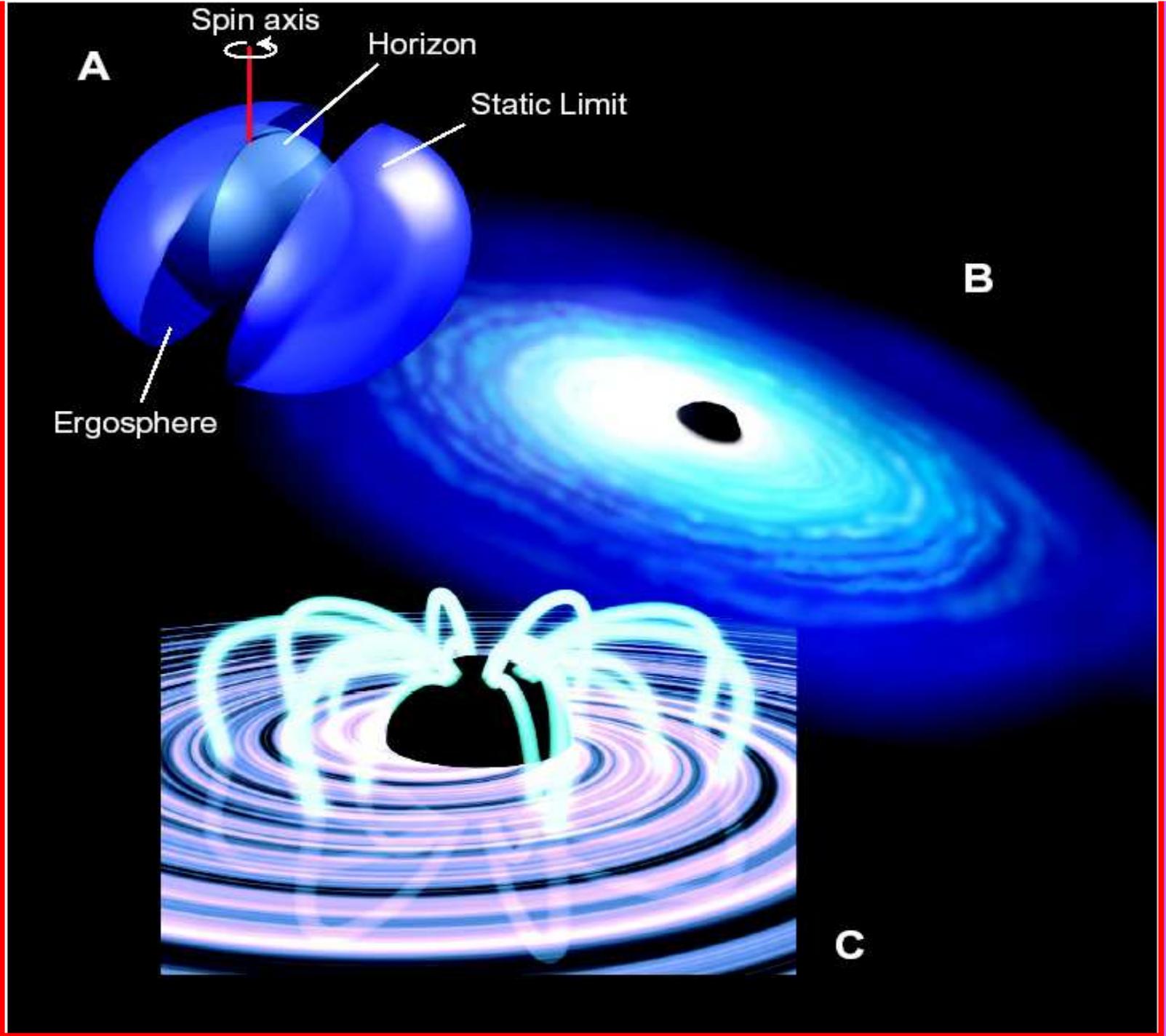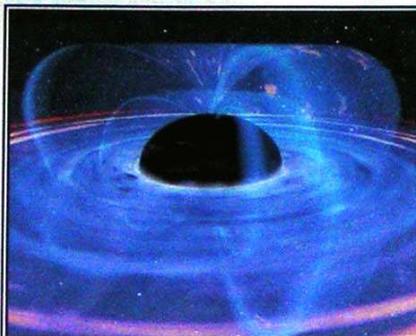
Spin axis

A

Horizon

Static Limit

Ergosphere

B

C

What Makes them B
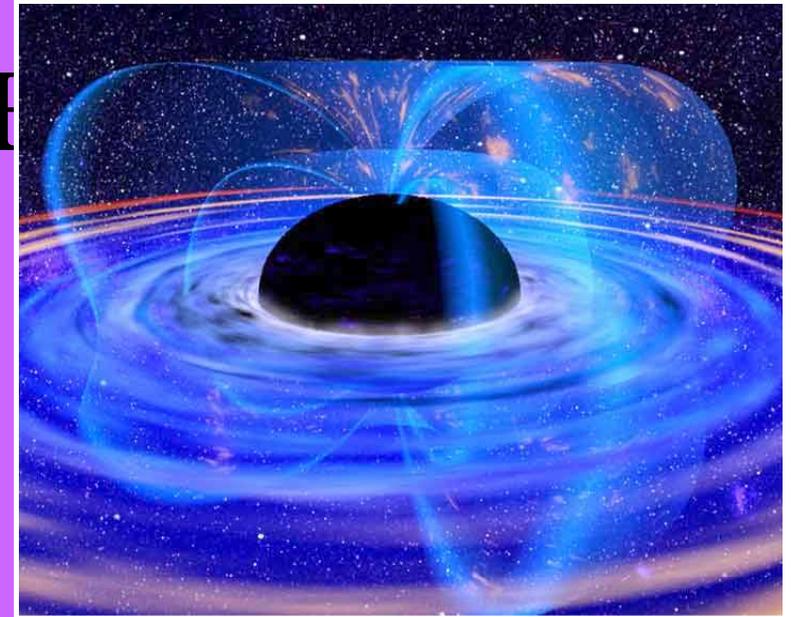
- Other than the classical Rees argument about efficiency, size and luminosity what observational properties make these objects black holes ?
    - High mass in a small volume via direct measurements
        SGR A*, NGC4258 etc
    - Mass functions of stellar systems
    For the vast majority of objects thought to be black holes such information is not available
    - We must use indirect observational data
        - Spectra
        - Timing
        - Spectral/timing (reverberation mapping)
        - Imaging (micro-lensing)

    For the vast majority of objects thought to be black holes such information is not available
    - We must use indirect observational data
        - Spectra
        - Timing
        - Spectral/timing (reverberation mapping)
        - Imaging (micro-lensing)
    - **E.g. things that look like other BHs are also BHs**

Why are black hole interesting today

- Black Holes and Strong Gravity
    - Spectral and timing probes of strong gravity
    - Astrophysics in the strong gravity region
- AGN Winds & effect of BHs on cosmic structure
    - Outflows from AGN
    - Cooling flow and cluster entropy problems
    - Role of AGN in galaxy formation
- Evolution of AGN and SMBH growth
    - Paradigm shift in AGN evolution

The next step : Constellation-X
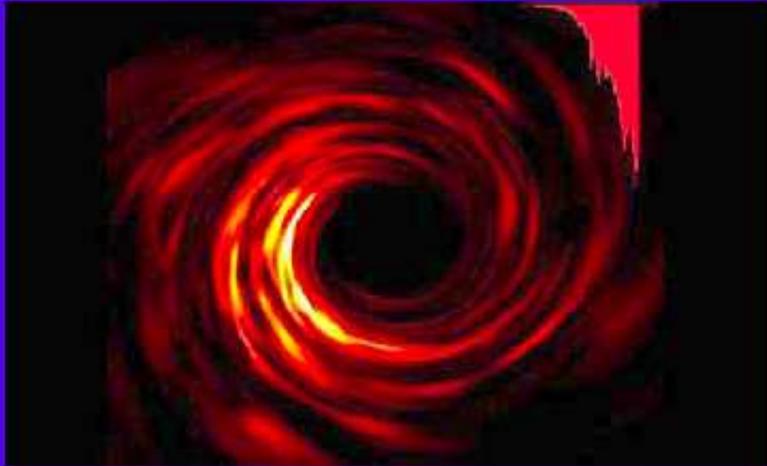
Reynolds et al
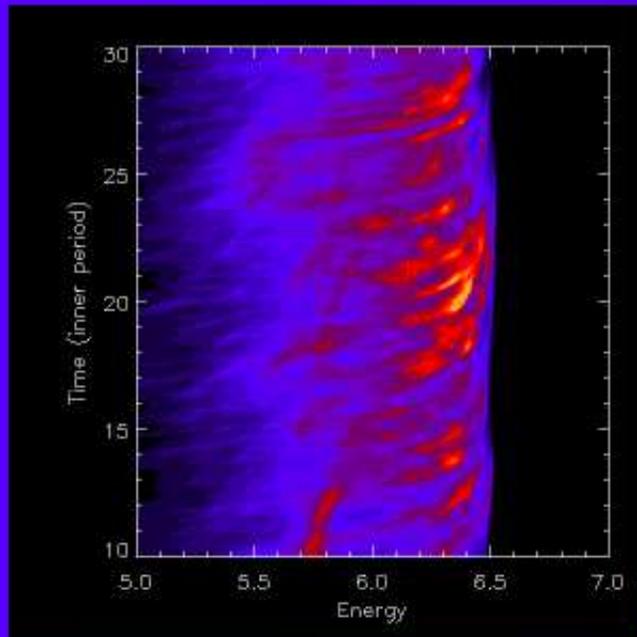
Analysis of iron line variability (from orbital motion of disk & reverberation effects) allows to to separate effects of
- Accretion disk physics
- Spacetime geometry

Requires superior collecting area of Constellation-X

7